Mapping Shellfish Distribution Using Hyperspectral Remote Sensing

By

Jeffrey S. Vincent

Bachelor of Science
New Mexico State University, 1997

Master of Applied Geography
New Mexico State University, 1999

Submitted in Partial Fulfillment of the Requirements

For the Degree of Doctor of Philosophy in the

Department of Geography

University of South Carolina

2006

_____
Major Professor
Chairman, Examining Committee

_____ _____
Committee Member Committee Member

_____ _____
Committee Member Dean of the Graduate School

Dedication

To My Family

This dissertation is dedicated to my wife Helen, my friend, inspiration and soul mate. My children, Paige, Sarah, Nevin, Kenny and Jeffrey, thank you all for enduring this process and sacrificing the time I needed. In my life, you are the most important.

Acknowledgements

This dissertation is the result of not just my efforts but from the inspiration and support of many people that proved to be invaluable throughout the dissertation process. I would like to thank the chair of my dissertation committee, Dr. John Jensen for his help and friendship. Dr. Dwayne Porter, a huge, huge thank you for your mentoring, guidance, and humor throughout. Your guidance and inspiration has helped shape my intellectual growth and will serve to guide me in the years to come. Dr. Michael Hodgson, thank you for your challenging classes and intellectual inspiration. It is refreshing and I value your inspiration. Dr. David Cowen, thank you for keeping me sane through this process. I admire your candor and energy for Geography. Dr. Loren Coen at the SC DNR, thank you for your friendship and guidance throughout the research, this research achievement would not be the same had I not had your help and encouragement. Dr. Steven Schill, the CICEET Principal Investigator, thank you for trusting me with the grant and allowing me to complete my goal. No acknowledgement would be complete without a big thank you from my colleagues in the GIP Lab. Your team work shows that anything is possible when good people work together. Undoubtedly, the last two years associated with the Baruch Institute's GIP lab has given me some of the best memories of South Carolina.

My intellectual formative years at New Mexico State University gave me the foundation and drive to achieve my goals at the University of South Carolina. Dr. Mike DeMers, my mentor and friend for life who inspired me to not only to go forward in my education but was also responsible for introducing me to Geography and GIS, a huge thank you! Dr. Jack Wright, Dr. Dan Dugas, and Robert "Bob" Czerniak, you all taught and showed me what it was to be a Geographer, thank you for your gift.

I would like to thank my mother-in-law, Linda Neslund. Your abounding energy and optimism helped enormously and kept me moving at times when the night was darkest. Thank you all!

Abstract

Mapping Shellfish Distribution Using Hyperspectral Remote Sensing

By Jeffrey S. Vincent

A majority of all baseline shellfish maps are currently produced through ground surveys and manual aerial photo interpretation, a tedious process which is time-consuming and prone to human errors. The first objective of this research was to investigate and document the feasibility of using remotely sensed imagery to identify and classify intertidal shellfish resources. A specific task was to spectrally identify the differences between mud and shellfish using a combination of hyperspectral remote sensing data and extensive *in situ* spectral data. A second objective was the identification of spectrally relevant portions of the electromagnetic spectrum that are useful in identification of shellfish and to determine if there is a statistical difference between mud and shellfish.

This research found that it was feasible to accurately identify shellfish and distinguish shellfish from mud. It was found that with the incorporation of *in situ* derived spectral endmembers, the accuracy of the mapping procedure was lower than deriving spectral endmembers directly from the remotely sensed imagery. It was also noted that changes within the habitat could have occurred between the acquisition of the remotely sensed HyMAP and AISA imagery and the acquisition of the *in situ* data may have contributed to lower accuracy results. Secondary objective results indicate that the visible and near infra-red portions of the electromagnetic spectrum are the most useful for discriminating between shellfish and mud. While statistical analysis showed there was a significant difference between mud and shellfish, there was also a high degree of

statistical differences within the collected shellfish data that a degree of uncertainty remains.

The use of remotely sensed imagery, *in situ* ancillary data and field verification does result in shellfish maps that are less error prone than previous methodologies and allows for the mapping of remote or hard to access areas of shellfish resources.

It is hoped that the creation of a repeatable, timely, and cost effective mapping technique that is less prone to error for the creation of baseline shellfish maps will benefit the coastal community at national and international levels.

Dissertation Director: John R. Jensen, Ph.D.

Table of Contents

List of Figures

List of Tables

Chapter 1. Introduction

Shellfish occupy a niche in the ecosystem that is between the land and oceans in an environment that is continually becoming more influenced by humans. Unfortunately with the rate of anthropogenic settlement along the coasts of the United States increasing, negative impacts on shellfish communities such as fecal coliform from diminished water quality, over harvesting, physical disturbance, and habitat degradation has forced the closing of shellfish harvesting grounds and the collapse of an entire industry in areas of the United States. Not only are the shellfish reefs in danger of collapsing but the larger ecosystem of fin fishes that are dependent on the oyster reefs will be adversely impacted as well. From a local to regional scale, these problems facing the shellfish ecosystem is forcing ecologists and other environmental scientists to focus on these long-term and regional scale questions (Michener, 1992). This research addressed the use of remote sensing as an application to detect, map and monitor coastal shellfish assemblages.

The interdisciplinary nature of this research merges the needs of shellfish biology with that of geography. Simply put, shellfish biologists need a tool that will allow them to map and monitor intertidal shellfish resources in a repeatable and cost effective process. Within the remote sensing community of geography is the need to apply spectral analysis from hyperspectral imagery to a marine coastal environment for technique validation. While neither remote sensing nor marine biology literature addresses the specific question of deriving oysters in a marine environment using this technique. These research questions were couched in terms of needs within the respective fields. The literature review elucidates the history of oysters on the Atlantic

coast of the United States, the function of oysters as part of a larger ecosystem process, oyster restoration efforts, and needs within the current resource management strategies. In remote sensing the rapid pace with which technology has advanced fueled by greater access to remote sensing data has created many techniques for deriving information from the environment, especially in the area of hyperspectral remote sensing. One such technique is Mixture Tuned Matched Filtering, (MTMF). Two images result from analysis and mapping, one is the MTMF score and the second is an infeasibility image. The MTMF score shows the probability that the pixel is contains the material that is being mapped and the infeasibility score shows the probability that the material in incorrectly mapped or are false positives. Used in conjunction with the MTMF score image, the user has the ability to refine the endmember selection and mapping process to increase accuracy.

This mapping research utilized two components for the MTMF technique: 1) using *in situ* shellfish spectral signatures to build a spectral library of oyster strata through the course of a year for input into the MTMF method, and 2) imagery derived spectral endmembers. A statistical comparison between image derived endmembers and *in situ* aggregated (and non-aggregated) endmembers was done to test for similarity. The main objective of this research was to test if shellfish could be differentiated from mud using remotely sensed hyperspectral imagery and classified to produce a map of shellfish distribution. Ancillary to this research was an accuracy assessment as a means of objectively assessing the utility of the two remotely sensed data sets used in the research.

Chapter 2. Literature Review

2.1 Disappearing Oysters

The dominant species of shellfish found along the eastern United States are *Crassostrea virginica* (Eastern Oyster) and *Mercenaria mercenaria* (northern quahogs). *C. virginica* is found predominantly within the intertidal zone of the South Atlantic and Gulf coast. They are ecologically and economically important suspension feeders that occur in estuaries from Nova Scotia to Florida and northern Gulf of Mexico. *Mercenaria campechiensis* (Southern quahogs) has a spatial range from New Jersey to Florida and along the northern Gulf of Mexico, (Grizzle, 1990) but today they are only found in the southern salt marshes.

The history of oysters and also its decline can be traced to the economic importance placed on the industry at the height of commercial harvest. The peak harvest years along the east coast of the United States was between the years 1880-1910 with 72.7 million kilograms of meat per year but declined to 18.3 million kilograms by 1995 (Coen, et al.1999b; 2000). The once highly productive areas of the Chesapeake Bay, Delaware Bay, and North Carolina were decimated and the industry collapsed. Many attributed the collapse of the industry to two principal diseases: *Haplosporidium nelsonii* (MSX) and *Perkinsus marinus* (Dermo) but recent studies cite other factors that have had a significant impact on the decline of shellfish such as habitat degradation (eutrophication), reduced water and habitat quality, natural and introduced predators and competitors, disturbance (boating, storm, dredging), shortages of oyster cultch, over-

harvesting, and interactions among these factors, (Coen and Luckenbach, 1999a; 2000: Smith and Greenhawk, 1998).

2.2 Oyster Reefs in an Ecological System

Coen et al., (1999a, 1999b, and 2000) believe that molluscan reefs are essential fish habitat and charges the Magnuson-Stevens Fishery Conservation and Management Act of 1996 as a legal basis for the protection, restoration, and enhancement of all "essential fish habitats" (EFH). An EFH is supported by the idea that oysters form a subtidal and intertidal structure in the estuary that supports a host of "fish" (fish is defined as crustaceans, mussels, finfish, and all other forms of marine life except mammals and birds).

Shellfish reefs are a community of organisms having multiple functions within an integrated ecological system. An understanding of the inter-relationships and functions of the various components of the shellfish reefs will not only sustain and enhance shellfish but will also lead to a greater understanding and better management practices of the macroinvertibrates, and fishes that are provided a habitat by the reefs. Small interstitial spaces between the shells serve as locations for settlement sites for spat growth and act as a shelter from predation for fish fry. The filtration capacity as contributing to the control of phytoplankton within the water column by dense molluscan communities has been well studied (Cloern 1982; Smaal and Haas 1997; Cohen et al. 1984; Roditi et al. 1996; and Dame et al. 1992 *in* Coen 1999). The ability to filter large amounts of water also helps to mitigate siltation of the water column. Breitburg (1999) defined three groups of finfish that that are ecologically associated with Chesapeake Bay oyster reefs; fish that are permanent residents of the reef; facultative residents; and transient residents

that use the reef to forage but are free ranging. Coen et al. (2000) lists many resident fish species, i.e. the oyster toadfish that use the reef microhabitats as nesting sites and as many as 79 species were found in a survey of reefs in Maryland, Virginia, North Carolina, South Carolina, and Texas. Sustainment of shellfish reefs are essential not only to the commercial and ecological value of the mollusks themselves but also the benefit of the commercial / recreational / ecological value of the finfish that utilize the reef as a habitat.

Currently in the literature there are three dominant approaches to management of shellfish resources; 1) to restrict the commercial/recreational use of the resource, 2) substrate or cultch addition, and 3) transplanting oysters. Hackney (2000) and Coen et al. (2000) recognized the need for an adaptive management approach that incorporates research with monitoring based information as inputs into restoration and management decisions. It allows for changes in restoration goals as the sites change with time. Monitoring as an approach was cited as a tool by Lyon (2001) for change detection of wetlands using aerial photography. An impediment to making specific goals for essential fish habitat is the lack of data on natural reef systems, (Coen et al. 1999 and 2000).

Uses of remote sensing with the marine or coastal resources have been historically limited. Applications of remote sensing of shellfish resources are scarce to virtually nonexistent. Grizzle (1990) details the use of aerial infrared photography for locating shellfish reefs and then conducting field surveys to determine the distribution of shellfish within a lagoon. Another use of remote sensing has been the use of side-scan sonar, acoustic sub-bottom profiling, and video equipment to access and chart the physical condition of the oyster habitat in Maryland's Chesapeake Bay (Smith and Greenhawk,

1998). Smith, Bruce and Roach (2001) also used side-scan sonar sub-bottom profiling systems, and acoustic seabed classification systems to access oyster habitat in the Chesapeake Bay with integration into a geographic information system. They found the side-scan sonar was superior at discernment of fine-scale bottom morphology, large object detection. The acoustic classification system was the best stand-alone technology for differentiating bottom composition, distribution, and quality of oyster habitat in sub-tidal environments.

2.3 Applications of Spectral Unmixing and Endmember Extraction

The goal of any remote sensing method is the ability to link remotely sensed data to the familiar frame of reference of the observer on the ground, (Adams, et al., 1993). The problem of classification becomes problematic when the spatial resolution becomes coarser than the objects being sensed. The result is a mixture of reflected energy by the constituents of a particular pixel. For hyperspectral imagery the problem becomes compounded further by the spatial autocorrelation of bands that contain similar information. To account quantitatively and qualitatively for the fractions of endmembers various methods have been developed that seek to extract the spectral signatures of materials within the pixel and then map the endmembers to produce an image of endmember probability. Depending on the type of mapping method employed the output also can contain either a root mean square image for error analysis or as in MTMF an infeasibility image is produced showing false-positive pixels.

Spectral mixture modeling is a technique for separating earth materials within a pixel into its constituent components by the use of endmembers which represent the spectral signatures of the cover type, (García-Haro et al., 1999). Endmembers are

recognizable features in a scene that are abstractions of objects regarded as having uniform properties that are meaningful to an observer (Strahler et al., 1986). The composition or number of endmembers may not be known so the problem is to decompose the mixture into constituent endmembers supported by the dimensionality of the data. Specular and diffuse reflectance from earth materials influence the delineation of the endmembers and contribute to noise in the modeling.

Generally, there are three methods described in the literature to deduce endmembers all of which have limitations. Bierwirth (1990) extracted endmembers directly from the image using the known spectral signatures of the dominant cover type. A second method uses principal component analysis (PCA) to enclose the pixel cloud within a solid geometric figure with the number of vertices equal to the dimensionality of the data (Garcia-Haro, et al. 1999). The preceding two methods assume that the spectral endmembers are contained within the dataset and are not realistic since most surfaces are not composed of homogenous materials. Endmembers not represented by the pixel composition are termed "external endmembers". Three other techniques based on endmember externality are the QMODEL, fuzzy algorithms, and parallel coordinate representation. These endmembers are derived from the relationship between samples located as vectors in principal component space (Garci′a-Haro et al., 1999). Johnson et al., (1985) uses an expert system to accept or reject imagery-derived endmembers by aligning reference endmembers against endmembers that are derived from imagery.

2.4 Selection of Endmembers:

The spectral mixing analysis method depends on the accuracy of the endmember selection. If the endmembers are incorrect then the probability scores are also incorrect.

An assumption of spectral mixture analysis is the linear mixing systematics where each pixel on the surface is a physical mixture of multiple components weighted by surface abundance and the spectrum of the mixture is a linear combination of the endmember reflectance spectra (Tompkins, 1997). The usual method for selecting endmembers is from an image cube "image endmembers" which best accounts for most of the spectral variance in a constrained least-square mixture model. These endmembers are then compared with "reference endmembers" which are field or laboratory generated spectra. Fraction images are the numeric abundance of the endmembers contained within the pixel. The advantage to having the fraction images is the relationship between physical processes and abundance of surface endmembers.

Tompkins et al. (1997) developed a method of selecting endmembers where ground truth was not available using a subjective and objective approach. The subjective approach is a statement of the subjectivity of *in situ* field measurements. For instance, the spectral endmember for a tree that is a percentage of a pixel is problematic when deciding how to represent all of the spectral variability such as leaves, bark, and shade. Which spectral profile best represents the tree? The other extreme is the objective approach for selection of endmembers using purely statistical methods such as principal component analysis (factor analysis) or convex hull geometry. Unlike the subjective approach, the objective approach assumes no *a priori* knowledge. Tompkins et al. (1997) combines the two approaches to find endmembers that were grounded in physical and spatial reality, (earth) but also are the best fit of the data cloud.

García-Haro et al. (1999) compared the constrained least squares method and factor analysis methods and found that both methods were able to estimate the fractional

abundance of the component mixture but the constrained least squares method had less biased estimates. They recommended that factor analysis is useful for finding the number and spectral signature of the endmembers.

2.5 Applications of Spectral Analysis:

In general terms hyperspectral remote sensing has application into seven broadl categories such as: rock and soil, vegetation, snow, ice, water, and atmosphere. Within the observed literature, most of the work being done using spectral mixture analysis has been in the area of vegetation, mineral, and soils mapping. Earlier use of hyperspectral imaging identified the unique contribution that can be made to vegetation mapping. Reflectance spectra in the 0.4 - 2.5μm region of the electromagnetic spectrum contain information on leaf cellular structure, leaf moisture content and plant pigment concentration (Jensen, 2005). This is used to assess vegetative health, chemical composition, and structure.

The use of spectral mixture analysis has not been limited to use in hyperspectral imagery but during the late 1980's through the 1995 most of the analysis using spectral mixture analysis has been done utilizing mutispectral platforms such as the Landsat Thematic Mapper. Applications using this platform include work done by Adams et al. (1995) and Garc′ia-Haro, et al. (1996 and 1999). Adams et al. (1995) classified multispectral imagery using fraction endmembers to detect land-cover change in the Brazilian Amazon. They used four reference endmember spectra: shade, green vegetation, nonphotosynthetic vegetation, and soil. They quickly recognized that reference endmembers could not account for the full natural variability of materials found on the ground which in turn affected the estimates of the fractions. What they were able

to provide with invariant endmembers was the consistent frame of reference for the four images. Using a four year TM sequence they found that endmember classification may be generally useful for comparing multispectral images in space and time and classification accuracy was improved for any one year by considering the multiyear context. Smith et al. (1992) used AVRIS and Landsat TM imagery to detect vegetation communities and changes in vegetation biomass using spectral mixture analysis. Using a range of vegetation communities, their study sites included a semiarid ecosystem in the Owens Valley, California and tropical rain forest in Manaus, Brazil. In the Owens Valley study using AVRIS imagery they identified two types of green vegetation and shade and two soil types. Using a Landsat TM image in the Manaus study they identified green vegetation and non-vegetated endmembers. The non-vegetated endmembers take into account the branches and stems exposed in the canopy as well as shade and soil. In both cases the *in situ* field measurements correlated well with the fraction maps. They cautioned that estimating biomass varied significantly with respect to the fraction maps at different times of the year.

The problem of endmember variability was also addressed by Bateson et al. (1996 and 1998). Their study was explicitly designed for hyperspectral imagery by first isolating the pure endmembers as seeds and then "grew" the spectra by including neighboring spectra. Criterion for inclusion was reflectance values are between 0 and 1 and they are sufficiently correlated (R = 0.99) to the seed endmember. They concluded that endmember bundles are a way of showing an understanding of the variability of endmembers and for quantifying uncertainty in fractional estimates.

Detection of seasonal changes in a semi-arid landscape using AVRIS data was studied by Yuhas et al. (1993), using convex geometry spectral unmixing techniques. They showed that seasonal changes can be detected both spatially and spectrally by the incorporation of the convex hull method. The convex-geometric unmixing utilizes the scatter points in spectral-space after a minimum noise transformation. The goal of the method is to geometrically determine the lowest dimensional subspace that the data spans, (Yuhas et al. 1993). A realized benefit of this method is the entire process is independent of user provided data when used in conjunction with the ATREM atmospheric correction model.

Most uses of spectral analysis are of the linear spectral mixture type. Linear spectral mixture analysis is best described as the modeling of each spectrum in a spectral dataset as a linear combination of a finite number of spectrally distinct signatures having fractional abundances between 0 and 1 and summing to one (Bateson and Curtiss, 1996). The use of linear mixture modeling was used by McGwire et al. (2000) to compare the differences between hyperspectral (Probe-1, Earth Search Sciences Inc) and multispectral (Analytical Spectral Devices, Inc from 0.4 – 2.5μm) instruments. They used the normalized difference vegetation index (NDVI), soil adjusted vegetation index (SAVI), and the modified soil adjusted vegetation index (MSVI) to test the relative ability of the hyperspectral and multispectral platforms to detect anthropogenic disturbance in an arid environment. Problems using traditional vegetation indices are pronounced in arid environments due to sparse vegetation and soil reflectance dominance. Vegetation cover for the study was calculated visually from the plot sites which were located in the Mojave National Preserve. Vegetation cover ranged from high (greater than 45%), medium (25-

31%), and low (12-16%). NDVI results from both the narrowband and broadband instruments were relatively similar, the SAVI performed worse than the NDVI and the MSVI did not show significantly better performance. The use of linear mixture analysis showed significantly better results, but when they incorporated multiple vegetation endmembers into the analysis they obtained significantly better results. The inclusion of multiple vegetation endmembers was determined after results indicated that a single plant species *Krameria erecta*, was strongly correlated with the residuals. This inclusion of more than a single endmember to represent endmember variability was consistent with studies by Adams et al. (1995), Garc′ia-Haro et al. (1996 and 1999), and Bateson et al. (1995) as discussed previously.

The use of multiple endmember spectral mixture analysis (MESMA) in an arid or semiarid environment does have practical limits when deriving the vegetation types using the MESMA method in an area that has less than 30% vegetation cover. Okin et al. (2000 and 2001) found that spectrally indeterminate vegetation types that are characterized by low spectral contrast are difficult to model even when species richness is high. The potential of unmixed spectra resembling an unknown material from the combination of soil and vegetation further confounds the ability of MESMA to retrieve accurate vegetation and soil types. The level of uncertainty only increases when the effects of nonlinear mixing are introduced.

Nonlinear mixing occurs when light is scattered by having multiple interactions with materials that are spatially close (Ray and Murray, 1996). Boardman and Kruse (1994) stated that linear mixing occurs in the instrument, but nonlinear mixing occurs in the material that is being sensed by the instrument. Ray and Murray (1996) are of the

opinion that shrub architecture plays an important role in nonlinear mixing and the error observed in linear mixing may be accounted for by the interaction of light and vegetation that has multiple endmembers.

Maas (1998) used Landsat TM imagery and linear spectral mixture analysis to estimate cotton canopy ground cover. In precision agriculture, remotely sensed parameters such as biomass, leaf area index, and plant canopy were correlated with empirical data and a mathematical curve was statistically fit to paired measurements. Problems were encountered due to the observations containing effects of factors specific to the place and time of the observations such as row spacing, plant height, soil color, texture, and shadows (Maas, 1998). Shadows affected scene reflectance which affected the independent variable (remotely sensed imagery) that was used to develop the empirical relationship with the dependent variable (cotton canopy). The result indicated that empirical relationships will differ from location to location under different times and conditions. To correct for the time and location Maas utilized a linear mixture modeling approach to calculate ground cover from scene reflectance in the red and near infrared wavelengths. Prior testing of the technique was done using ground based spectroradiometer measurements from different years and locations and aircraft observations (Maas, 2000). The study done in 2000 used a commercially available Landsat TM image in a continued validation of earlier findings. Conclusions suggested that observations in the red and near-infrared spectrum that were derived from Landsat TM imagery can be used to accurately estimate cotton canopy ground cover by compensating for shadows cast by the plants on the soil between rows. Maas' results concurred with earlier findings that estimates are independent of location and year and

were based solely on remote sensing observations without additional field information (Maas, 2000).

Peddle et al. (1999) used a combination of spectral mixture analysis and geometric-optical reflectance techniques to compare biophysical parameters derived from NDVI and MMR radiometer data from 31 stands of black spruce. The biophysical parameters they tested were net primary productivity (NPP), leaf area index (LAI), and solar zenith angle (SZA). Problems observed with NDVI derived biophysical parameters as previously reported by Peddle include data that is influenced by background soil, forest floor effects, canopy geometry, and leaf optical properties at subpixel scales (Peddle et al. 1999). Peddle et al. (1999) built upon the work by Hall (1995) by using component reflectances that were obtained by both a simple cylinder-based geometric-optical model and measurements used as inputs into the spectral mixture analysis. Peddle (1999) sought to validate Hall's earlier findings and improve upon earlier work by considering the importance of solar zenith angle variations for estimating component endmembers, a more sophisticated cone and spheroid representations of canopy geometry, and an independent method for determining the accuracy of pixel fractions on their overall approach. Using linear regression analysis of forest biophysical variables and detailed analysis using aerial photography to validate scene fractions, they concluded the spheroid model was more accurate than the cone and cylinder models for solar zenith angle corrections. Using the spheroid model, a solar zenith angel of 45^{o} proved to provide the best overall shadow fractions (canopy mutual shadowing). The spheroid model that was used to estimate the sunlit fraction proved to provide the most consistent

results. Over all, the method outlined above represent a substantial improvement over parameters derived from NDVI for all variables and at all solar zenith angles.

A novel approach in the use of MESMA has been the use of image fusion in conjunction with MESMA. Image fusion merges two images of differing spatial and spectral resolutions. The use of a high spectral resolution image allows for the identification of materials in the image using MESMA and high spatial resolution allows for locating the materials within the image. Gross and Schott (1998) explored the use of linear unmixing by first unmixing an image into its constituent fraction maps and then fusing with a high spatial resolution image. They were able to quantify their results by knowing and controlling the radiometric, geometric and spatial properties of the images through the use of Synthetic Image Generation (SIG) software. While there are many techniques for image fusion such as component substitution techniques, the goal here is not a review of the fusion techniques but an elucidation of the applications of spectral mixture analysis. In this particular study the authors used a nonlinear constrained optimization algorithm they developed to locate the endmember fractions at a higher degree of spatial resolution for fusing the two images. Their conclusions showed that using the synthetic image generation provided optimal conditions for the study and using the nonlinear constrained optimization technique they were able to quickly locate subpixel endmembers into higher spatial resolution. In cases where the materials have similar reflected radiances in the panchromatic band, the optimization technique returns fractions that are equal to the lower spatial resolution and no sharpening will occur without the introduction of further degradation. Robinson et al. (2000) built upon earlier work in image fusion by comparing three methods of image fusion and spectral

unmixing. They compared three methods of image fusion and unmixing: the first method fuses images and then unmixes them, the second, unmixes the image using an adaptive unmixing algorithm and the third option also unmixes and then fuses the images but use a traditional image wide unmixing method. The adaptive unmixing technique is a step-wise regression technique that adaptively selects a spatially varying set of endmembers and solves for the fractions of the selected endmembers within each pixel. The traditional unmixing approach assumes a fixed number of endmembers through out the entire image and attempts to find fractions for $K(x,y)$ endmembers in each pixel (Robinson et al. 2000). In areas with few materials present, the fractions may be overestimated and in areas where there are many materials (such as an urban landscape) endmembers maybe missed. This problem is the same as previously discussed with endmember variability in sparse landcover. The step-wise method requires, "that for each pixel, a library of endmembers be searched for the *n* members that are in that pixel. These endmembers are those that minimize the error without "overfitting" the sensor measurement" (Robinson et al. 2000). Regression mixing is based upon the ANOVA aspect of "Extra Sum of Squares" from Draper and Smith (1981). As in previous studies they were able to control for spatial, radiometric and geometric variables through the use of synthetic imaging software and then they verified their findings using a DAEDALUS multispectral image with 12 bands (they omitted the two thermal bands) and fused it with a synthetically derived image to insure that no artifacts were introduced during the parameter optimizations in the SIG processing. Their conclusions showed the step-wise unmixing was superior to traditional linear or multiple endmember mixture analysis. They based this on step-wise unmixing "always" producing lower squared error than the

traditional methods. Further, they stated that because traditional unmixing performed poorly, the majority of their work focused solely on the step-wise/fuse method to the fuse/unmix method. As to which method works better the authors couch their conclusions in the context as to the purpose of the work. If accuracy is desired then the step-wise unmix/fuse method is best but if visually enhanced fraction maps are the purpose then the fuse/unmix method should be the choice.

Depending on the purpose of the study many applications for ecological research do not need high spatial resolution. An ecological application using a simple linear mixture analysis was done by Sabol et al. (2002) to determine stages of regrowth in forested areas of the Pacific Northwest. Forested areas in different structural stages will have different ecological functions than areas of young or old growth. The ability to determine forest age using remote sensing is a benefit to ecologists studying forest function and age. In this study the authors used a four endmember constrained linear unmixing method and applied it to a Landsat TM image of the Gifford Pinochet National Forest. The endmembers represented the green vegetation, nonphotosyntethic vegetation, shade, and soil. Shadowing due to topographical effects was resolved by the use of a digital elevation model to remove the unresolved shadows from the imagery prior to mixture analysis. They were able to derive the age of forested areas through the use of a ratio between green vegetation and the shade and soil endmembers. Mature or climax forest will have a higher level of green vegetation relative to the other endmembers and conversely, a young forest in the early stages of regrowth will show a greater level of soil and non photosynthetic vegetation relative to green vegetation. Using field analysis of 495 forest stands they were able to access the accuracy and precision of the predicted

stand ages. They did caveat their findings with associated uncertainties when mapping stand characteristics. They use as an example the parameter stand age and discussed the source of uncertainties. As example they listed instrument and atmospheric effect, spectral variability of surface components, incomplete removal of topographic effects, variations in management practices to erroneous USFS data. They listed spectral variability as one of their uncertainties but as discussed above one wonders if the use of a single green vegetation endmember is sufficient to encapsulate the total spectral variability.

Spectral mixture analysis has been applied extensively in terrestrial applications and tested with synthesized spectra in the laboratory. Terrestrial applications include the ability to discriminate between vegetation, soils, and shade, García-Haro et al. (1999 and 1996), Huete (1986), Tomkins et al. (1996), and Adams et al. (1995).

A portion of the literature that was surveyed covered the geological biogeochemical uses of spectral unmixing most of which has its application in the development of the unmixing algorithms. Boardman and Kruse (1994) showed the utility of unraveling mixed pixels from AVRIS to separate spectral endmembers that show subtle differences between dolomite and calcite minerals without any *a priori* knowledge in the North Grapevine Mountains, Nevada. The North Grapevine Mountains in Nevada has been the site of extensive geological study using spectral mixture analysis.

The use of spectral mixture analysis to convolve a pixel into its constituent endmembers by the use of a reference library or through techniques that do not use any *a priori* information has its use primarily in the application of vegetation or mineral separation where endmembers are distinct. What are not discussed in the literature are

applications of this method in a coastal estuarine environment where the objects are assemblages of marine animals found in a variety of substrates.

Chapter 3. Methodology

3.1 Introduction

The field methodology portion identified 6 locations within the North Inlet-Winyah Bay National Estuarine Research Reserve that were partially representative of the spectral variability of shellfish spectral and strata characteristics. The objectives and treatments used in this research were;

- Treatment One: Create a spectral library to map spectral endmembers within remotely sensed imagery using the MTMF methodology.
- Treatment Two: Derive oyster spectral endmembers from remotely sensed imagery and map their distribution within the study areas using AISA and HyMAP imagery.
- Treatment Three: Compare classification accuracies between *in situ* and the two image derived spectral endmembers. Compare accuracies between AISA and HyMAP imagery.
- Treatment Four: Ascertain whether it is possible to distinguish spectrally or statistically between mud and oysters

The methodology that was implemented for the mapping portion of this research is shown in figure 3.1. Spectral characteristics of sites were obtained using a hand-held GER 1500 spectroradiometer (Geophysical and Environmental Research Corporation, Millbrook, NY) that had a calibrated spectral range from 350 nm – 1093 nm with 512 channels and a bandwidth 1.5 nm. Readings were gathered from selected field sites once

a month for the period July 2003 through July 2004. The objective was to obtain a record of the spectral variability of the shellfish strata during the sampling period under varying environmental and atmospheric conditions. The mean of apparent reflectance of the readings for a specific sample point and stratum by month constituted the spectral reference in the spectral reference library.

The two data sets of remotely sensed imagery used in this research differed greatly in both spectral and spatial attributes, the HyMAP imagery is considered a "true" hyperspectral image with 126 many narrow contiguous bands, spectral range from 0.439 – 2.488 μm and 4 X 4 spatial resolution. The AISA imagery has 7 bands with a spectral resolution of 0.498 – 0.819 μm and 0.5 X 0.5 meter spatial resolution.

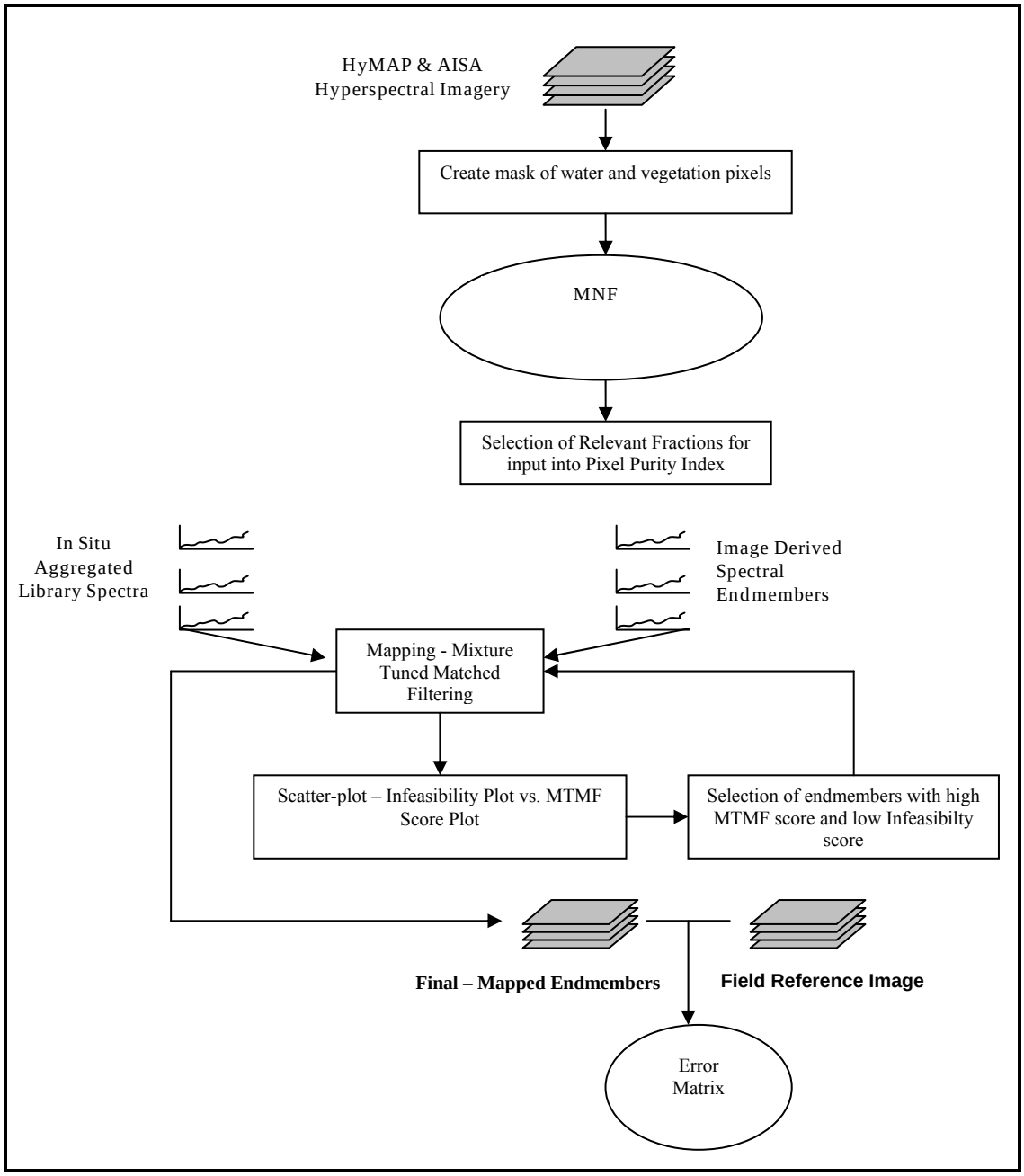

Figure 3.1 - Spectral Analysis Data Processing Flow Chart

3.2 Research Objectives and Hypothesis

With all the applications of MTMF occurring within terrestrial ecosystems there is a natural logical extension to applying this method to an estuarine ecosystem. The broad question concerning the use of MTMF is: can MTMF analysis be used in an

estuarine ecosystem? Is there a transferability of results and problems that are found in terrestrial applications the same as in an estuarine ecosystem? Are the confounding issues of MTMF analysis such as spectral endmember variability the same in an estuarine ecosystem as in a desert ecosystem? The background in an estuarine ecosystem is a soil/mud matrix, water, and vegetation. Healthy shellfish filter suspended material and mud from the water then deposit it on the shellfish reef. A problem in classifying shellfish is the very small size of the object being sensed and the confounding effect of shellfish covered in various degrees in the mud substrate. A narrower question in the application of MTMF analysis in an estuarine ecosystem is: Can shellfish be *quantitatively* remotely sensed and separated from the soil/mud matrix by MTMF analysis? The main objective of this research is to spectrally differentiate and separate the shellfish endmember from mud, vegetation and water endmembers for the purposes of classifying and mapping within a geographic information system. Additionally, If shellfish can be spectrally differentiated from the soil/mud matrix, can shellfish be further differentiated between live and dead (washed) shellfish?

3.2.1 Hypothesis

Null Hypothesis one H_o1: There is no difference between maps produced by either reference library spectra and derived endmembers through MTMF analysis.

Null hypothesis two H_o2: There is no spectral difference between live oysters and mud.

3.3 Study Area

North Inlet-Winyah Bay National Estuarine Research Reserve covers about 80 km^2 of barrier islands, low-lying coastal forests, and intertidal salt marsh near

Georgetown, South Carolina. It is an estuarine environment that is bordered on the east by the Atlantic Ocean and two rivers on the west-southwest: the Waccamaw and the Great Pee Dee that feed into Winyah Bay which is south of North Inlet. The 2,630 ha primary research area includes high salinity *Spartina alterniflora* marsh and 715 ha of tidal creeks with an average channel depth 3m, and a seasonal temperature range of 3-33^{o} C (Porter et al.1996). Land cover composition at mean tide is *Spartina alterniflora* marsh is 73.0%, tidal creeks 20.6%, oyster reefs 1.0%, and exposed mud flats 5.4%, (Porter et al. 1996). There were a total of nine named study sites located within the Jones Creek / Duck Creek (aka Bob's Garden) area and No Man Friend's Creek. The North Inlet sample sites are shown in figure 3.2. Each sample site had its location pinpointed using a Trimble XR Pro global positioning system with real time differential correction and was processed further using the Charleston, SC ground receiving station. Each sample site was identified by a four foot section of PVC pipe that was hammered into the oyster bank and given a unique identification code. Additionally figure 3.3 shows a photo essay of the sample sites and a sampling of the strata found.

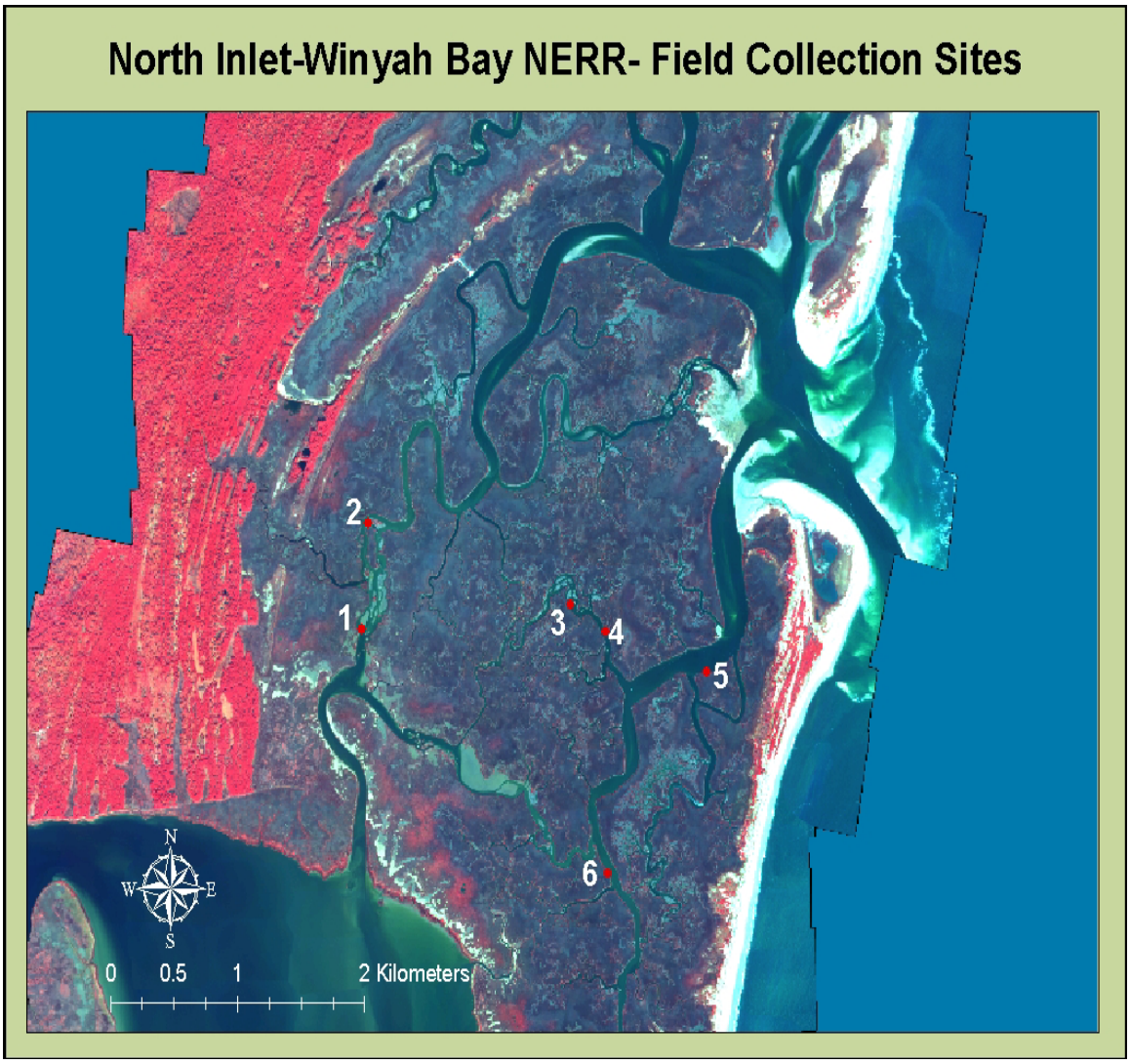

Figure 3.2 - North Inlet Study Area with Sample Site Locations

Number 1 in the above image shows the location of No Man's Friend 1 which was a patch reef that was approximately 4 meters wide by 10 meters in length and was primarily composed of shellfish and *Spartina alterniflora*. Number 2 was No Man's Friend 2 sample site which was representative of mud. The site was approximately 12 meters wide by 15 meters in length. Number 3 on the image was Bob's Garden sample site #4 which was a large patch reef that is approximately 70 meters long and 15 meters wide. Number 4 was a composite of three sample sites, Bob's Garden 1 through Bob's

Garden 3. These three sample points were composed entirely of shellfish with the patch reef measuring approximately 3 meters wide by 8 meters long. The geographic locations of Bob's Garden sample sites were located within Duck Creek. Number 5 was Jones Creek sample points 1 and 2 that measured roughly 2 meters wide and 15 meters long. These sample points were located on a narrow fringing reef that was composed of very few live shellfish. Number 6 in the above image was Jones Creek sample point #3 located on a narrow fringing reef like Jones Creek 1 and 2 but composed manly of dead washed shell. Washed shell is a nomenclature given to shell that has been exposed for an extended portion of time to the water and sun. Exposure to the elements has had a "bleaching" effect upon the shell thus giving it a "washed" appearance.

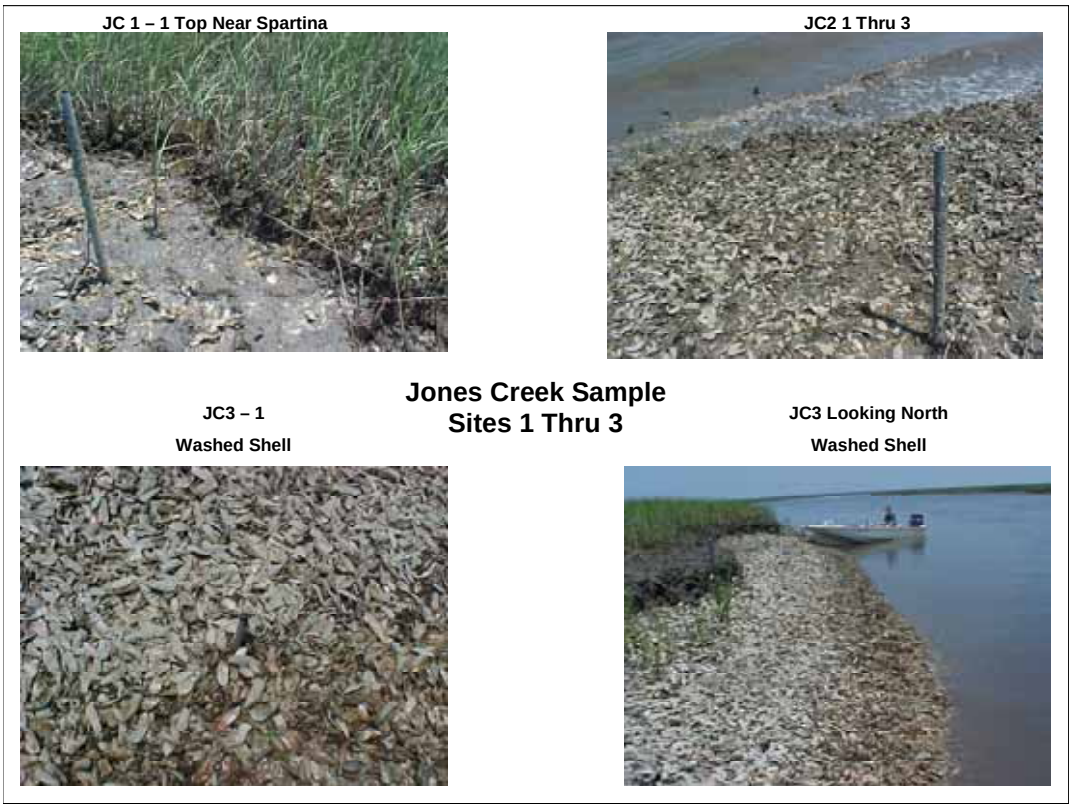

Figure 3.3 – North Inlet, South Carolina Sample *In Situ* Sample Sites

Figure 3.3 - Continued

Figure 3.3 - Continued

3.4 Selection of Appropriate Platform

The HyMAP image extent around the BOB4 sample site did not have the same extents as the AISA image sample area extents due to the spatial arrangement of the flight-lines. The HyMAP regions of interest were spatially subset from the larger HyMAP flight-line. The HyMAP image subset is 258 columns by 189 rows. HyMAP has 126 bands covering the spectral range from 452 nm to 2482 nm effectively covering from the visible (VIS) to the short wave infrared (SWIR) regions of the electromagnetic spectrum. The region of interest subset of the HyMAP image was spectrally subset into two regions of interest to ease computational loads and isolate more nuanced differences in spectral responses. Subset 1 (ROI_1_Bands2_44) and subset 2 (ROI_1_Bands45_126) include 452.9 nm to 1078.8 nm and 1.093.8 nm to 248.2 nm respectively. All bands were

used in the analysis with the exception of some water absorption bands that occur at bands 63-65 (1.4044 – 1.4328 nm), 94-97 (1.8034-1.9877 nm), and band 126 (2.4822 nm) due to a lack of image cohesion.

As with the AISA region of interest, a mask was constructed of the water and vegetation using the 2-dimensional feature space viewer. Both georectified flight lines of the HyMAP apparent reflectance images are shown in figure 3.4 and in figure 3.5 the region of interest subset with the masked subset. The masked subset was the same mask applied to the both the two spectral subsets, ROI_1_Bands2_44 and ROI_1_Bands45_126.

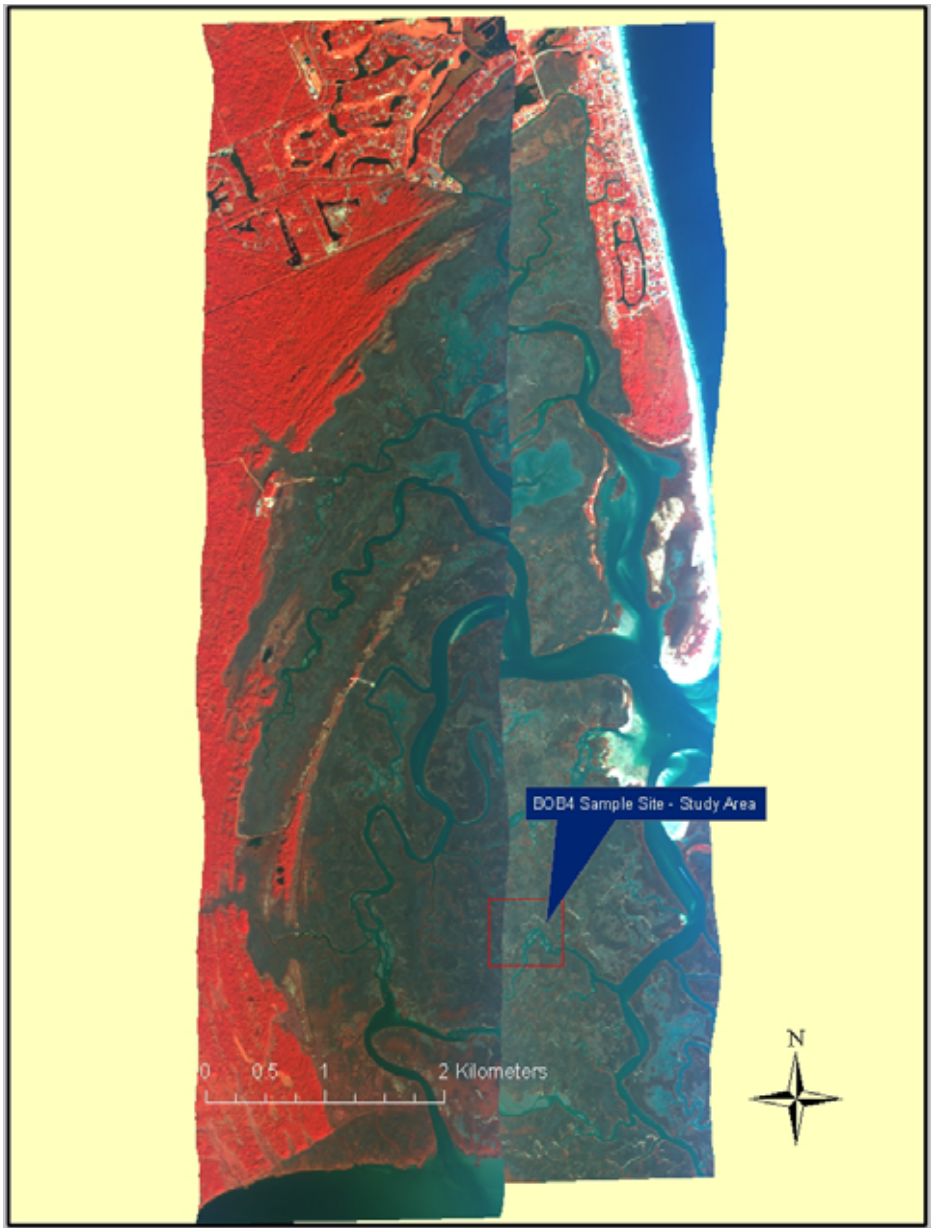

Figure 3.4 – HyMAP Image of North Inlet/Winyah Bay NERR, South Carolina

Both flight lines were atmospherically corrected using the ACORN (Atmospheric Correction Now) algorithm and georectified using the GLT (Geographic Look-Up Table) using the nearest neighbor approach that preserves the original pixel location. No color balancing was performed on the imagery or histogram normalization procedures to maintain the originality of the digital number values.

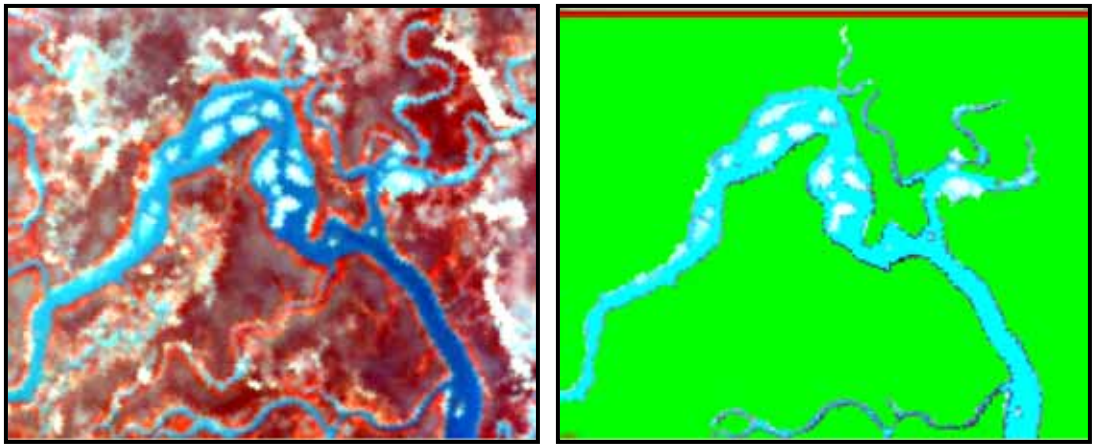

Figure 3.5 – HyMAP BOB 4 Study Area & Mask Image

As stated above the HyMAP imagery was initially subset into two subsets for ease of computation and to isolate any smaller variances in the mid-infra red region that would not be apparent if the visible region was analyzed in the same subset. An additional aspect is the subset of bands 2-44 is also the same spectral range of the hand-held GER field spectroradiometer. In order to map *in situ* derived endmembers the image subset had to match the spectral range as that of the *in situ* endmembers. The *in situ* spectral library endmembers were then convolved to match the spectral range of the HyMAP imagery and a minimum noise transformation performed for inclusion in mapping with the *in situ* endmembers.

HyMAP was one of the two principal sources of remotely sensed data was a rectified and radiometrically corrected HyMAP (Analytical Imaging and Geophysics, Boulder, CO.) image of North Inlet-Winyah Bay that was acquired at low tide in October of 2000. This HyMAP sensor is a "whisk broom" array with data acquisition at an altitude of 2100 meters and has 126 bands at a spatial resolution of 4 x 4 meters. The IFOV is 2.5 mr along track and 2.0 mr across track with a field-of-view of 61.3 degrees (512 pixels). This imagery was collected in support of an EPA-funded Coastal Intensive

Sampling Network (CISNet) project. The second data set is a rectified and geometrically-corrected AISA.

The AISA imagery used in this research has a spectral resolution of seven bands and a range of 498 nm – 819 nm. The spatial resolution is 0.5 X 0.5 meters which is adequate for visual identification of shellfish aggregates on patch reefs but are more difficult for visual identification of fringing reef structures. The imagery was acquired by the Center for Advanced Land Management Information Technology (CALMIT) using the AISA sensor (Specim Corporation). The AISA Plus sensor that was used for the North Inlet-Winyah Bay NERR over-flight has seven bands between 498 and 819 nanometers and a spatial resolution of 0.5 X 0.5 meters. This sensor has a push broom configuration with a narrow spectral resolution, configurable number of narrow spectral bands (~6 nm wide).

Spectral analysis was done using the photogrametric and remote sensing software, The Environment for Visualizing Images (ENVI) versions 3.5, SP1 and 4.1, by Research Systems Incorporated, of Boulder, CO.

Before treatments of the AISA or HyMAP imagery could be initiated, a mask of the study area was constructed. Figure 3.6 shows the AISA image of the BOB4 study site showing bands 6, 4, and 2 (RGB). This study site was selected due to its large patch reef with a variety of shellfish strata types present both on the reef and on patch reefs surrounding the study site. The mask in effect negates pixels of water and vegetation for the Mininum Noise Transformation and subsequent analysis. Using the 2-dimensional feature space viewer using ENVI, clusters of water and vegetation were classified and

used in construction of the mask. Pixels not classified using the above method were hand-selected and classed.

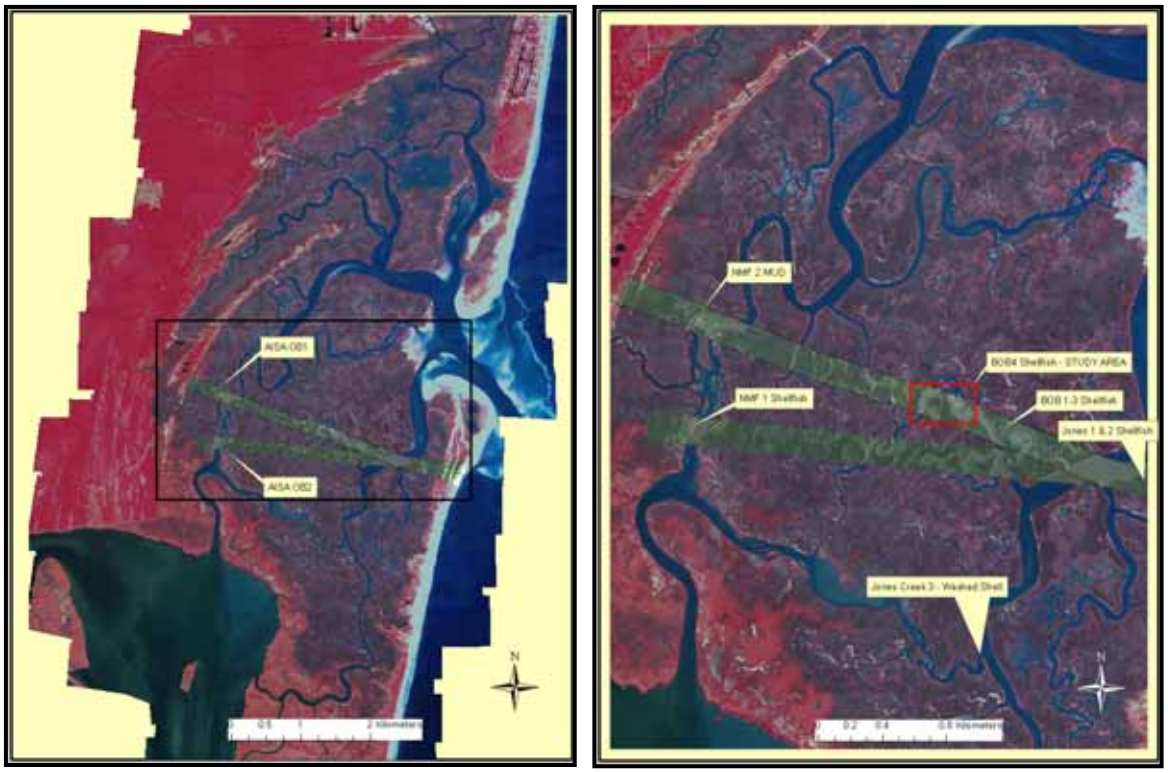

Figure 3.6 - AISA Flight Lines and Image Subset in North Inlet, South Carolina

Figure 3.7 shows the BOB4 study site of the AISA image while the second image shows the mask that was constructed and utilized for the Minimum Noise Transformation.

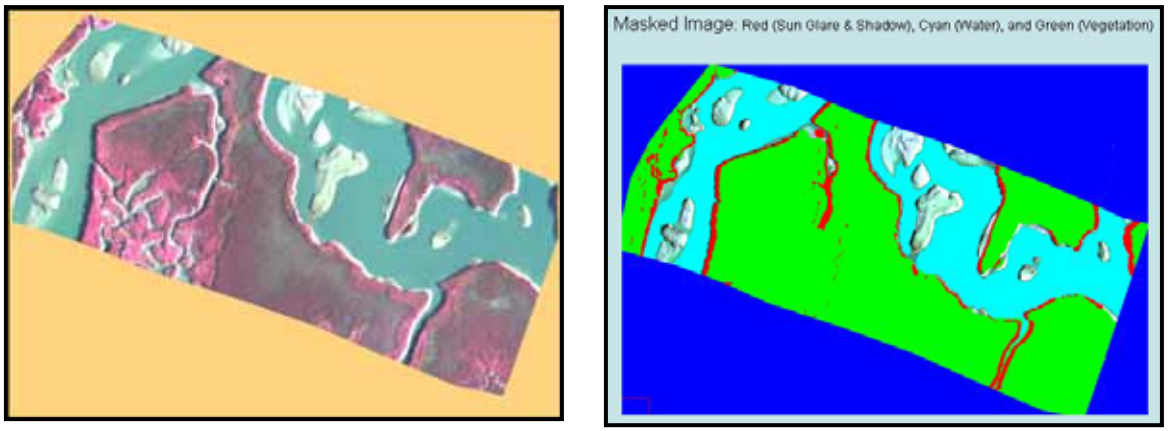

Figure 3.7 – AISA Image Study Site & Mask

The mask was constructed using the feature space viewer within ENVI where larger groups of dense pixels or classes of pixels can be isolated and marked for masking. In Figure 3.7 the three different classes of pixels that were isolated are vegetation, water and sun glint and shadow. The sun glint and shadow is an artifact within the data and not representative of the earth materials typically found in these areas. This issue is explored in more detail in the Discussion section of this report.

3.5 Radiometric and geometric correction

The HyMap data set required no instrument radiometric correction as evidence in a Fast Forward Fourier Transform performed in ENVI. Atmospheric correction of the HYMap data set was accomplished using the radiative transfer model algorithm Atmospheric Correction Now (ACORN) prior to spectral analysis. Prior to spectral analysis, all derived images were geometrically corrected using the georeference from input geometry files that are supplied in the HyMap dataset. Using the Input Geometry file (IGM) that is supplied with the HyMap Dataset, a super Geographic Look-up Table (GLT) is derived. The IGM file contains the geolocation information for each original raw pixel. The derived images are then georeferenced using the super Geographic Look-up Table. A HyMap image that is not spectrally unmixed will be geometrically corrected

and the two flight lines will be joined in a mosaic to produce a geometrically corrected reference image to use in image-to-image geometric correction.

The AISA image was atmospherically corrected using a proprietary algorithm that is similar to an atmospheric radiative transfer model. Down-welling irradiance information and atmospheric information was collected at the time of image acquisition with image georectification and atmospheric correction being accomplished in near real-time. Both the AISA image and HyMAP images were tested for geolocational accuracy with the use of ground control points within the study areas. Global positioning system ground control points were collected during the field portion of the research and compared visually within each of the two images. The HyMAP image incurred the greatest geopositional inaccuracy of approximately 3-5 meters. While the AISA image had approximately 1 - 2 meter geopositional accuracy. These measurements are only approximations due to a level of uncertainly associated with measuring GPS points to a known location within the study area.

3.6 In-Situ Field Sampling and Spectral Library Creation

3.6.1 Sample Site Delineation

The study sites were delineated for the gathering spectral signatures of shellfish for a wide range of environmental conditions. Figure 3.8 shows the location of each of the sample sites and the approximate location of each sampling point within the sample site and Table 3.1 lists the field study sites that were identified by their strata for spectral observations. Conditions such as: abundance of shellfish, positions, (vertical and horizontal), and environmental condition, (wet/dry, various amount of mud present, algae, and detritus). Site characterization of the oyster reefs were delimited using

definitions from the Shellfish Management section of the South Carolina Department of Natural Resource's Intertidal Oyster Survey Field Data Sheet codes. The Oyster Survey describes the reef strata with respect to bushels of live oysters per acre, presence or absence of vertical clusters, proportion of live oysters to shells and amount of mud

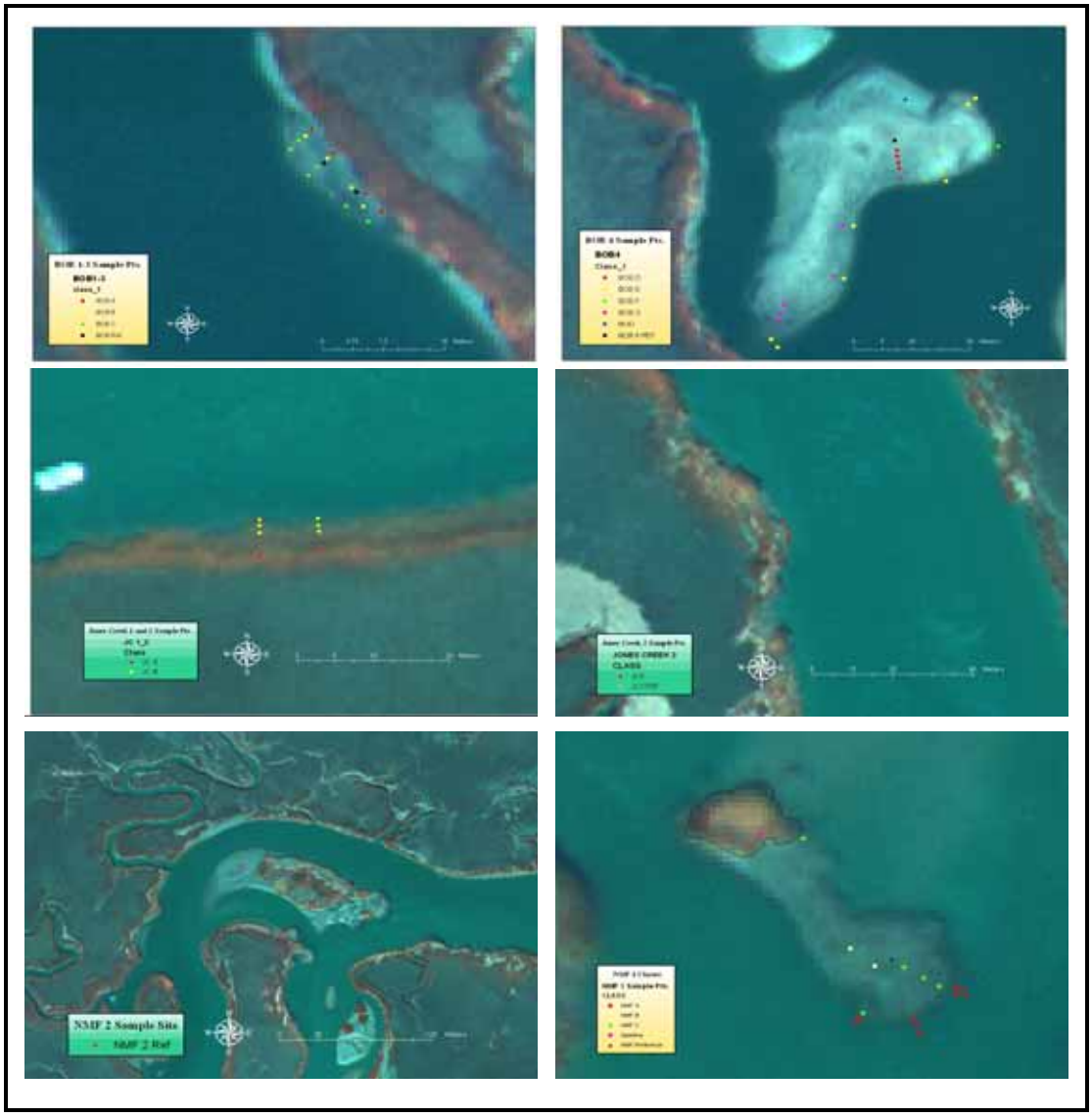

present. Each of the 10 listed strata or classifications are identified by a letter code. Appendix 7.1 includes a description of the Intertidal Oyster Strata descriptions and their letter designations.

Figure 3.8 – Sample Sites in North Inlet / Winyah Bay NERR, South Carolina

Each sampling point was aggregated into like shellfish classes. For each month the triplicates for each sampling point and for each shellfish class was averaged to obtain spectral curves for twenty classes.

3.6.2 *In-Situ* Endmember Collection and Spectral Library Creation

The nine identified sampling locations exhibited a variety of mixed strata's within the sample sites, clusters of shellfish that were representative of relatively homogenous strata were identified and demarcated. Transects were demarcated to represent vertical relief of the sampling reef from the waters edge, (below mean low tide) to the top of the oyster bank. No Man's Friend 1, Bob Creek 4, and Jones Creek 3 sample points have a GPS point and distance measurement from the reference post to the sample point and demarcated using lengths of small diameter PVC pipe that has been placed into the reef. Bob Creek 1 through 3 and Jones Creek 1 and 2, have their sample point distance measured only relative to the reference post. This was due to the relatively short distance to the reference post within a smaller sampling area. The triplicates were averaged and converted to reflectance to obtain a single spectral curve for each sample point.

Sampling points or clusters were classified according to South Carolina Department of Natural Resources Field Data codes for Intertidal Oysters. There was some subjectivity in assigning strata to the DNR classifications, but the intent was to use the DNR classification as a means to describe and differentiate between groups of shellfish.

All spectroradiometer measurements were taken using the GER 1500 spectrometer held to a height at ~1.5 meters above the sample point. This height resulted in an IFOV of ~ 1 inch square. The washed shellfish at the Jones Creek #3 sample site

was read when dry and then again read wet. This was to document any changes in the spectral reflectance due to the presence of water. Relative terms were used to describe the wet/dry conditions included; dry (maximum dryness of the tidal cycle), semi-dry (more dry than wet), semi-wet (more wet than dry), and wet (wet shellfish and pooling of water interstitially). Notes included descriptions of the amount of mud encrusting (heavy/medium/light/none), and any noted detritus, such as seaweed, leaves, grasses, etc. All spectroradiometer readings, descriptions, measurements, and records were documented in a bound field notebook and sampling points were digitally photo documented. Endmembers of water, mud, vegetated areas such as *Spartina alterniflora*, and the concrete pad near Clambank Landing were used as controls.

As illustrated in Figure 3.9, monthly spectroradiometer files were organized according to strata and condition (wet or dry). The files were then converted from an Excel spreadsheet format to ASCII text file for importing into ENVI's Spectral Library. All monthly ASCII exported files for each stratum were aggregated into a single folder. At the end of the sampling period, each strata folder contained all spectroradiometer readings converted to reflectance. The spectroradiometer values were averaged into a single spectral reflectance curve for each stratum. Appendix II contains sampling dates from June 2002 through July of 2003.

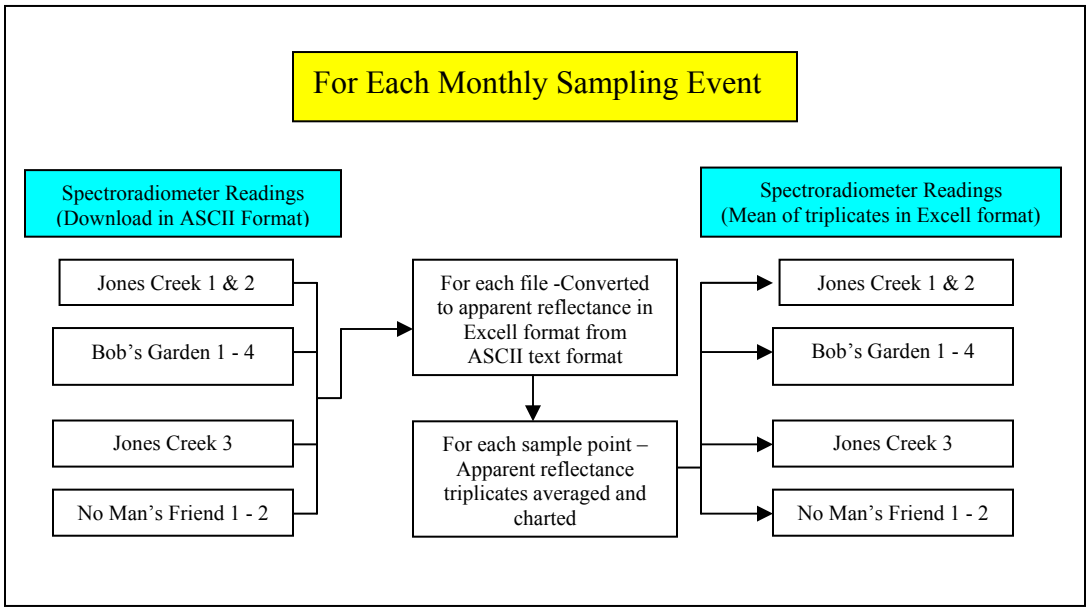

Figure 3.9 – Aggregation of Spectral Files

Primary aggregation was the importation of each spectral file into Microsoft Excel, conversion from radiance to reflectance, the averaging of the triplicates for an average signature of a particular sample point, and charting of the individual reflectance and average signatures. The file structure was organized in Excel by month with the raw data, radiance and averaged triplicates in reflectance. Further aggregation was necessary to have each strata represented and reduce the number of individual spectral signatures for mapping.

As shown above in Figure 3.9 the individual sample points were further aggregated by averaging all the individual reflectance signatures for a given area to create an averaged reflectance across a larger spatial extent with similar strata. Each sampling point had a spectral reference signature recorded to calculated reflectance so it was not possible to average individual radiance signatures and process into reflectance. Appendix 7.3 explains which individual sample points were aggregated into secondary groupings.

From Appendix 7.3, BOB A through C was comprised from BOB 1 through 3 sample sites. These sample points were located within the same geographic proximity and were differentiated by strata that corresponded with the vertical rise of the reef. Another aggregation from the averaged triplicates was the aggregation by sample site showing all twelve months of spectral signatures. This is useful for visual discrimination for annual phenological changes that may occur within the sample points. A good example of this was BOB4_12 which is characterized by washed bright shell but during the winter months there is a preponderance of macro-algae growth that partially obfuscates the washed shell. Another use of this type of aggregation was any noted spectral changes with the concrete pad. It is noted that the acquisition of spectral signatures were taken at precisely the same point on the concrete pad that is used as a de-facto control but shows slight variations in the spectral response due to slight variations in the concrete pad. Figure 3.10 shows this graphically with the triplicate averaged spectral signatures for all months. Additionally the spectral files were averaged into a single monthly averaged spectral curve for each sample site to look for changes throughout the year for each sample site. Figure 3.11 shows a comparison of BOB4_13 and NMF2 (mud) with BOB4_15, BOB4_2, and NMF1_11 shellfish (both wet and dry separate curves). This graph also shows and visual differences between shellfish and mud.

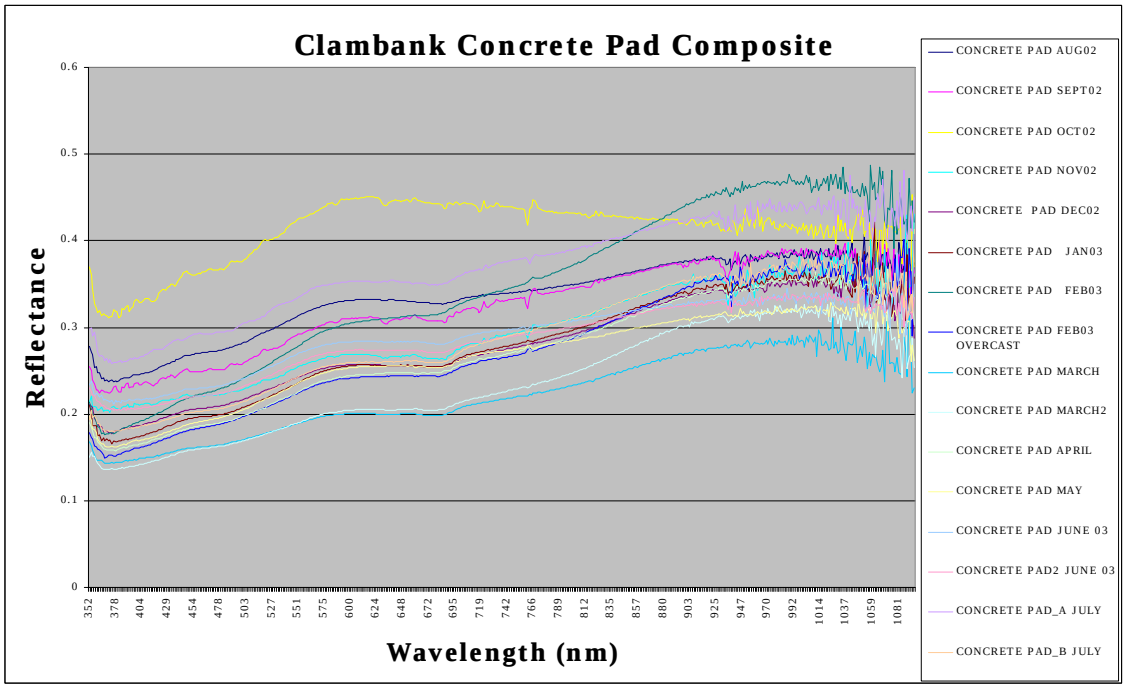

Figure 3.10 – Clambank Concrete Pad Composite

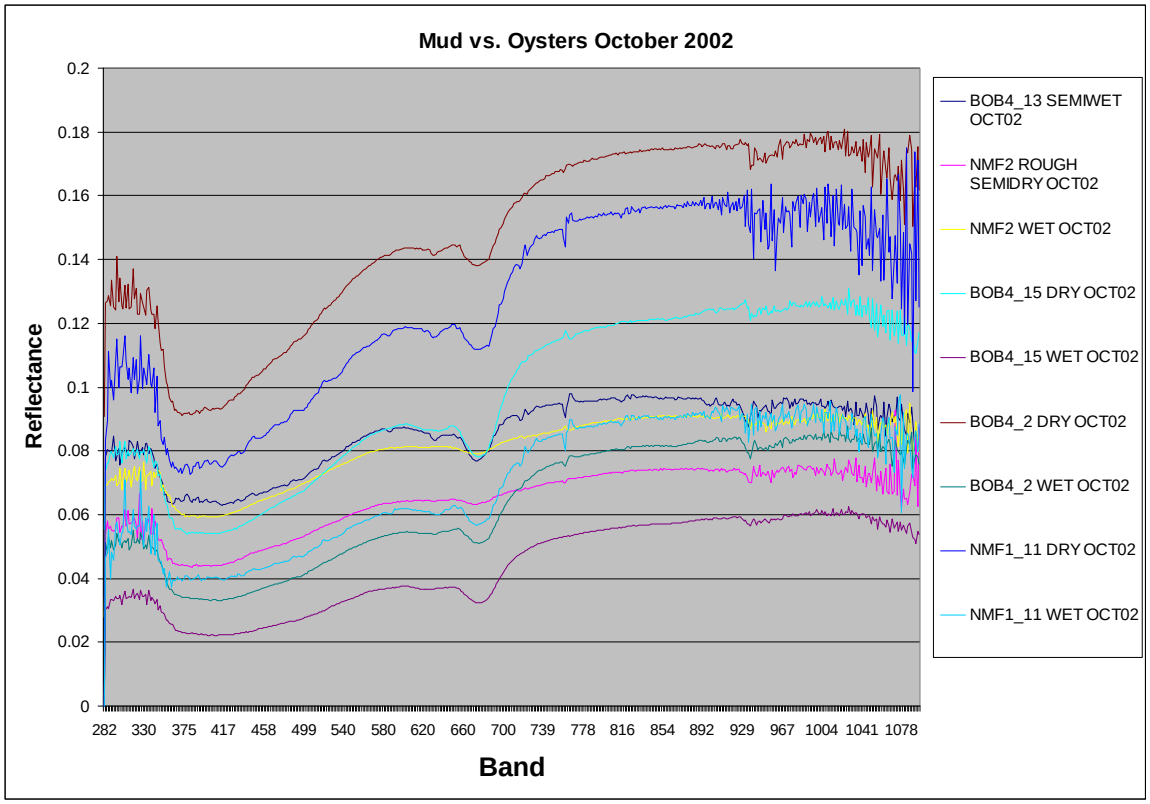

Figure 3.11 – Time Composite Comparison of Mud and Shellfish

3.7 Statistical Analysis

Statistical analysis design involved the analysis of the spectral signatures from the year-long *in situ* sampling that resulted in the creation of a spectral library and spectral image endmembers that were derived from the HyMAP imagery. The HyMAP imagery was the imagery of choice for statistical analysis owing to the greater number of contiguous bands (126 bands from ~450- 2400 nm) and narrower band widths than the AISA (7 bands from 498 nm – 819 nm). Pixels were delineated that correspond with areas where the *in situ* spectral signatures were collected as part of the annual field collection regimen. Selected pixels were analyzed individually and averaged spectral signatures to represent the aggregated spectral and spatial characteristics of the *in situ* endmembers.

The objectives of the statistical analysis were:

- Objective One: With regard to *in situ* sample points, such as BOB4_1, there were three spectral readings taken at slightly different points around the sample point. If the earth material (shellfish) present within the sample point is considered to be of similar shellfish strata, how similar or different statistically are the three spectral readings? Does the type of oyster strata or material such as mud or the concrete pad make a statistical difference in the spectral signature of the triplicates?
- Objective Two: The sample points were aggregated by similar strata in larger areal spectral representations by averaging the individual spectral reflectance signatures but how different are the sample points that were aggregated together,

i.e. does the average of triplicates from BOB4_1 differ from the average of the triplicates from BOB4_2?

- Objective Three: With a sampling of pixels from the HyMAP imagery from locations of the in situ sampling as described above, do the spectral signatures from the HyMAP imagery differ from the *in situ* spectral signatures?

The process of selecting image endmembers is done through the Pixel Purity Index and the N-Dimensional Visualizer by a trial and error process of selection and aggregation of individual endmembers. The criterion for merging endmembers into "bundles" that represent the spectral variability of the earth material of interest is by implementing the Jeffries-Matusita Transformed Divergence algorithm. Transformed Divergence is computed using the mean and covariance matrices from the imagery and measures the degree of divergence or separability of two classes (Jensen, 2005). This technique works well with endmembers derived from the imagery using the above process but this algorithm cannot be used on *in situ* endmembers independent of the imagery. Thus there was not parity in the research design when comparing imagery spectra that was derived using the above method with *in situ* spectra. As a compromise, image endmembers utilized for the MTMF mapping were exported as ASCII text and analyzed using the non-parametric Wilcoxon Signed-Rank test.

The Wilcoxon Signed-Rank test is the non-parametric version of the paired t-test that tests whether the median for a data set has a particular value. Using the two-sided or signed rank of the Wilcoxon test has the ability to test a null hypothesis that the two variables have equal centers of symmetry. It does not assume the distribution is Gaussian

in nature. The Wilcoxon Signed Rank test was used for the last objective as described above.

Although ANOVA is usually used with normally distributed data, we used ANOVA 2-Factor analysis to test the hypothesis of no difference between triplicates of *in situ* samples taken in three different spots at a single sample point, i.e. BOB4_1 triplicates (objective one from above). The ANOVA 2-Factor test was used for the first two statistical analysis objectives.

For this portion of the research we did not examine all sample point triplicates, or all possible combinations of aggregated *in situ* data to determine differences or similarities between aggregated *in situ* or image endmembers. Given time constraints it was decided to use a small group of *in situ* sample of data points within the BOB4 sample area, the No Man's Friend Sample sites and final image endmembers from the HyMAP imagery. In comparing the HyMAP image endmembers with the in situ endmembers it should be noted that comparisons were done with *in situ* data that were convolved to match the HyMAP imagery and the HyMAP imagery was subset to reflect the spectral range of the *in situ* data. This aspect of the research while intriguing is not central to the purpose and intent of the research but should be the subject of future research using an intense and rigorous statistical analysis.

The ANOVA 2-Factor analysis of triplicates found results that were consistent with the type of material being analyzed. Triplicates from more homogeneous materials tended to have less overall variance. Mud from No Man's Friend 2, and bright sand from the beach fronting the ocean were some of the materials that exhibited the least amount of overall variance. Conversely, variance was greatest with materials that exhibited the

greatest heterogeneity such as live, vertical, densely clustered oysters on the west side of BOB4. Principally BOB4 sample points 14 through 16 and 19 through 22. Oyster strata such as "D", "B" or "F" stratums had mixed results for variances between triplicates.

Analyzing regions of the electromagnetic spectrum individually (blue, green, red and shortwave infrared regions) between triplicates resulted with the smallest variances in the blue, green and red regions and the greatest variances found further out in the short wave infrared regions. Analysis of the spectral regions was carried out on BOB4_1 through BOB4_4 sampling points and is representative of "D" oyster strata. These findings may not reflect results from more or less homogenous oyster strata.

Using the Wilcoxon test it was found that the averages of triplicates are significantly different than the averages from another sample point within the same oyster strata. This analysis was performed between BOB4_1 and BOB4_2. In addition, averaged image spectral signatures were statistically different than averaged *in situ* spectral endmembers for the same area of BOB 4 sample site. This is significant because when mapping shellfish reefs using *in situ* derived endmembers, lower mapping accuracies have been reported than when image derived endmembers are used (Elmore, et al., 2000).

3.8 Remote Sensing Spectral Analysis

The methodology of this research utilized spectral endmembers derived from remotely sensed imagery and *in situ* data collection of spectral signatures of shellfish strata. Imagery was radiometrically and geometrically corrected to insure accurate GPS location and pixel registration agreement. The imagery was spatially subset into Regions of Interest, (ROI's) to ease computation and memory burdens. The use of the MTMF

methodology was first used to map shellfish distributions using image derived spectral endmembers. The steps taken were to place the data in minimum Noise Transformed (MNF) space, create a Pixel Purity Index (PPI), define extreme endmembers using the n-Dimensional Visualizer, and then the refined endmembers were mapped using the MTMF methodology. *In Situ* data was convolved to match a specific imagery data set then placed into MNF space for mapping using the MTMF method.

Mapping shellfish resources using *in situ* derived endmembers first required a decision regarding the level of aggregation of the *in situ* spectroradiometer signatures that would best yield a spectral signature as found at the same scale within the imagery. This is a very small area of interest and consequently the second level of aggregation as described above was used as inputs for spectral unmixing. The second level of aggregation of the *in situ* spectral endmembers was aggregated to represent the same patch type of shellfish aggregation and health. The *in situ* spectral reflectance sampling points that fell within an area of similar shellfish groups such as the SCDNR strata representations of "F" or "F1" were averaged. These averaged spectral signatures convolved to match the AISA wavelength as described above and then a minimum noise transformation was applied to the spectra. They were then saved as a spectral library within the ENVI software to be utilized as inputs for mapping using the MTMF methodology. The AISA and HyMAP imagery was treated as shown in figure 3.12 showing the steps that were used in the spectral analysis process as described in the ENVI User's Manual.

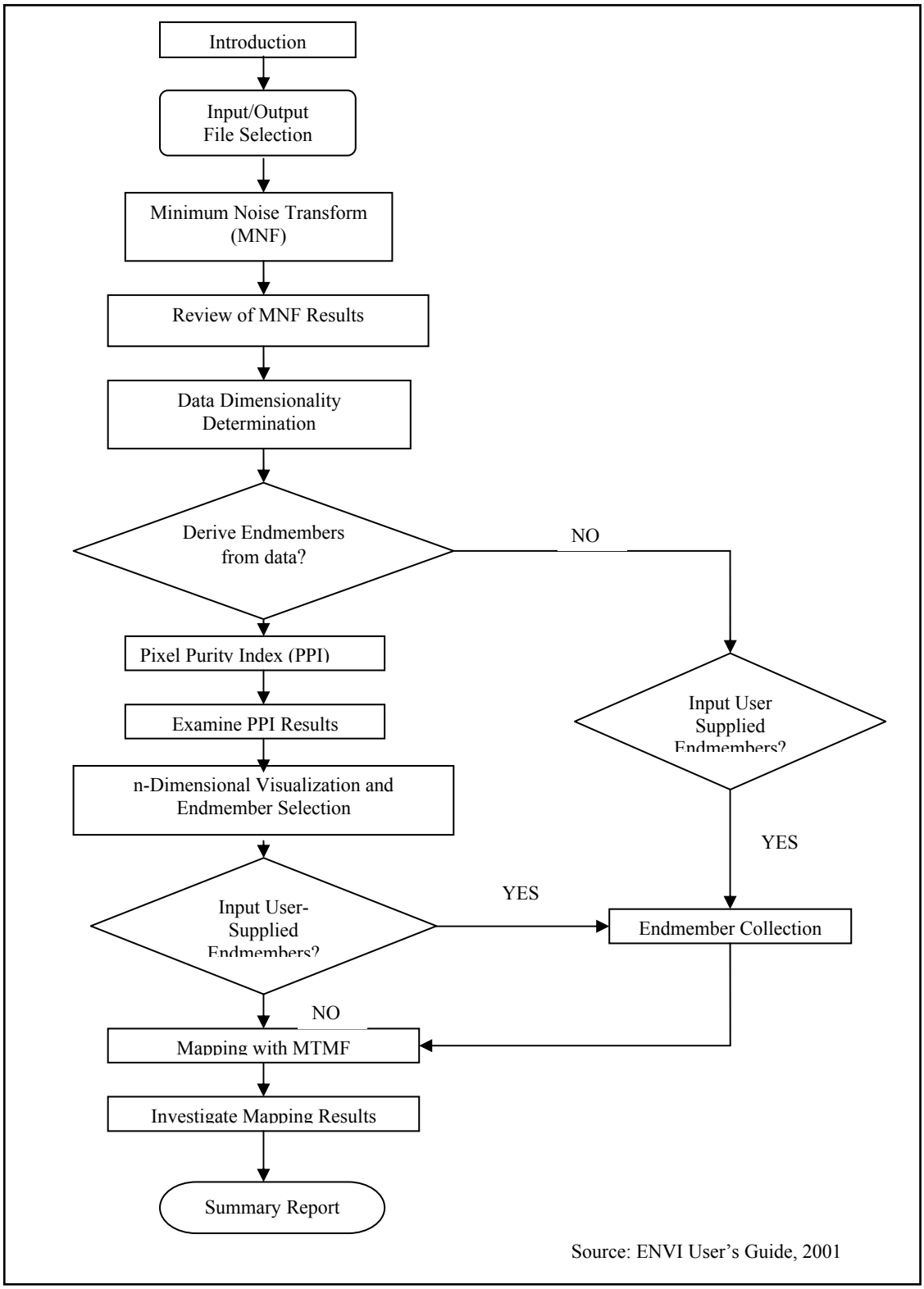

Figure 3.12 – Spectral Analysis of Remotely Sensed Imagery

3.8.1 Minimum Noise Transformation (MNT)

The first treatment of the imagery was the elimination of any earth materials of non-interest such as water and vegetation within the region of interest. All shellfish to be mapped were assumed to be near the waters edge or reposing on the patch reef. We were interested only in patch or fringing reef structures. The process of masking was carried out by using the 2-dimensional feature space viewer within the ENVI software. The 2-dimensional feature space viewer places the pixel values of one band on the axis of a scatter-plot and another band on the opposing axis. Usually the bands chosen have one band that characterize the material of interest, such as a band in the near infrared for vegetation and another band to act as contrast. The resulting "shape" of the data cloud is then density sliced to show higher areas of denser pixels. These areas are synonymous with a material within the imagery. When selected, the pixels are colored within the scatter-plot and appear within the imagery as colored pixels. In this way materials of interest within a scene were selected and placed into a class. Once all the pixels of unwanted materials were selected, a masking band was created from the selected pixels which were applied during the Minimum Noise Transformation process.

The next treatment was the reduction of the spectral dimensionality of the imagery. Hyperspectral imagery is usually defined as having many contiguous spectral bands (Jensen, 2001). Many of these bands contain redundant information and the Minimum Noise Fraction Transform (MNF Rotation) is designed to eliminate redundancy and segregate any noise in the image (Boardman and Kruse, 1994). This is a process with two cascaded Principal Component transformations. The first Principal Component transformation is based upon the estimated noise covariance matrix which

then decorrelates and scales the noise within the data resulting in no band-to-band correlations and the noise has unit variance. The second stage takes the noise-whitened data and performs basic Principal Component transformation. For further spectral processing the associated images (often called in this report eigenimages) and the eigenvalues (or eigenvectors). There was a parsing of the images and statistics into two groups; those with the highest eigenvalues and coherent eigenimages and those composed of the lower eigenvalues (with near-unity values) and eigenimages that were noise-dominated. By selecting the eigenimages that have the highest eigenvalues and thus the most variance the image dimensionality was reduced to the bands with the most information for further processing.

3.8.2 Pixel Purity Index (PPI) and the n-Dimensional Visualizer

The third treatment relates to the input of either in situ endmembers that have also been transformed via the above process or endmembers of interest can be derived from the imagery itself through a process known as the Pixel Purity Index (PPI). The Pixel Purity Index was used to find the most spectrally pure pixels or extreme pixels. They are extreme in the sense that they are on the furthest edges of the pixel data cloud. The PPI is computed by repeatedly projecting n-dimensional scatter-plots onto a random unit vector (ENVI User's Guide, 2005). Pixels at the end of the unit vector are counted as extreme and the pixels are then indexed as to the number of times they are marked as extreme. The output is a single band image with pixel brightness denoted as the count or number of times it was marked as extreme. Parameters the user can set are the threshold factor setting that determines the threshold for extreme pixels. A threshold factor setting of 5 marks all pixels at the end of a vector extreme that are within five digital numbers (high

and low) of the extreme pixels as extreme. The higher the setting, more pixels will be counted as extreme but are less likely to be spectrally pure. The other parameter that is set is the number of iterations that the algorithm will run. To know when all extreme pixels have been found and marked, a graph is displayed showing the number of iterations (x-axis) and the number of pixels marked as extreme (y-axis). When the curve flattens out at the top for a number of iterations then it is safe to assume that most of the significant extreme pixels have been marked and indexed.

If *in situ* endmembers were used to map an earth material, then the pixel purity index process was not needed. To utilize *in situ* endmembers as input for mapping they must be in the same Minimum Noise Factor transformed space as the image and placed into the ENVI spectral library for use in the MTMF algorithm.

The next treatment is the visualization of the PPI in n-dimensional space. This allows the user to view and refine the number of endmembers in multiple dimensions of space to visualize the PPI data cloud from as many different angles as necessary to select the most spectrally pure endmembers. The user then has the options of exporting the endmembers to view the pixels within the image in geographic space and saving the bundles or collections of endmembers that represent a single class of earth material. Endmembers that are exported for viewing within the imagery are treated as roi's (regions of interest) which can then be tested statistically using the Jeffries-Matusita Transformed Divergence test for endmember separability. Endmembers that are statistically similar can then be merged together into a single class. The selection and refinement of endmembers presents one of the most subjective portions of spectral analysis. The inclusion or exclusion of endmembers within a class is most problematical

when trying to gather endmembers that represent the spectral variability of the earth material within the image.

3.8.3 Mixture Tuned Matched Filtering

The last treatment is the mapping of the endmembers using one of the available mapping algorithms. The two algorithms that were considered for mapping in this research are Linear Spectral Unmixing, which was originally proposed and MTMF, which was the method chosen for this research. MTMF was chosen over Linear Spectral Unmixing because in Linear Spectral Unmixing all endmembers contained within the image must be derived. With both Linear Spectral Unmixing and MTMF there is an inherent limitation in the number of endmembers that can be mapped, there can only be n-1 endmembers mapped, where n is the number of eigenimages used in the analysis. A limitation of the method becomes apparent when the image may contain more endmembers than there are available eigenimages. Since the object of the research is to map shellfish and not water or vegetation, it makes sense to mask these elements and not include them in the analysis. Additionally, when the Minimum Noise Fraction transformation is ran on the image, the vegetation and water will usually encompass the majority of the variance within the image and variances between mud and shellfish are much smaller by comparison. Thus when the eigenvalues are calculated the higher values will be for the water and vegetation with the smaller eigenvalues relegated to mud and shellfish, which may be lost within the noise dominated (near unity variance) eigenimages. MTMF is also called partial-unmixing because it looks just for the endmembers of interest while suppressing the remaining spectral signatures as background noise.

The results from MTMF include two gray-scaled images for each mapped endmember. The first is the MTMF Score image that shows the relative degree of match to the reference endmember scored from just above zero to one being a perfect match. Pixels mapped just around zero are background pixels that were suppressed. It is common to stretch the values in the right hand side of the histogram from just above zero to one to show pixels that are mapped correctly. The second gray-scaled image is the infeasibility image that shows values in noise-sigma units to indicate the feasibility result. Figure 3.13 shows a diagram of how "noise-sigma units which vary in digital number scale with matched filter values", (RSI ENVI, 2004).

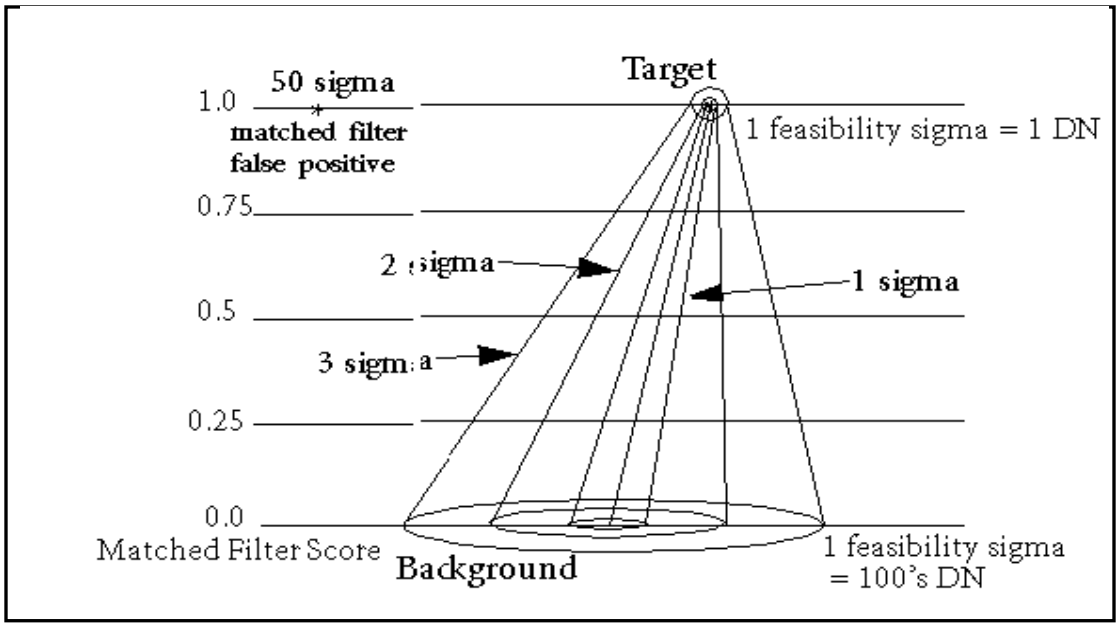

Figure 3.13 – MTMF- Noise Units

Pixels that are correctly mapped will have a high MTMF value and a low infeasibility value. Pixels that have a high MTMF value and a high infeasibility value are "false positive". To refine mapped endmembers and identify correctly mapped pixels the two-dimensional viewer is used to show the MTMF score on one axis and the

infeasibility scores on the other. Pixels that are identified as correctly mapped can be exported as regions of interest and treated as inputs into additional rounds of mapping.

3.9 Accuracy Assessment

3.9.1 Introduction

Assessing the relative accuracy of the mapped oysters presented some unique challenges, such as what constitutes a "true" map of oysters with which to compare against. In creating the "true" map of oysters, the issue of assessing a raster map of one spatial resolution against another raster based of a differing spatial resolution becomes problematic. Traditionally, remotely sensed imagery has an accuracy assessment implemented by comparing the number of pixels classified of one class against the number of "true" pixels but when the spatial resolutions of the mapped images are different than the "true" image, this method will not work. An alternative technique of deriving the accuracy of a classified image is by converting the image from raster to a vector image and compare by areal coverage rather than number of pixels. This method is not without problems since it assumes a near perfect conversion from raster to vector without loss of area.

The use of a relatively large pixel size as compared to the material of interest one must take into account the large areal extent of the pixel. The HyMAP imagery pixel size, as stated above is 4 X 4 meters. The digital number of each pixel is the composite of the earth material found within the pixel. A 4 X 4 meter rectangle within the estuary may include areas of water, mud, vegetation, (although attempts have been made to exclude vegetation and water) and shellfish. The MTMF method only identifies the probability of the presence of the earth material of interest. It does not include the relative abundances of the material of interest or and more importantly, the location of the shellfish within the 4 x 4 meter area. This presents a unique problem when

comparing the areal extent of two different vector polygons. It is assumed for this research that the presence of oysters, (presence is binary, yes or no) is complete and evenly distributed within the areal extent of the pixel. The problems of performing the classification accuracy assessment are inaccuracies generated through the georectification process and are exhibited in spatial misalignment between the three layers. Each layer must align correctly within a very small tolerance since the size of the oyster reefs range from small clusters to large patch reefs. Establishing image geocorrection within a small RMS is problematic by itself. Positions of ground control points are not easily found within the estuary. A point of land may or may not be in the same geographic location from one time frame to another as forces of accretion and degradation may have altered the position of the point of land in a relatively short period of time. Moreover, correct alignment may not be attainable since level of tide stage when each image was acquired was different so a visual "rubbersheeting" or re-geolocation based upon visual cues is misleading and inaccurate. But an accuracy assessment with these caveats in mind was performed to assess the relative accuracies of using two different spatial and spectral resolution sets of imagery in conjunction with comparing *in situ* derived and image derived endmembers.

The term "relative accuracy" used here in this research is used to denote the inherent problems faced when assessing the Producer's and User's Accuracy. The process that was used to create the accuracy assessment follows the steps of converting the raster classed images to vector and implementing a model that was developed using ESRI's ArcGIS Model builder. The model developed basically creates a GIS layer that is the intersection of the mapped or "found" oysters with the "true" map of oysters. The

output layer is the "correctly" mapped oysters and then the symmetrical difference is found between the "truth" oyster map and the "correct" oyster map. The out put from this operation results in oysters that were not mapped but should have been included or errors of omission. The correct oyster map also has the symmetrical difference found between the correct oyster map and the found or mapped oysters to derive oysters that were mapped but should not have been included, or errors of commission.

Jensen (1996) defines Producer's Accuracy as the total number of correct pixels in a category divided by the total number of pixels of that category and is a measure of omission. The User's Accuracy he defines as the total number of correct pixels in a category divided by the pixels actually classified in that category. Since this research converted the pixels to polygons instead of using number of pixels, area of the polygons was substituted in lieu of pixel counts.

3.9.2 AISA and HyMAP Accuracy Assessment

The creation of the reference image was accomplished using a GeoVantage 0.25 X 0.25 meter spatial resolution image of the BOB4 study area and surrounding oyster reefs. The spatial resolution is small enough that larger patch oyster reefs and fringing reefs are easily identified visually. The methodology used to create the reference image was to use Visual Learning System's Feature Analyst to classify the larger patch reefs and fringing reefs. Feature Analyst uses an iterative process of hierarchical learning with user input to "learn" correct objects that are classified by context and shape. The Feature Analyst is an extension to ESRI's ArcGIS. Smaller isolated clusters usually found in the middle of patch reefs surrounded by mud or on the fringing reefs are harder to classify using Visual Learning System's Feature Analyst and were identified and classified using

field images and *a priori* field knowledge collected during the extensive field data collection phase of the project.

Prior to the accuracy analysis the raster images the data was explored to define the class of oysters to be exported to vector. Since we were concerned only with presence or absence of oysters, the data was parsed into a single class that held only the probability of oysters being present. The cut-off from approximately above zero to the maximum data value needed to be elucidated. Knowing the data range the raster image was reclassed to include only one class, the class that indicates the presence of oysters. The other classes of data were eliminated that did not include the presence of oysters. The second treatment was then to convert the raster oyster class to polygons. There was no generalization of the polygons in the conversion process. The third treatment of the rasterized polygons was to accurately as possible "rubbersheet" the HyMAP imagery to spatially match the patch reefs and fringing reefs location. This was undoubtedly the most subjective aspect of the accuracy assessment process. User input was utilized to match the rasterized polygons with specific entities displayed in the GeoVantage "apparent truth" oyster map. User input relied heavily upon *a priori* field experience, field notes and photographic documentation to rubbersheet the HyMAP polygons.

The fourth treatment in the accuracy assessment section describes the procedure used to assess the relative accuracy of the AISA and HyMAP oyster classification. The assessment was implemented in two AISA trials that utilized image derived and in situ endmembers. Because the HyMAP imagery was spectrally subset into two spectral subsets, bands 2-61 and 2 – 44. The original band subset was created to increase the number of bands into the near infra-red region to incorporate unique spectral information

which to map oysters. The data sets were subset spectrally and spatially for two reasons: 1) creating a smaller spectral and spatial subset decreases computation time and file sizes. This is especially important because in the spectral analysis many intermediate files are created, creating a potential problem for storage. 2) Spectral regions of the electromagnetic spectrum may be weighted higher in the MNF process than other regions and by creating spectral subsets, smaller variances will not be lost in the MNF process. The band 2- 61 utilized just image derived endmembers and in situ endmembers were not used with this set. The spectral range of the bands 2-61 set was greater than the range of the field hand-held spectroradiometer. HyMAP spectral subset 2-44 was assessed from mapping utilizing image derived spectral endmembers, bright shell endmembers (image derived), mixed shell (image derived), and in situ endmembers. There were six separate accuracy assessments done between the AISA and HyMAP images.

Figure 3.14 shows the data processing steps that were implemented in ArcGIS's Model Builder to shorten analysis time and automate the steps required to process the data.

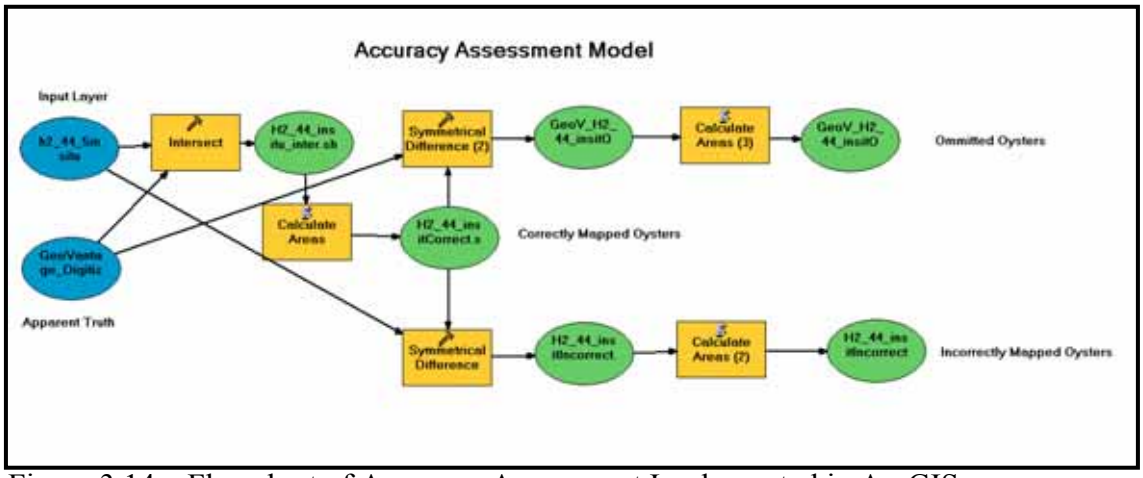

Figure 3.14 – Flowchart of Accuracy Assessment Implemented in ArcGIS

The two base coverages utilized for the accuracy assessment were the GeoVantage "apparent truth" oyster map and the coverage of "found" or mapped oysters from the MTMF process to be assessed. The first treatment was to intersect the coverages to create a correctly mapped oyster coverage or polygon area of commonality. The area was then calculated for the correctly mapped oyster polygons. Second treatment was the calculation of the symmetrical difference between the correctly mapped oysters with the "apparent truth" GeoVantage polygons. The area was again calculated from the resulting coverage from this operation. This treatment resulted in the areas that were omitted from the classification but should have been included, errors of omission. The third treatment was the same as the last treatment with the exception that the symmetrical difference was done between the correctly mapped oysters and the found or mapped oysters with a concomitant area calculation. This resulted in errors of commission or oysters that were mapped as initially correct (found) but should have not been included.

The final treatments were to export the table record that contain the area of the polygons from the correctly mapped coverage, omitted polygons, and incorrectly mapped polygons. Only those polygons that fell within the common area of the "apparent truth" GeoVantage coverage and the coverage that was assessed were included in the final calculations. This was done to exclude polygons that were outside of the spatial extents of one or both coverages. The exported data from the coverages were imported into Excel and percent relative accuracies were calculated for each of the coverages.

Chapter 4. Results

4.1 Introduction

The results presented in this section show the most recent effort of mapping after several revisions using the 2-dimensional scatter-plot to review and select endmembers. The purpose in showing the last two mapping trials is twofold: first, to illustrate the technique of using the scatter-plot to isolate and refine endmember bundles and secondary, remarkable changes in the results showing the before and after effect of using this technique. The results section, like the Methodology section, presents the results of the *in situ* spectral libraries that were collected and constructed through the course of a year and applied to the AISA and HyMAP imagery. The principal study sites used to map the in situ and image derived endmembers were BOB4, No Man's Friend 1 and No Man's Friend 2 (mud) field sampling sites. The process of deriving the spectral shellfish endmembers from the AISA and HyMAP data sets are shown and the results are then applied to mapping the shellfish distributions from the study sites in both the AISA and HyMAP datasets.

Mapping shellfish using field derived spectral endmembers first entailed adjusting the bandwidth of the spectral endmembers of the GER 1500 Spectroradiometer to mimic the number of bands and spectral range of the remotely sensed imagery that is to be used to map the shellfish. Specifically, the GER spectroradiometer that was used to collect the in situ shellfish spectral signatures has 512 bands (spectral range of 350nm – 940 nm),

AISA has 7 bands (spectral range 498nm – 819 nm) and HyMAP has126 bands (spectral range 0.4529 – 2.4822 nm). Depending upon the spectral range and number of bands, each remotely sensed data set needs to have the *in situ* spectral signatures convolved to match the specific remotely sensed imagery platform. The in situ spectral signatures were then processed through a minimum noise transformation in the same manner as the imagery. The last step in processing the in situ spectral data is to compile then into a convolved spectral library that was then used as input into a mapping process such as the MTMF mapping.

4.2 In-Situ Spectroradiometer Data

4.2.1 Field Sampling Sites

The study sites were selected and delineated for the gathering of spectral signatures of shellfish in a wide range of environmental conditions. These conditions include the: abundance of shellfish, positions (vertical and horizontal), and environmental state, (wet/dry, various amounts of mud, algae, and detritus present). Site characterization of the oyster reefs were conducted using definitions from the Shellfish Management section of the South Carolina Department of Natural Resource's Intertidal Oyster Survey Field Data Sheet codes. The Oyster Survey describes the reef strata with respect to bushels of live oysters per acre, presence or absence of vertical clusters, proportion of live oysters to shells and amount of mud present. Each of the 10 listed strata or classifications are identified by a letter code. See Appendix 7.1 for a complete description of the Intertidal Oyster Strata descriptions and their letter designations. Table 4.1 lists the field study sites that were identified by their strata for spectral observations.

Table 4.1 - In situ Spectral Sampling Sites

Site	Description	Notes
JC 1	Jones Creek – "F1" Strata	Contains F1 and F strata. Linear feature along bank of creek with *Spartina a.* on top of bank.
JC 2	Jones Creek – "C" Strata	Island feature in creek
JC 3	Jones Creek – Washed Shell	Little to no live shellfish, all horizontal, some with inside of shell face up.
Bob 1	Bob Creek – "G" Strata	Island feature in creek
Bob 2	Bob Creek – "E" Strata	Island feature in creek
Bob 3	Bob Creek – "C" Strata	Island feature in creek
Bob 4	Bob Creek – "D" Strata	Island feature in creek
NMF 1	No Man's Friend Creek – "G" Strata overall	Large island feature with *Spartina A.* on west side of island. Also contains "D", F1", and "B" strata
NMF 2	No Man's Friend Creek – Mud	Control for mud endmember. No vegetation present. Also has enough vertical relief to obtain semidry and wet mud spectroradiometer readings.
60 Bass	60 Bass Creek – "E" like strata	Shellfish with sand filled interstitial spaces, tightly packed and completely covering the substrate.

Each field sampling point was aggregated into like shellfish classes. For each month, the triplicates for each sampling point within each shellfish class were averaged to obtain spectral curves for twenty classes.

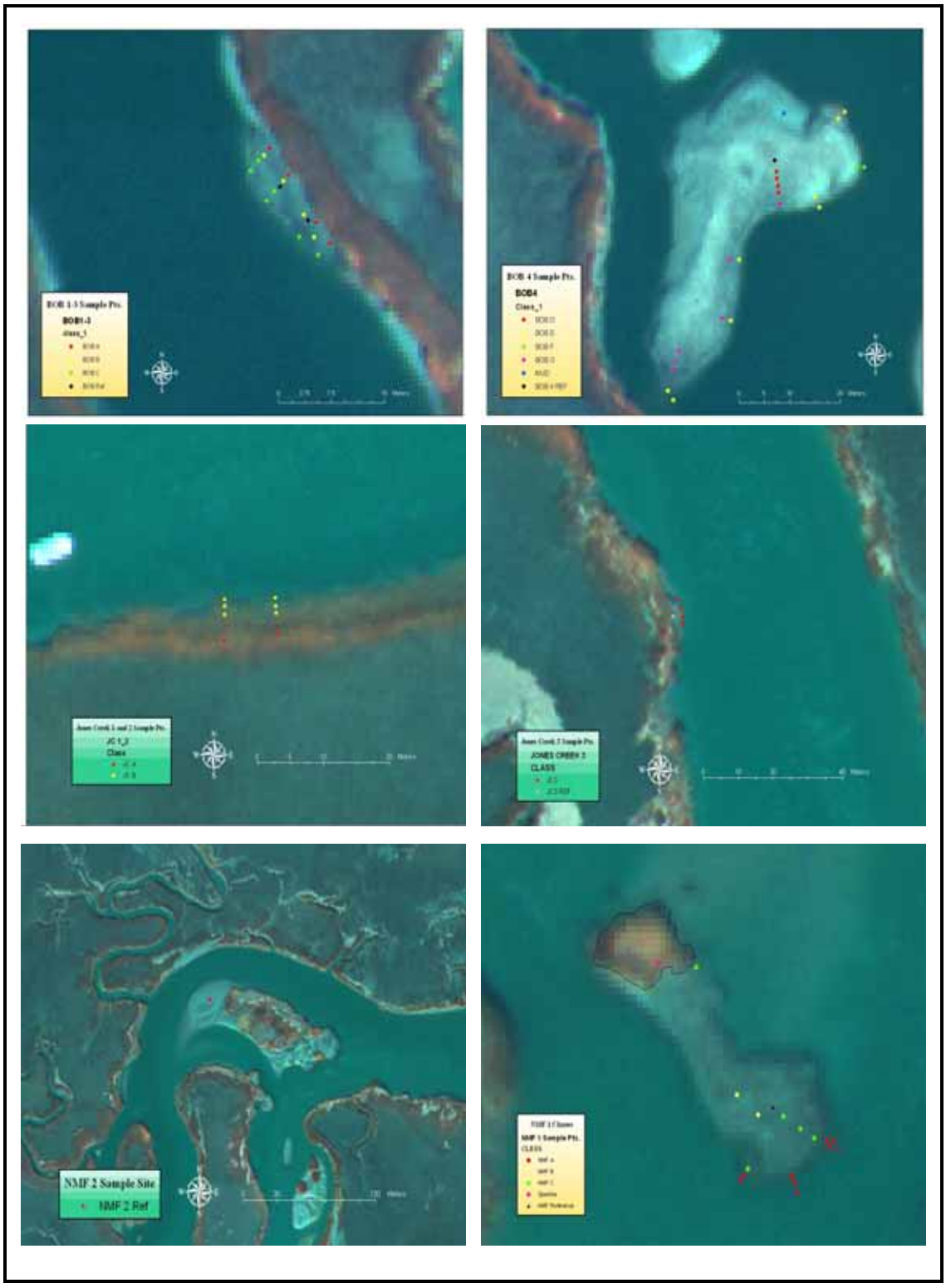

Figure 4.1 – Sample Sites North Inlet, South Carolina

Within the nine identified sampling locations, there were clusters of shellfish representative of "relatively" homogenous strata as well as a variety of mixed strata in and around each sampling locations. Transects were demarcated to represent vertical relief of the sampling reef from the waters edge, (below mean low tide) to the top of the oyster bank. No Man's Friend 1, Bob Creek 4, and Jones Creek 3 sample points have GPS point and distance measurement from the reference post to the sample point and demarcated using lengths of small diameter PVC pipe that was placed into the reef. Bob Creek 1 through 3 and Jones Creek 1 and 2, have their sample point distance measured only relative to the reference post. This is due to the relatively short distance to the reference post and a smaller sampling area. Figure 4.1 shows the locations of the sample points for each of the sample sites which were color coded to indicate which group each sample point belonged to in the secondary level of aggregation. In post-processing, the triplicates were normalized to apparent reflectance, and then averaged to obtain a single spectral curve for each sample point.

Sampling points or clusters were classified according to South Carolina Department of Natural Resources Field Data codes for Intertidal Oysters. There is recognition that there are some ambiguities in the DNR classification, but the intent is to use the DNR classification as a means to describe and differentiate between groups of shellfish.

All spectroradiometer measurements were taken using a GER 1500 (Geophysical & Environmental Research Corp (Millbrook, NY)) held at a stable height of ~ 1.5 meters above the sample point, (the height of holding the spectroradiometer at chest high, ~6 ft. tall). This height resulted in an IFOV of 1" x 1". The spectroradiometer is calibrated

from 350 nm to 1050 nm which roughly correlates with the long wave ultraviolet to the near infrared region (Jensen 2000). There are 512 bands with a spectral resolution of 3 nanometers at Full Width Half Maximum. The washed shellfish at the Jones Creek #3 site was sampled in dry and wet conditions. This was to document any changes in the spectral reflectance due to the presence of water. Relative terms were used to describe the wet/dry conditions included; dry (maximum dryness of the tidal cycle), semi-dry (more dry than wet), semi-wet (more wet than dry), and wet (wet shellfish and pooling of water interstitially). Notes included descriptions of the amount of mud encrusting (heavy/medium/light/none), and any noted detritus, such as seaweed, leaves, grasses, etc. All spectroradiometer readings, descriptions, measurements, and records were documented in a bound field notebook and sample points were digitally photo documented. Endmembers of water, mud, vegetated areas such as *Spartina alterniflora,* and the concrete pad near Clambank Landing were used as controls.

As illustrated in Figure 4.2, monthly spectroradiometer files were organized according to strata and environmental condition (wet or dry). The files were then converted from an Excel spreadsheet format to ASCII text file for importing into Research Systems, Inc. (Boulder, CO) The Environment for Visualizing Images (ENVI) software version 4.1 Spectral Library. All monthly ASCII exported files for each stratum were aggregated into a single folder. At the end of the sampling period, each strata folder contains all spectroradiometer readings converted to reflectance. The spectroradiometer values were then averaged into a single spectral reflectance curve for each stratum. Appendix 7.4 contains sampling dates and tide levels from June 2002 through July of 2003.

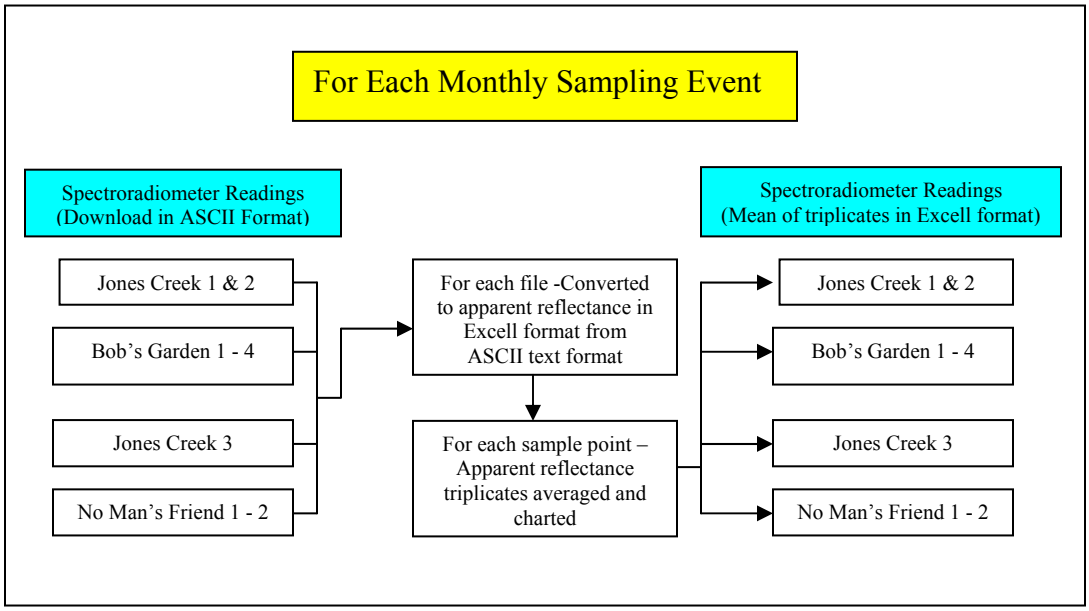

Figure 4.2 – Aggregations of Spectral Files

Primary aggregation was the importation of each spectral file into Microsoft Excel, conversion from radiance to reflectance, the averaging of the triplicates for an average signature of a particular sample point, and charting of the individual reflectance and average signatures. The file structure is by month and contains raw data, Excel format radiance and reflectance, and averaged triplicates. Further aggregation was necessary to have each strata represented and reduce the number of individual spectral signatures for mapping.

As shown above in Figure 4.2, the individual sample points were further aggregated by averaging the individual reflectance signatures at monthly intervals. Since each sampling point had a spectral reference signature recorded, it was not possible to average individual radiance signatures and post-process into reflectance. Appendix 7.3 shows the aggregation process of how individual sample points were aggregated into secondary groupings.

From Appendix 7.3, there were 14 sample points associated with sample sites BOB 1 through BOB 3, these sample points were averaged together to form BOB A through C (4 sample points from BOB 1, 4 sample sites from BOB 2, and 6 sample points from BOB 3). Since these sample points are located within the same geographic proximity, they are differentiated by strata that align with the vertical rise of tide. Another aggregation from the averaged triplicates used all twelve months of spectral signatures by sample site. This is useful in looking at the annual phenological changes that may occur within the sample points. For example, sample point BOB4_12 is characterized by mostly washed bright shell but, in the winter months, there is a preponderance of macro-algae growth that obfuscates the washed shell. Spectral changes can be monitored using the aggregation of the monthly spectral data acquired on the concrete pad at Clambank.. Figure 4.3 shows these monthly triplicate averaged spectral signatures. These data were acquired at precisely the same point on the concrete pad and were used as a de-facto control, showing subtle variations in the spectral response due to slight surface variations in the concrete pad.

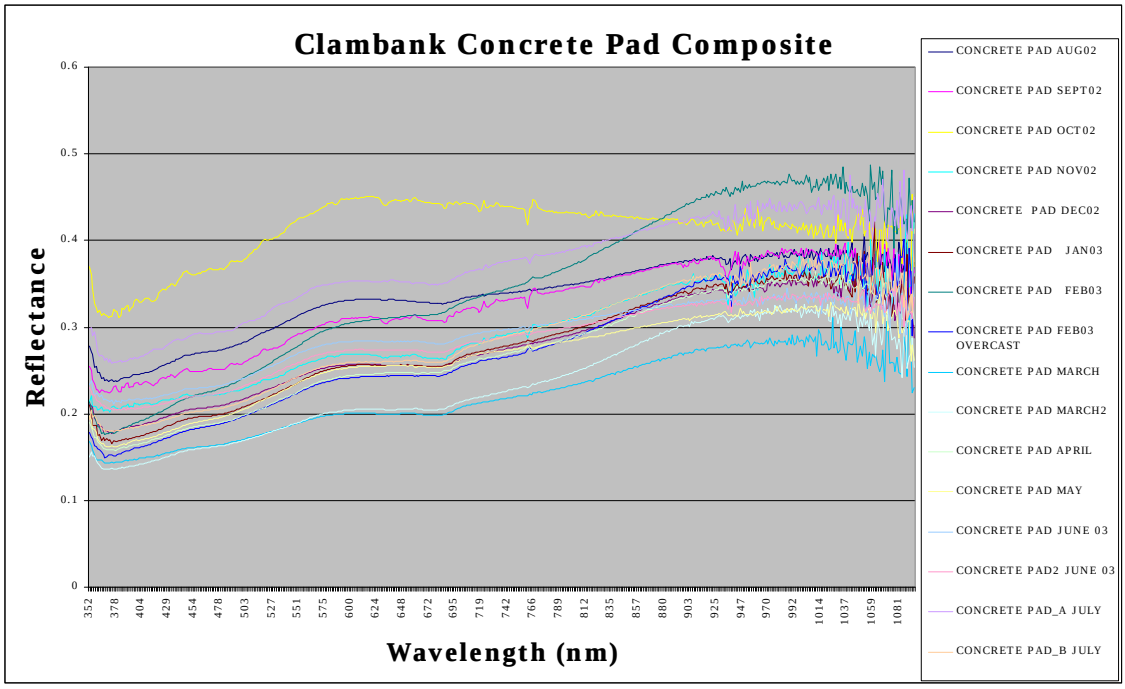

Figure 4.3 - Concrete Pad Composite at Clambank Site, North Inlet, SC

4.3 Remotely Sensed Spectral Data Analysis

4.3.1 Introduction - Spectral Data Analysis

The methodology of this research utilizes spectral endmembers deduced from remotely sensed imagery and *in situ* data collection of spectral signatures of shellfish strata. Both sets of imagery (AISA and HyMAP) were subset into Regions of Interest (ROI's) to ease computation and memory burdens. Regions were subset to be inclusive of the *in situ* sampling sites and surrounding oyster reefs. There were 6 Regions of interest for each set of imagery: 1- Jones Creek 1 and 2, 2 - Bob's Creek 1 through 3, 3 - Bob's Creek 4, 4 - Jones Creek 3, 5 - No Man's Friend 1 and 6 – No Man's Friend 2 (mud).

The spectral analysis within ENVI for decomposing endmembers from imagery can be performed using the Spectral Mapping Wizard. The wizard is a set of independent functions that can be used though the wizard or each function by itself. For this research

each of the functions for the spectral analysis was implemented individually. In this way, functions were re-run until results were fine tuned and a greater understanding of the data was achieved. Spectral analysis on each of the image subsets was done once to derive oyster endmembers from the imagery but was mapped using the MTMF function twice. Once with image derived endmembers and the second time using *in situ* derived spectral endmembers. All field collected spectral signatures were first convolved to match the wavelength scale of each of the remotely sensed images and minimum noise transformations were performed for inclusion in the MTMF process.

4.4 Minimum Noise Transformation

4.4.1 AISA 0.5 meter; BOB4 Sample Site

Spectral analysis was done using the photogrammetric and remote sensing software, The Environment for Visualizing Images (ENVI) version 3.5, SP1 and 4.1, by Research Systems Incorporated, of Boulder, CO.

Before analysis of the AISA or HyMAP imagery could be initiated, a mask of the study area was constructed. This study site was selected due to its large patch reef with a variety of shellfish strata types present both on the reef and on patch reefs surrounding the study site. The mask in effect negates pixels of water and vegetation for the Minimum Noise Transformation and subsequent analysis. Using the 2-dimensional feature space viewer using ENVI, clusters of water and vegetation were classified and used in construction of the mask. Pixels not classified using the above method were hand-selected and classed.

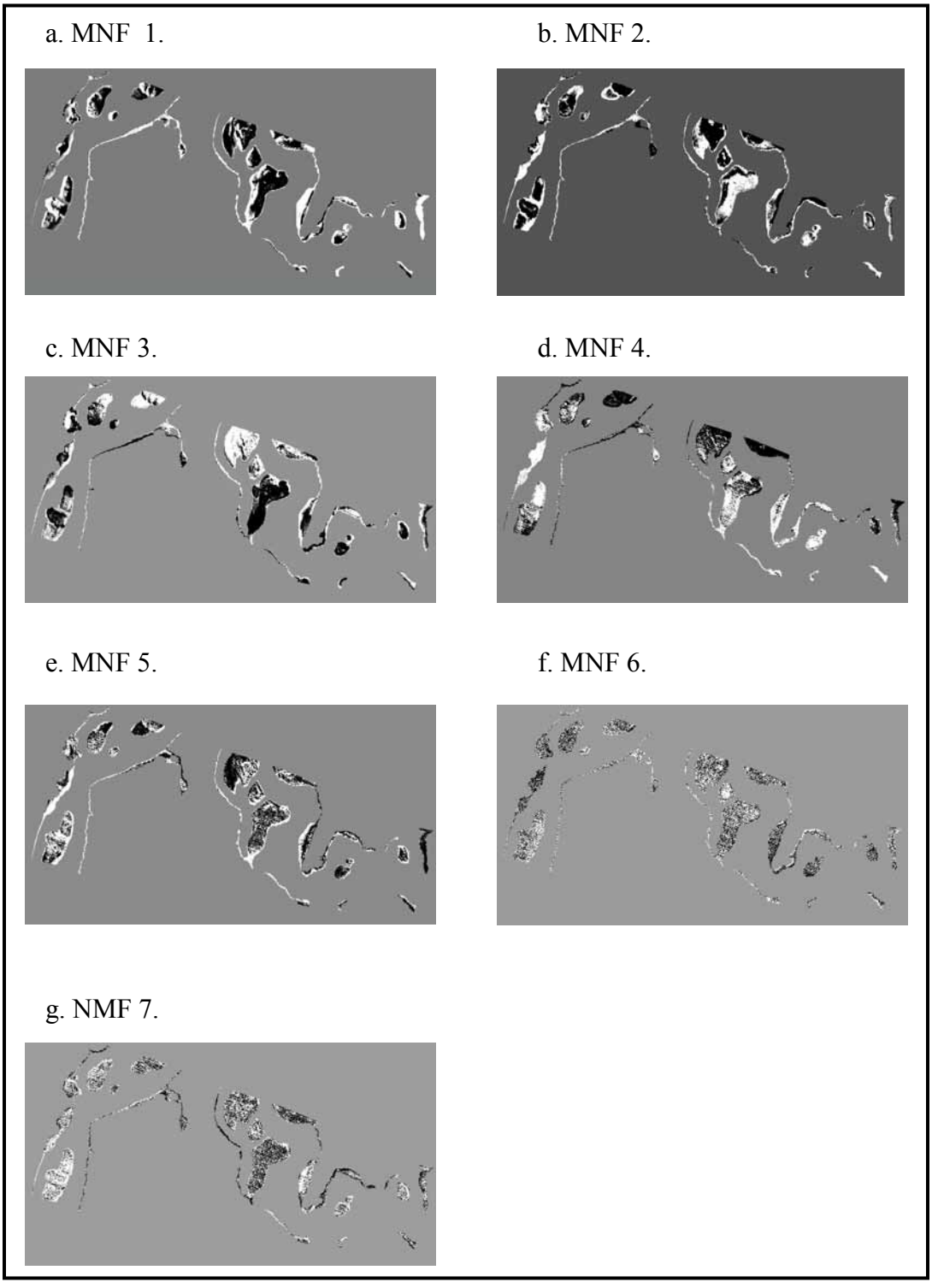

Figure 4.4 - Minimum Noise Transformation Fractions for AISA 0.5 meter BOB4 Site

A visual and statistical inspection of the AISA MNF rotation in Figure 4.4 allows the analyst to identify the eigen image(s) that convey the most useful information and identify the eigen image(s) that best represents the materials of interest. Minimum noise fractions 1 through 5 show the best image cohesion but from *a priori* field experience of the study site fractions 2 and 4 show the best fractions for shellfish. An examination of figure 4.5 shows a graph of the eigen values shows that the plot descends rapidly from eigen image 1 to 2 but is mostly level at eigen image 6, confirming the earlier visual inspection that eigen images 1 through 6 show the best image cohesion. Table 4.2 below shows the contributions of each band to the eigen vectors (principal components). The greatest contribution to eigen vector 1 (principal component #1) are bands 1, 2, and 5. Bands 7, 1, and 6 respectively contribute the most to eigen vector 2 (although band 7 has a much higher weighting than any other weights and the eigen image shows the bright shellfish areas within BOB4). Bands 4, 2, and 3 respectively contribute the most to eigen vector 3 and bands 5, 6, and 4. Examination of the contributions of each of the bands to the eigen vector images, one sees the yellow highlights the highest contribution for each eigen vector, bands 6 (713.82 nm) sums to 88.52 with band 1 (498.98 nm) sums to 87.59 and we can surmise that these two bands contribute the most to the discrimination of shellfish.

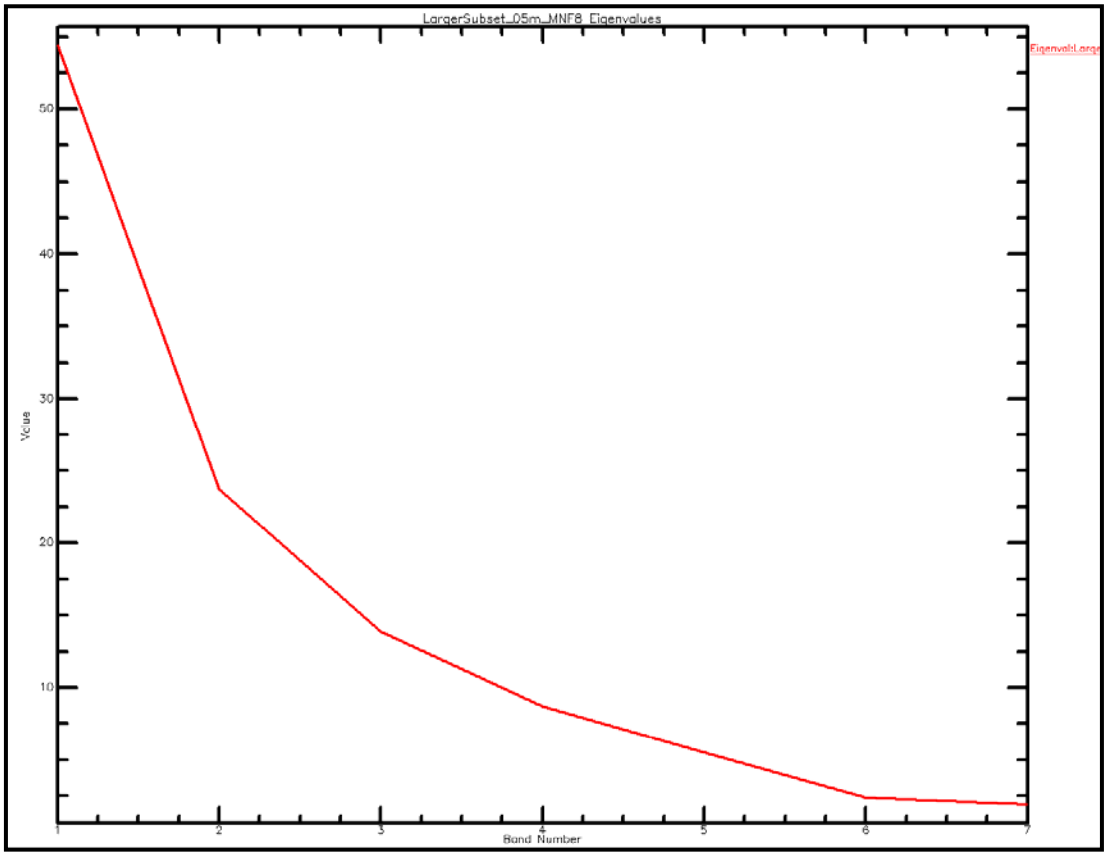

Figure 4.5 - LargerSubset_05m_MNF8 Eigenvalues Plot

Table 4.2 - AISA Principal Component Band Weightings

Contributions to Principal Components for: LargerSubset_05m_NMF8							
PC #	Band 1-498.980	Band 2-549.540	Band 3-584.300	Band 4-669.240	Band 5-700.140	Band 6-713.820	Band 7-819.840
PC 1	39.461132	30.967971	3.7874552	1.6658845	19.701317	0.10766289	4.3085771
PC 2	13.753507	0.1117656	3.5168846	5.4145362	0.78053759	7.0317692	69.391
PC 3	1.2678803	21.83554	20.607179	39.846817	7.1041205	0.4042573	8.9342059
PC 4	1.5524154	13.996682	0.012908533	18.530118	33.042241	32.728787	0.13684773
PC 5	14.624366	1.3457968	56.981885	11.534314	0.15615138	10.970003	4.3874836
PC 6	9.5766675	2.0882763	12.99604	7.7534701	39.205715	16.608796	11.771036
PC 7	19.764032	29.653968	2.0976477	15.25486	0.009917925	32.148725	1.0708496

The eigen values was used in conjunction with the eigen-images to visually verify and select those principal component bands that exhibit the greatest degree of spatial cohesion. Eigen-images 6 and 7 are dominated by noise and constitute the smallest contribution to the scene variance. Table 4.3 shows the percent contribution of variance

explained by each band. There is a total of 98.24% of the variance explained by the seven eigen-images and 94.24% explained by the usable bands 1-5.

Table 4.3 – Percent Contribution of Bands

Band	Eigenvalue	Percent
Band 1	54.403262	50.80967884
Band 2	23.713668	78.55858451
Band 3	13.898252	87.43348369
Band 4	8.706524	92.12773837
Band 5	5.543738	94.98746504
Band 6	2.395308	97.83421131
Band 7	1.936741	98.24883824

4.4.2 HyMAP 4 X 4 meter; BOB4 Sample Site

It was found that the best subset of the 126-band HyMAP imagery were bands 2-61. This is contrast to the use of bands 2-44 that were used for the *in situ* mapping. This is the difference between the optimal use of bands and limitations imposed for the use of the GER field data. For the sake of comparison, HyMAP bands 2-44 were spectrally analyzed so as to compare the final mapping accuracies with the *in situ* derived endmembers. Bands from 61 to 126 were found to contribute very little to the weights of the Minimum Noise Fractions when bands 41 to 126 or bands 2 to126 are subjected to the Minimum Noise Transformation. This report shows the results from using bands 2-61 and 2-44 in using image derived endmembers and *in situ* spectral library endmembers. Band one was not included due to the preponderance of noise within the band. Since the interest is in shellfish and mud, a mask was constructed and applied in the same manner as was done for the AISA image to effectively negate water, vegetation and areas outside of the image that would otherwise be considered in the MNF transformation. As described above, the inclusion of water and vegetation in the MNF transformation skews the eigenimages to favor the water and vegetation effectively relegating mud and

shellfish to the lowest end of the eigenvalues. Any of the subtle variances within mud and shellfish are lost within the larger variances of the vegetation and water. The MNF transformation from the use of the *in situ* endmembers is the same mask that was applied to the image endmember analysis.

As with the AISA region of interest, for the HyMAP images a mask was constructed of the water and vegetation using the 2-dimensional feature space viewer. The masked subset was the same mask applied to ROI 1 Bands2_44 and ROI 2 Bands2_61.

All bands from 2-61 were utilized in conjunction with the mask band that was produced from the use of the 2-dimensional feature space viewer. The result of the transformation was 60 eigenimages and descriptive statistics that included the eigenvalue of each of the transformed bands. Figures 4.6 and 4.7 show the eigenvalues versus eigenvectors graphs with the steep descent of the curve followed by a longer flatter curve graph of both HyMAP spectral and spatial subsets.

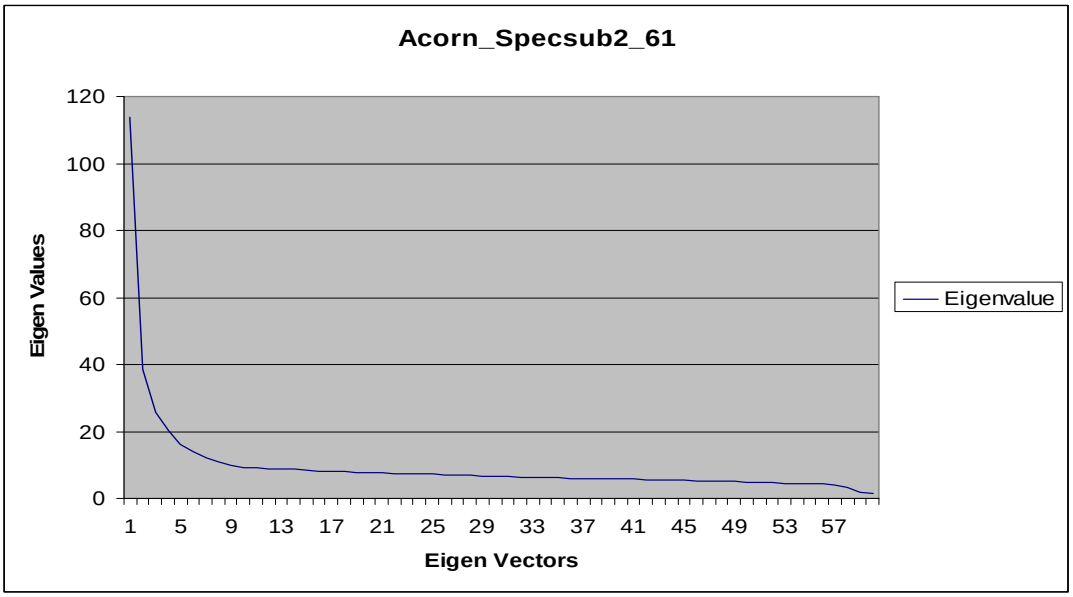

Figure 4.6 – Eigen Values of ACORN_SPECSUB_2_61

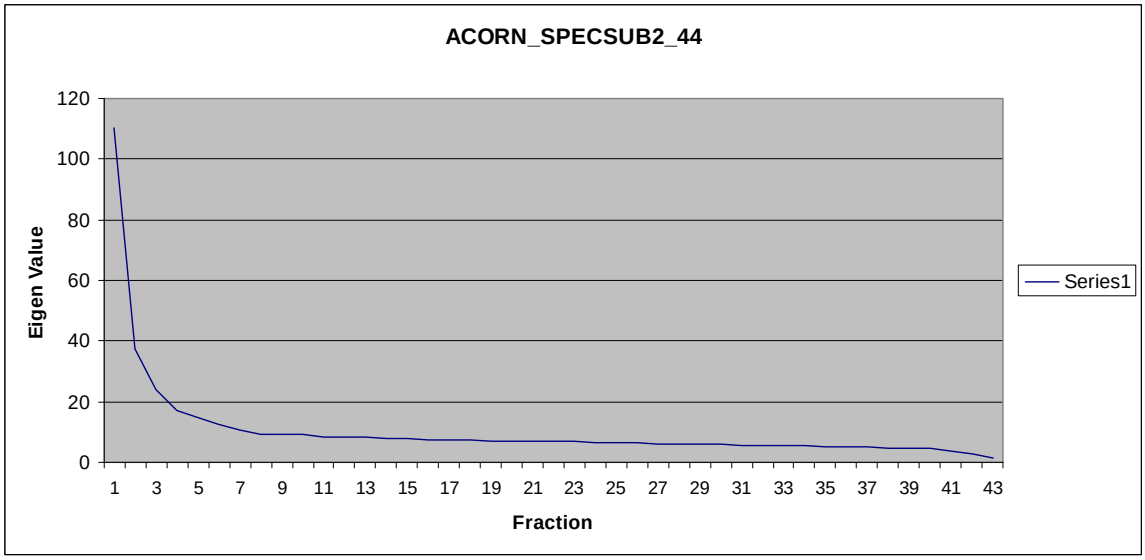

Figure 4.7 - Eigenvalues of ACORN_SPECSUB2_44

In both figures the curve starts to flatten out around the 6th eigenvector and is flat by the 10th eigenvector. When significance between eigenvectors diminishes, very little information is contributed to the explained variance. This ability to reduce the dimensionality of a hyperspectral image is a key component in the analysis of hyperspectral imagery. Since many of the bands within a hyperspectral image have a

high degree of colinearity, the ability to eliminate redundant information or information that is of no use, is an important step. The next step was to visually and statistically examine the eigenimages to select the eigenimages that are the most discriminating of shellfish and eliminate eigenimages that were noise dominated. Tables 4.4 and 4.5 below show the top three bands for the first ten eigenvectors that contributed the most to each eigenvector. This is interesting as it gives clues as to which portion of the electromagnetic spectrum is best suited for discerning shellfish. By knowing which eigen image shows the brightest pixels for shellfish we can know which bands were weighted the highest for a particular eigen image.

Table 4.4 - ACORN_SPECSUB2_61_MNF1 Weights

Band Contributions and Weightings:						
Principal Component Analysis for Acorn_SpecSub2_61						
PC Number	BANDS			WEIGHTS		
PC 1	Band 6	Band 2	Band 3	11.987379	9.2760573	8.5539724
PC 2	Band 8	Band 6	Band 16	29.277465	18.890562	7.220803
PC 3	Band 5	Band 4	Band 12	41.006034	7.734877	6.4461721
PC 4	Band 15	Band 13	Band 19	15.454924	14.655724	9.3147558
PC 5	Band 2	Band 15	Band 26	10.631192	10.335425	8.0594018
PC 6	Band 16	Band 17	Band 35	16.724908	4.6216271	8.6137405
PC 7	Band 28	Band 18	Band 16	8.4118245	7.4878084	6.9099657
PC 8	Band 39	Band 31	Band 20	11.9482	11.251051	9.9917252
PC 9	Band 47	Band 22	Band 16	7.5668694	6.7345066	6.6067521
PC 10	Band 16	Band 50	Band 31	15.394009	8.2520497	7.0312418

Table 4.5 Acorn_Specsub2_44_MNF1 Weights

Band Contributions and Weightings						
Principal Component Analysis for Acorn_Specsub2_44						
PC Number	BANDS			WEIGHTS		
PC 1	Band 6	Band 8	Band 2	24.544642	21.270713	10.625006
PC 2	Band 7	Band 6	Band 4	22.94082	22.624914	11.595337
PC 3	Band 5	Band 9	Band 4	48.837544	12.746763	8.2575101
PC 4	Band 8	Band 10	Band 11	18.174939	12.163735	7.4630977
PC 5	Band 21	Band 20	Band 10	21.841274	14.430288	12.215388
PC 6	Band 9	Band 13	Band 20	17.400769	12.358863	9.2249532
PC 7	Band 13	Band 8	Band 12	24.131268	9.3414639	9.0000087
PC 8	Band 10	Band 17	Band 18	12.042941	12.041463	11.333438
PC 9	Band 9	Band 13	Band 11	15.258824	11.084697	10.771905
PC 10	Band 15	Band 12	Band 11	21.328123	14.473929	8.5607029

Viewing the individual Minimum Noise Fraction images below for both HyMAP subsets in figures 4.8 and 4.9, around fraction nine or ten the image becomes grainy and there is no pattern to the light / dark pixels that would correspond to either mud or shellfish. Taking all the pertinent information together, MNF 1 through 10 minimum noise fractions were the most valid eigen images for further refining of the pixels via the pixel purity index. If the better MNF eigenimages for analysis are 1 through 10 how

much of the total variance is accounted for when utilizing just 10 out of a possible 59 eigen images? Tables 4.6 and 4.7 below show the cumulative variance that is associated with each successive eigen image. For bands 2-61 in table 4.6, within the first 10 eigen images there is a total of only 46% and 56% for the bands 2-44 subset of the total variance in the image explained in the first 10 eigen images. This was an unexpectedly low value but there could be a number of causes for this low value. Most prominent is the large number of bands used as input and there is not the presence of any single or group of bands that carry a disproportionate amount of the variance in the scene. Hence the variance maybe spread out some what evenly over all the bands. Examination of the table of weights in tables 4.4 and 4.5 by eigen vector reveals that bands. Examining the eigen vector images in conjunction with the weightings tables gives insight into which bands may have the greatest influence in discerning shellfish from mud. From these examinations, optimal bands for identifying mud and oysters are the visible bands (blue, green and red). Although the principal component that has the highest weight is in principal component 3 and lists band five (0.4972 μm) as having the highest weighting, with band eight (0.5439 μm) in principal component 2 having the second highest weighting. Band five is in the blue region of the electromagnetic spectrum and band eight is in the green region although the two bands are relatively close the lower limit of band five is around the maximum of clear water while band eight is in the lower area for the detection of chlorophyll. In this case the presence of diatoms maybe influencing the reflectance.

Table 4.6 – Cumulative Percent ACORN_SpecSub2_61

MNF Band	Eigenvalue	Cumulative Percent
Band 1	113.715216	19.68291099
Band 2	38.496547	26.34625944
Band 3	25.867514	30.82365476
Band 4	20.076597	34.29870309
Band 5	16.016936	37.07106669
Band 6	14.004451	39.49509025
Band 7	12.275391	41.61983166
Band 8	10.877002	43.5025266
Band 9	9.760726	45.19200588
Band 10	9.31478	46.80429659

Table 4.7 – Cumulative Percent ACORN_SpecSub2_44

Band	Eigen Value	Cumulative Percent
1	110.300974	24.26741907
2	37.464643	32.51004975
3	23.821269	37.75098912
4	17.034562	41.49877882
5	14.877893	44.77207779
6	12.584281	47.54075707
7	10.536101	49.85881437
8	9.389293	51.92456139
9	9.297237	53.97005508
10	9.041847	55.95936018

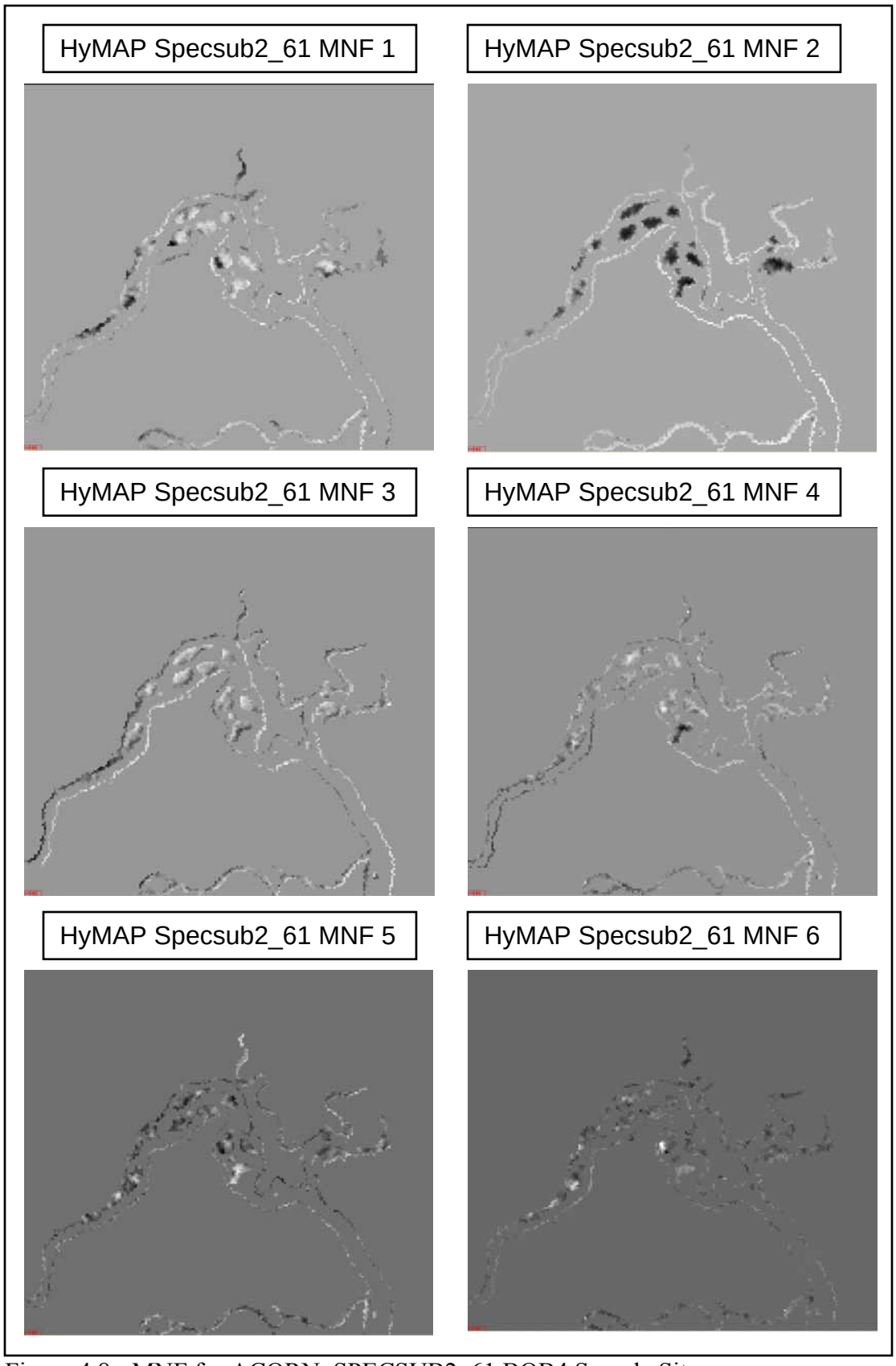

Figure 4.8 - MNF for ACORN_SPECSUB2_61 BOB4 Sample Site

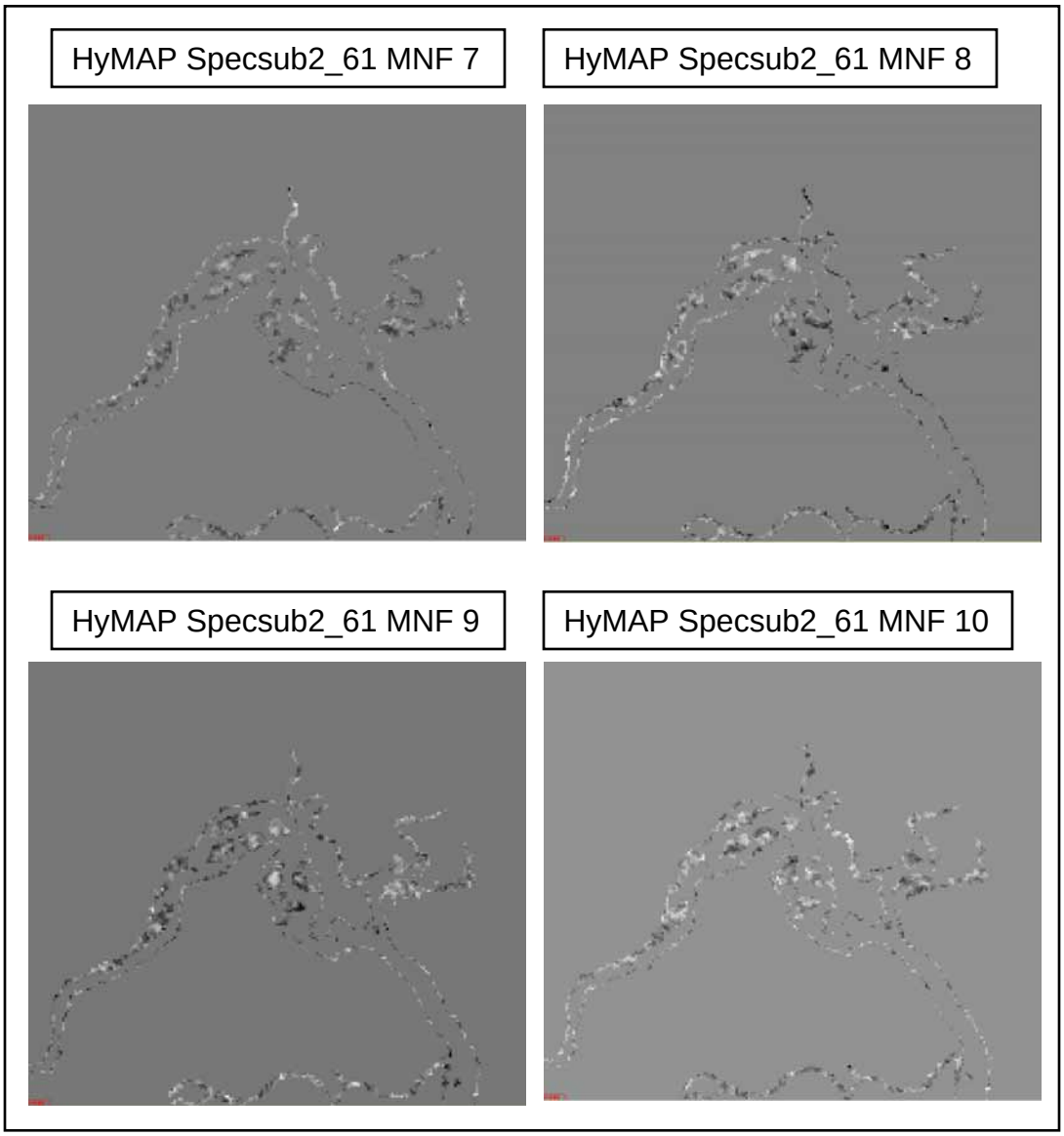

Figure 4.8 Continued - MNF for ACORN_SPECSUB2_61 BOB4

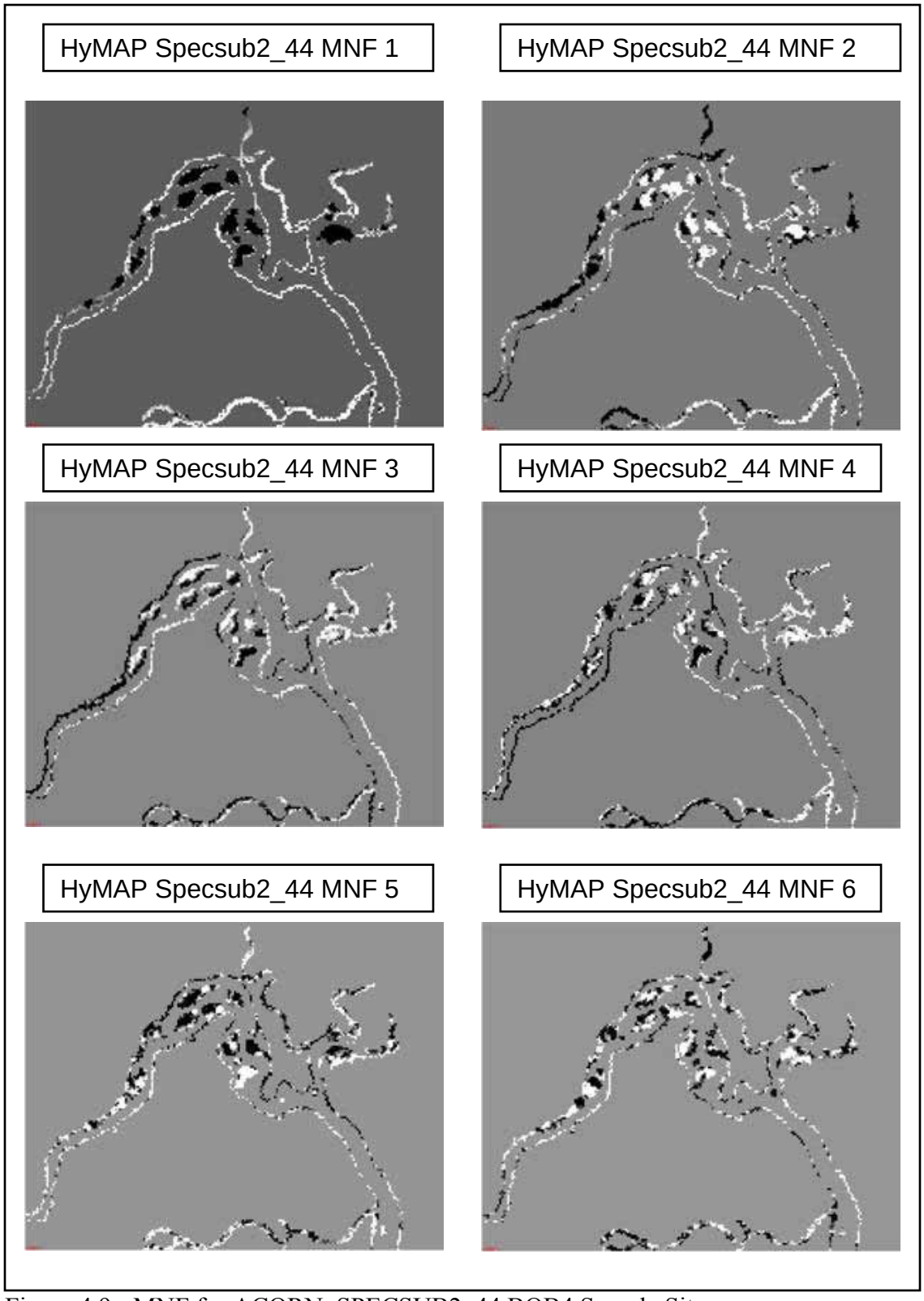

Figure 4.9 - MNF for ACORN_SPECSUB2_44 BOB4 Sample Site

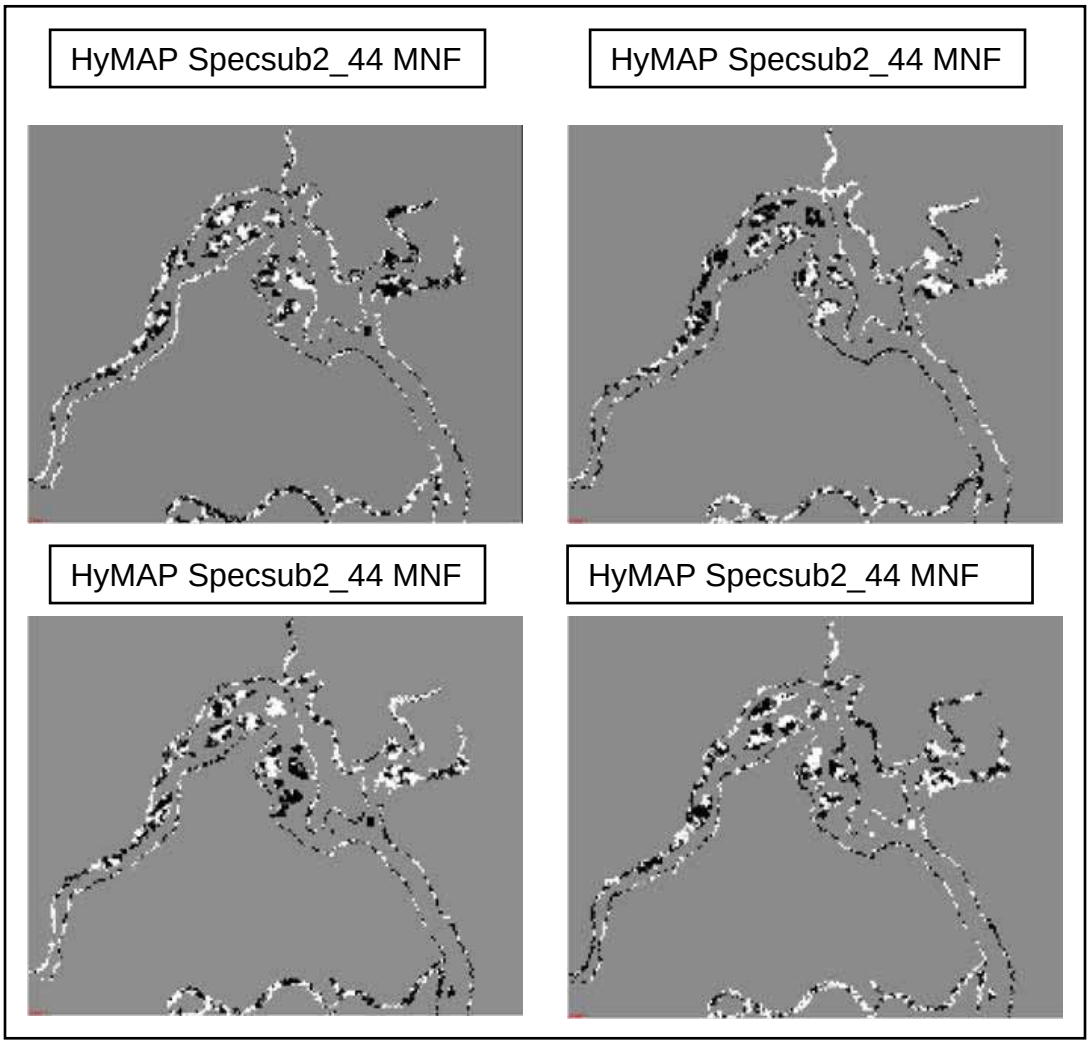

Figure 4.9 Continued - MNF for ACORN_SPECSUB2_44

4.5 Pixel Purity Index

4.5.1 AISA Pixel Purity Index (PPI)

The parameters used for the Pixel Purity Index was a threshold factor of 2 and 10,000 iterations. The curve describing the number of spectrally pure pixels was relatively flat after the initial round after finding 1853 pixels that were designated as spectrally pure. Figure 4.10 shows the image produced from the process over-laid on the AISA image and density sliced by value for better viewing.

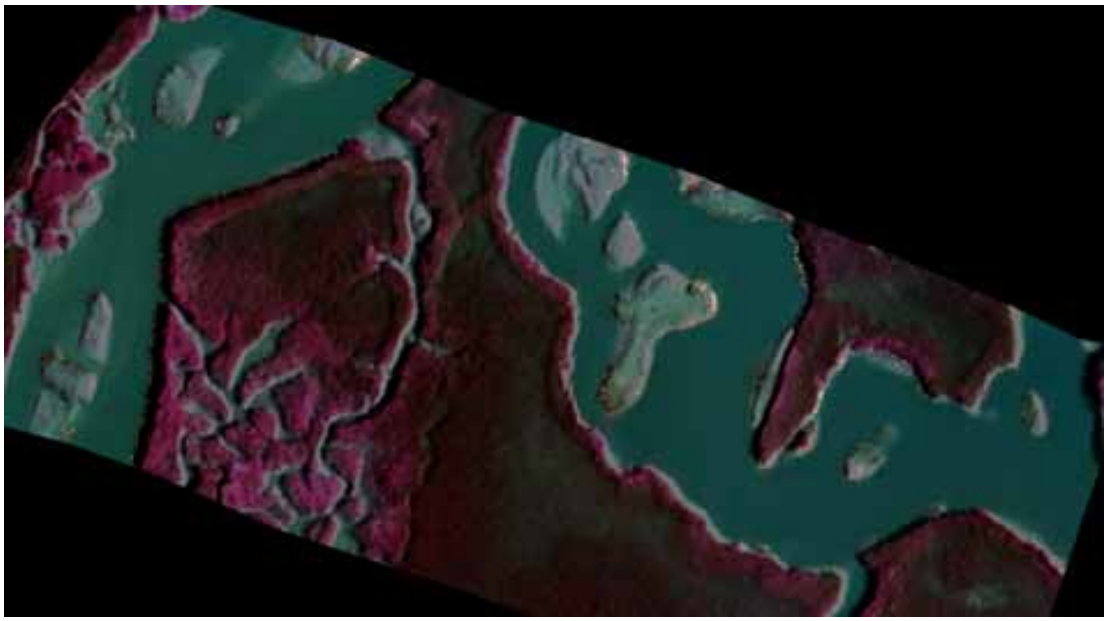

Density Color Values	
Value	**Color**
1 – 162	Red
163 - 326	Green
327 – 490	Blue
491 – 654	Yellow
655 – 818	Cyan
819 – 982	Magenta
983 – 1146	Maroon
1147 - 1310	Sea Green

Figure 4.10 - MNF Iteration 9 Pixel Purity Index

From the pixels that were marked as spectrally pure, these were then processed in the *n*-Dimensional Visualizer within ENVI. The *n*-Dimensional Visualizer assigns the pixels to classes and displays the results of the colored classes visually in a multiple dimensional viewer. The user can manipulate these classes in various dimensional axes as well as rotate and turn to inspect the data cloud. The user has the option of including additional endmembers within the class or endmember bundle, delete classes or add more classes. The user also has the option of exporting a class of pixels to the Region of Interest (ROI) viewer to view the pixels within the image. This is helpful in deciding if a certain class of endmembers correlates with *a priori* knowledge the user may posses of the image. This inspection of the data is the most subjective portion of the analysis and is discussed in greater detail in the Discussion section. Figure 4.11 illustrates the two classes of endmembers that were collected using this technique. There were 20 endmembers that were collected to represent the shellfish. This was to ensure enough spectral variability to adequately map most or all of the shellfish found within the study area. Only six endmembers were selected to represent the mud class. Fewer mud endmembers were found but this may reflect the narrower spectral variability of mud within the scene. Figure 4.11 illustrates graphically the two classes with the Pixel Purity Index image overlaid on the AISA image for two sample sites within the study area. There were 6 pixels representing the mud endmember and 20 pixels representing the shellfish endmember. A final proof of separability between the two classes is the use of a statistical test named the Jeffries-Matusita Transformed Divergence test. The two classes are termed separate if the score is above 1.8, a score below this value indicates they

should be merged into a single class. The results of this test yielded a score of 1.895, which indicates these two classes (shellfish and mud) are distinct and separable.

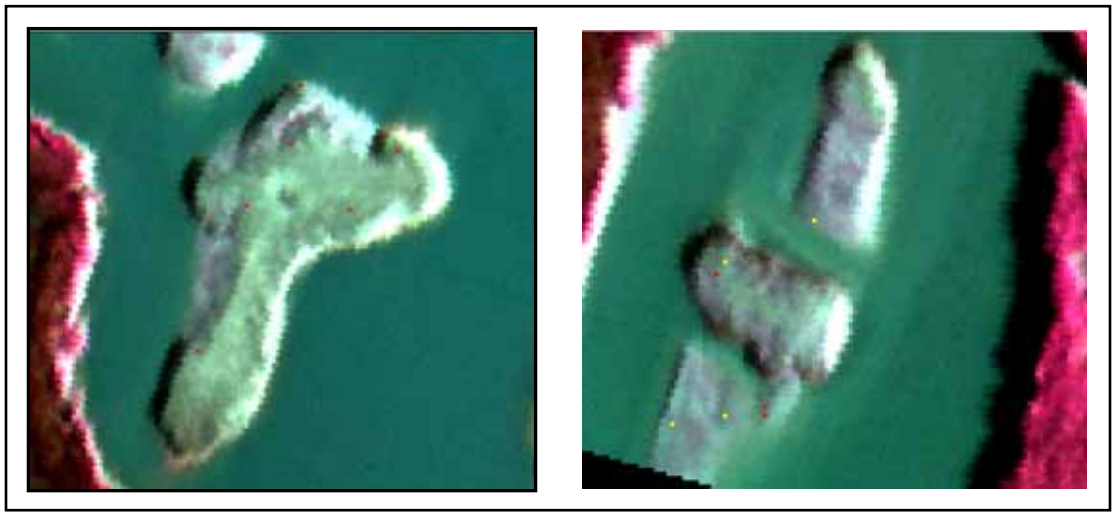

Figure 4.11 – Portion of ROI for Image Derived Endmembers - AISA

4.5.2 HyMAP Pixel Purity Index (PPI)

As stated above, the purpose of the Pixel Purity Index (PPI) is to transpose the pixels from the MNFT image into multiple dimensions and rotate the data cloud, then mark the number of times certain pixels on the extreme edge of the data cloud are captured. This technique was derived from the convex hull geometry concept (Boardman, 1993). The purpose is to compile a list of pixels that are the most extreme and thus the most spectrally pure. These pixels were then utilized to map the image for a specific earth material or endmember. There was a large degree of subjectivity that depended upon the analysts experience and *a priori* field conditions that were injected into the analysis by the analyst in the sense that many endmembers have the ability to be selected with varying degrees of pureness. It is up to the analyst to determine which ones were of most utility and represent the material of interest. Additionally, one spectra or endmember may not adequately reflect the full range of spectral variability found *in situ*.

To counter this endmember "bundles" with multiple endmembers have been produced in an attempt to encompass the spectral variability. This approach has limitations since there can only be *n -1* number of endmembers compared to the number of input eigenimages used in the mapping (Bateson et al.1998).

In the course of this research there were dozens of permutations of the mapped imagery and parameters computed for both 2-44 and 2-61 band subsets. For purposes of this report only the results obtained from the most successful run of the endmember selection and mapping are discussed from the band 2-61spectral subset. The first ten eigenvectors were used with five thousand iterations with a threshold factor of 1.0 resulted in finding 999 spectrally pure endmembers within the image subset. In Figure 4.12, the Pixel Purity results show the full range of the pixel values in a density slice of the bands 2-61 spectral subset. As a matter of reference, pixels with a higher score are considered more "spectrally pure" than pixels with a lower score (the number represents the number of times the pixel is marked as extreme). Only one pixel had a score greater than 754 (the most spectrally pure) and two pixels were in the 646 - 753 range. From *a priori* knowledge, both of these sets were located within the shellfish reef areas. These sets were utilized as input into the MTMF mapping method and then subsequently refined to obtain more accurate shellfish mapping.

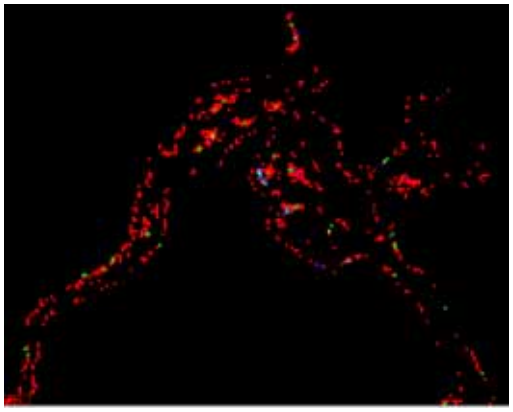

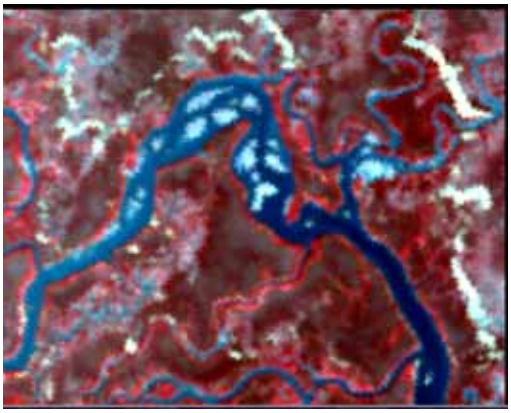

Value	Color
1 – 106	Red
107 - 214	Green
215 – 322	Blue
323 – 430	Yellow
431 – 537	Cyan
538 – 645	Magenta
646 – 753	Maroon
754 - 861	Sea Green

Figure 4.12 – PPI Image Showing Full Range of Pixel Values Band Subset 2-61

Viewing the results, most of the pixels were low scoring and thus do not represent spectrally pure pixels. To isolate the higher scoring pixels, the pixels were held to a threshold value (441 - 816) to isolate the higher values. The higher scoring pixels are shown in figure 4.13 exclusively with the elimination of lower scoring and less pure pixels for the spectral subset bands 2 – 61 with the values labeled. After further refinement of the shellfish and mud endmembers by successive iterations of mapping, figure 4.14 shows the endmember results that were used for the final MTMF mapping. The endmembers shown in figure 4.14 also happen to be located within the BOB4 sample site within an area that contains few live oysters and washed shells.

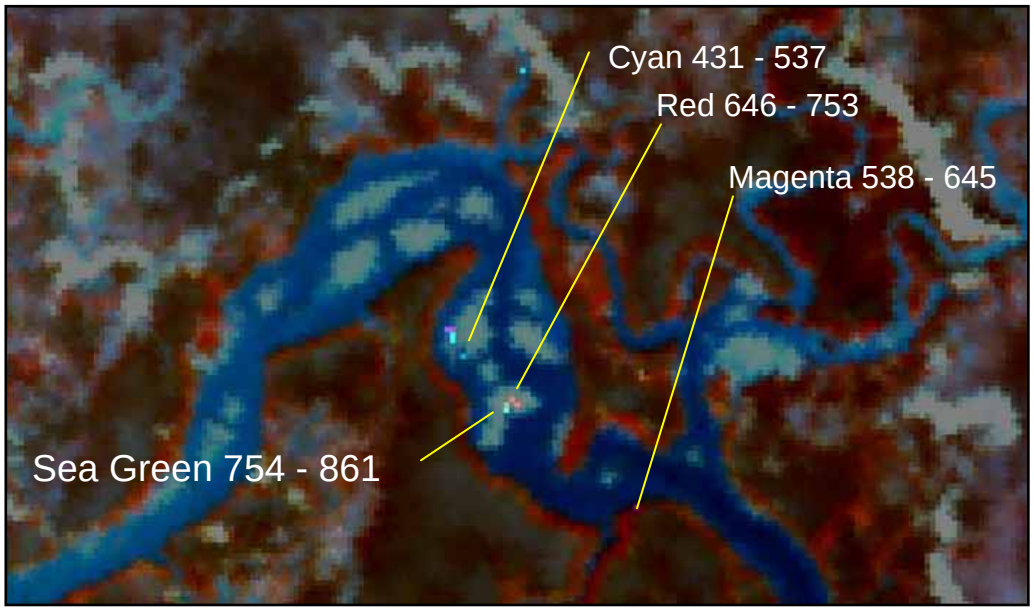

Figure 4.13 - Pixel Purity Index Showing Values From 441-861

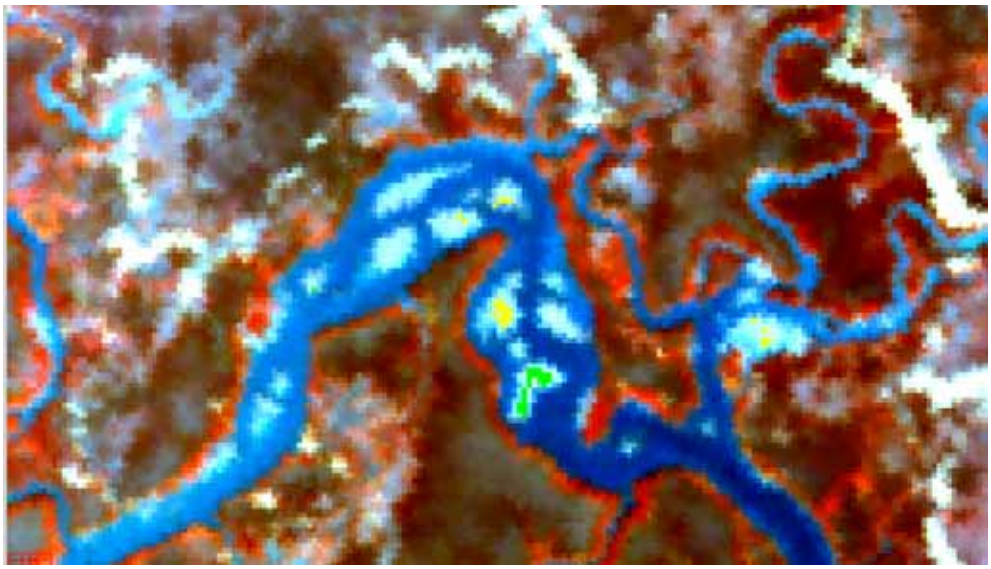
Figure 4.14 - Shellfish and Mud Endmembers HyMAP Bands 2-61 Shellfish (Green) and Mud (Yellow) Extracted Endmembers

Figure 4.14 shows all the endmembers selected from the field sampling site BOB4 which had a higher spectral reflectance than the surrounding mud patch reef.

There were 23 green pixel endmembers which represented shellfish and 25 yellow pixel endmembers that represented mud.

4.6 MTMF Using Image Derived Endmembers

4.6.1 AISA Mixture Tuned Matched Filtering

A MTMF Score and Infeasibility Score (two images for each endmember bundle) was calculated using the endmembers from the BOB4 study site as input into the MTMF. Results of several MTMF runs are shown above in Figure 4.16. This figure shows the pixels mapped as shellfish with values linearly stretched between zero (the background pixels) to one. Displayed in figure 4.15 is the 2-dimensional scatter-plot of the MTMF Score (x-axis) and Infeasibility Score (y-axis) showing most of the pixel values residing between zero and one with a relatively low score on the infeasibility axis.

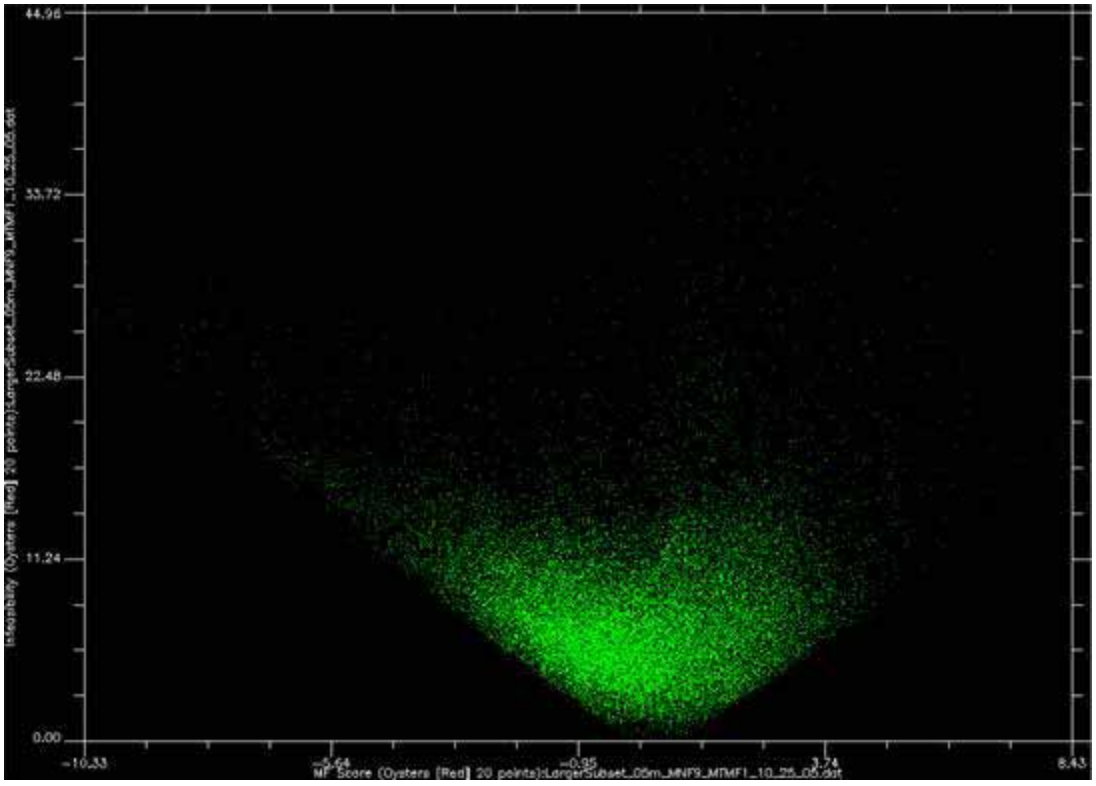

Figure 4.15 – MTMF Results for Shellfish AISA Imagery BOB4

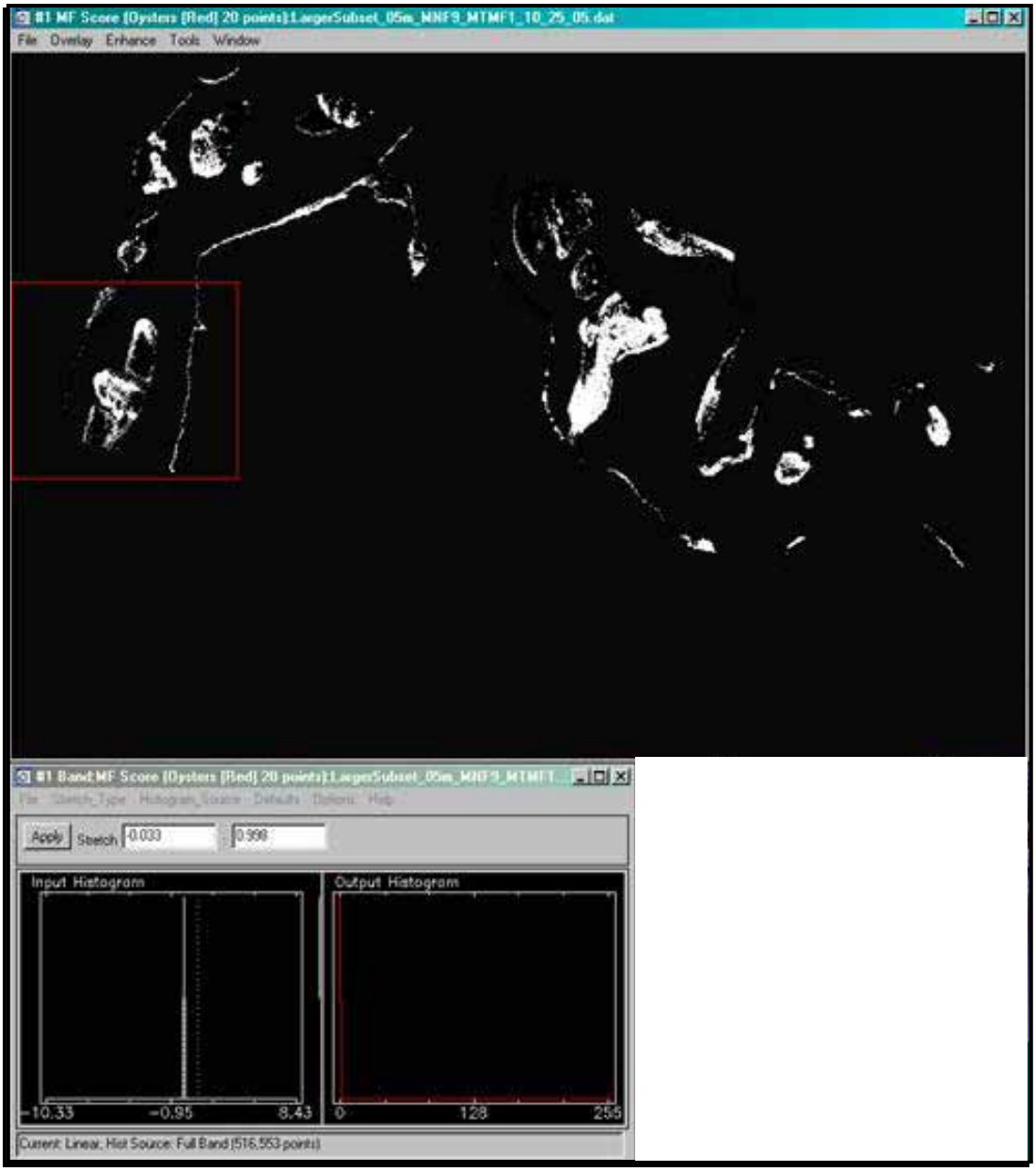

Figure 4.16 – MTMF Results for Shellfish AISA Imagery BOB4

Interactive stretching uses set minimum and maximum values (0.0 to 1.015) and "stretches" those values over the whole range of values that can be displayed. The results obtained for mud using the MTMF process and stretching the pixel values from zero to one are shown in figure 4.18. This image represents mud features, and has values from -0.014 to 0.968 stretched to isolate and map the mud pixels. The scatter-plot (figure 4.17)

shows the majority of pixels with the lowest infeasibility values centered from zero to one, thus illustrating a successful endmember mapping process.

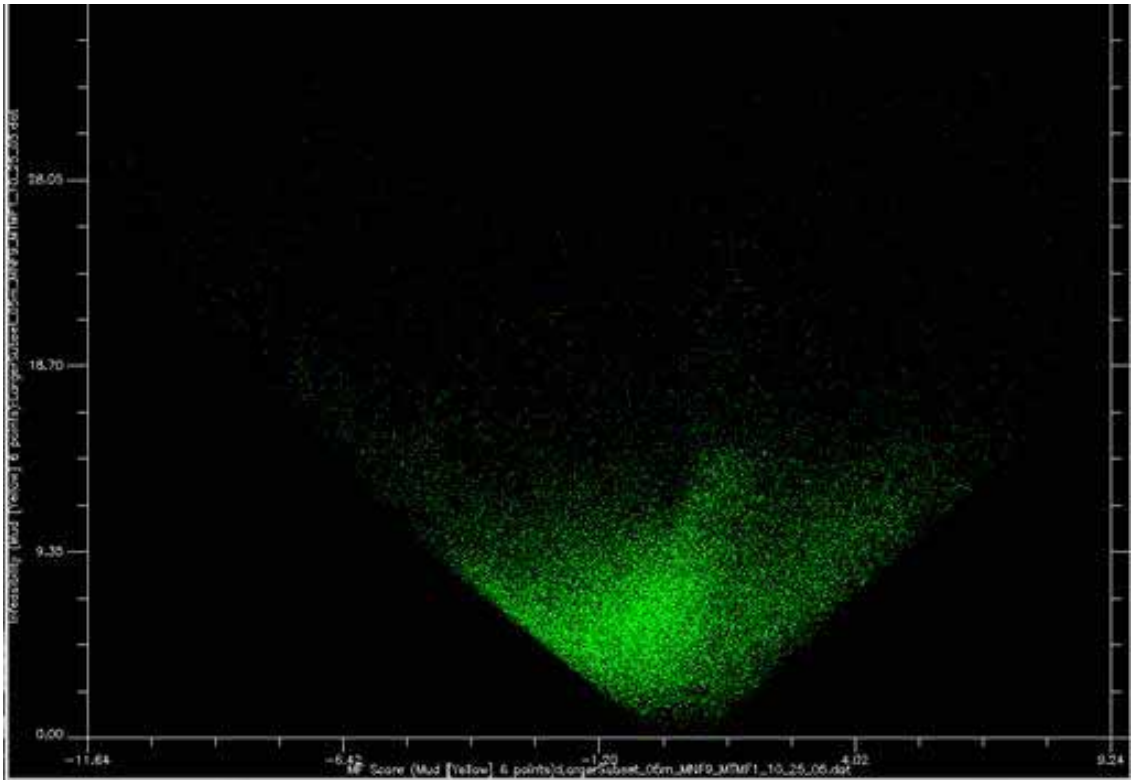

Figure 4.17 - MTMF Infeasibility Score for Mud Endmember AISA Image BOB4

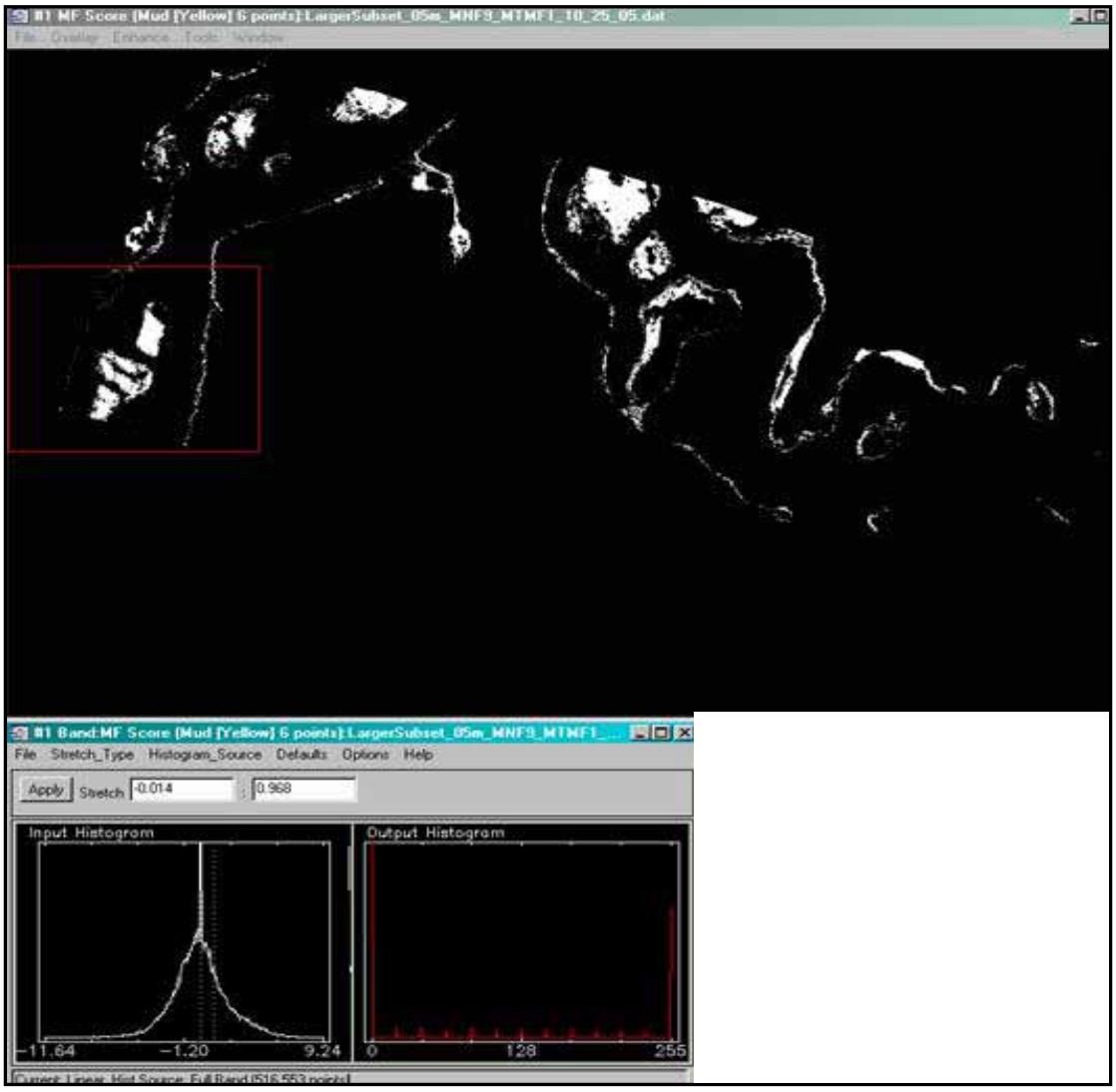

Figure 4.18 – MTMF Infeasibility Score Mud Endmember AISA BOB4

4.6.2 HyMAP ACORN_SpecSub2_61 - Initial Mapping Round

The first ten Eigen images from the Minimum Noise Transformed file ACORN_SpecSub2_61_NMF1 were used as input to map the shellfish and mud endmember bundles. Endmember spectra used for input were obtained from the Pixel Purity index rather from the n-Dimensional Visualizer. Since familiarity with the area allowed *a priori* knowledge of the study site, specific endmembers are known to be shellfish or mud. The endmembers are designated for analysis by simply dragging-and-

dropping the endmember into the endmember collection dialog box. These endmembers were collected from an image that was already rotated in MNF space, so there was no need to convert the endmembers into MNF rotated endmembers.

Each endmember that was used as input produced two output images: 1) MTMF Score image showing the mapped pixels with their DN designating the probability of the pixel matching the reference endmember, 2) an Improbability Score shows the degree of probability of a pixel being not correctly identified. Figure 4.19 and 4.20 show the MTMF Score for shellfish and mud overlaid on the HyMAP subset image with values stretched between 0-1 with a color density slice. Interestingly, mud is found in the same locations as shellfish although pixels classed as mud indicated a lower probability of correctness but pixels classed as shellfish indicated a higher probability of correctness.

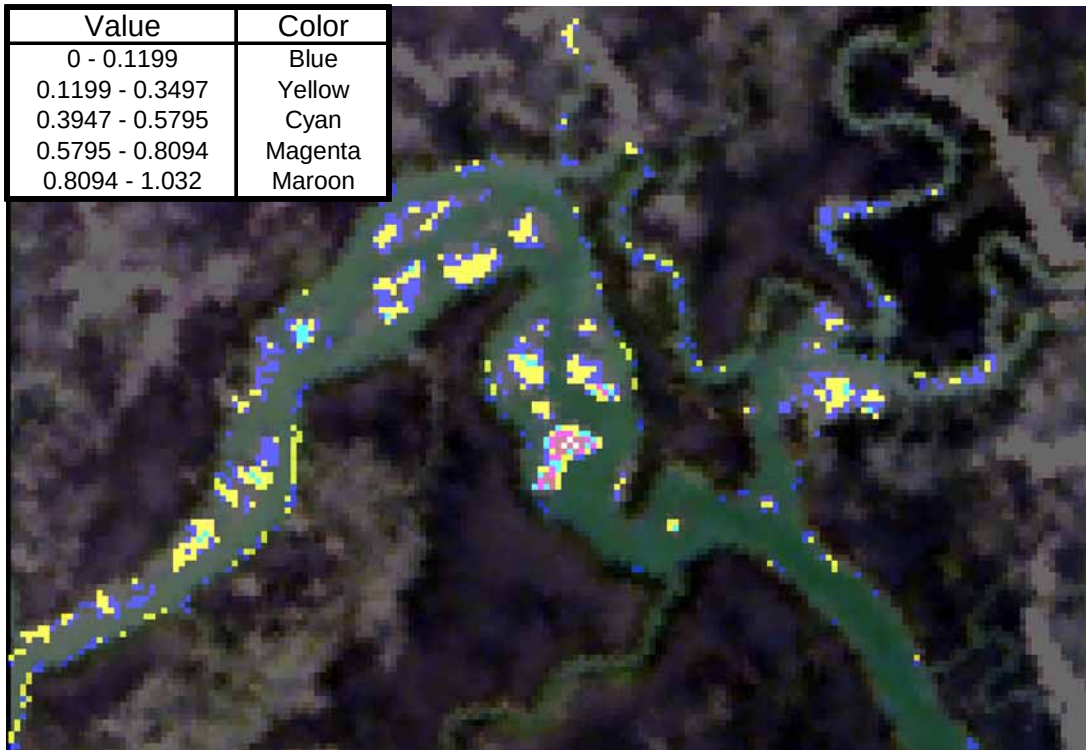

Figure 4.19 - MTMF Oyster Result with HyMAP Bands 2-61 Image

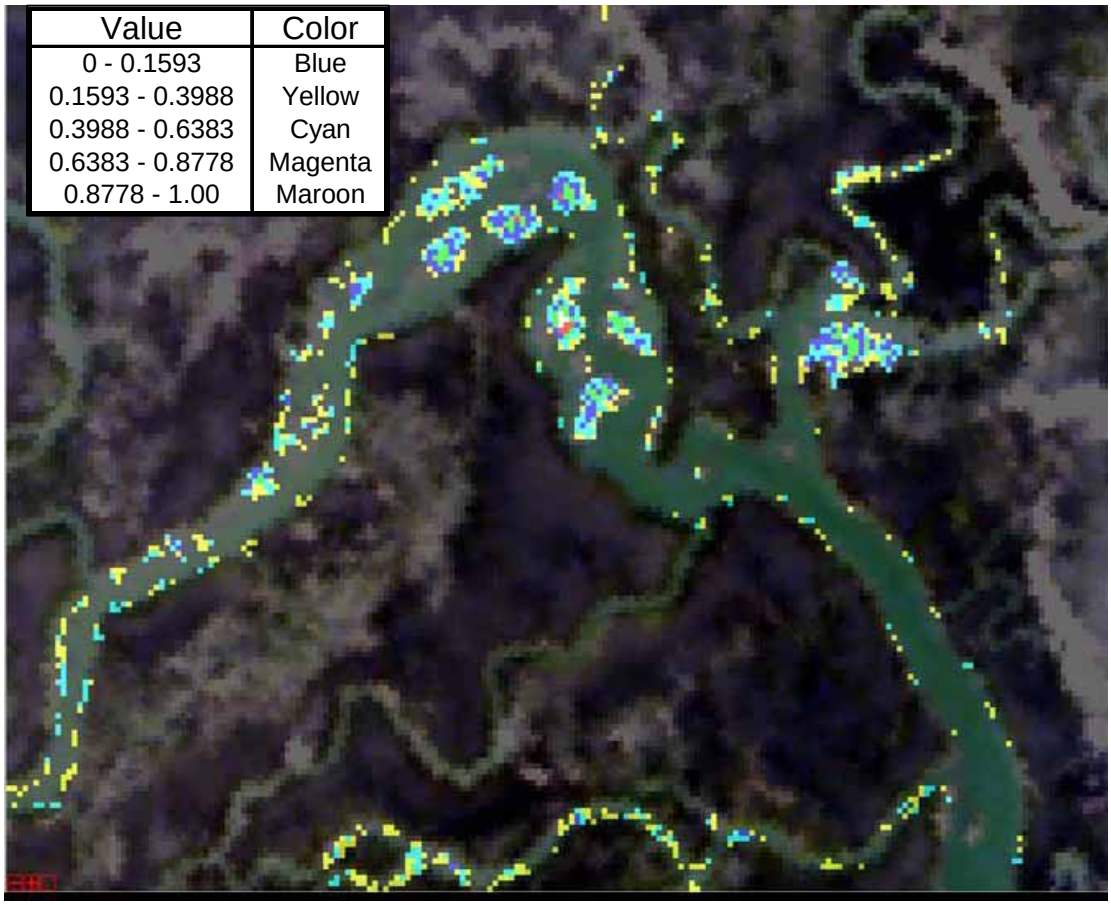

Figure 4.20 - MTMF Mud Result with HyMAP Bands 2-61 Image

Mud was also found to have a greater areal extent than shellfish. From *a priori* field work, there are areas known to contain shellfish but were not classified as shellfish. Using the 2-dimensional scatter-plot of the MTMF Score versus the Infeasibility Scores, we can select endmembers with a high MTMF score and low Infeasibility Score. The 2-dimensional scatter-plot in figure 4.21 shows the distribution of endmembers with the MTMF scores along the *x*-axis and the infeasibility scores plotted along the *y*-axis with selected endmembers. Selection of endmembers that have a low infeasibility and high MTMF score are shown in the figure.

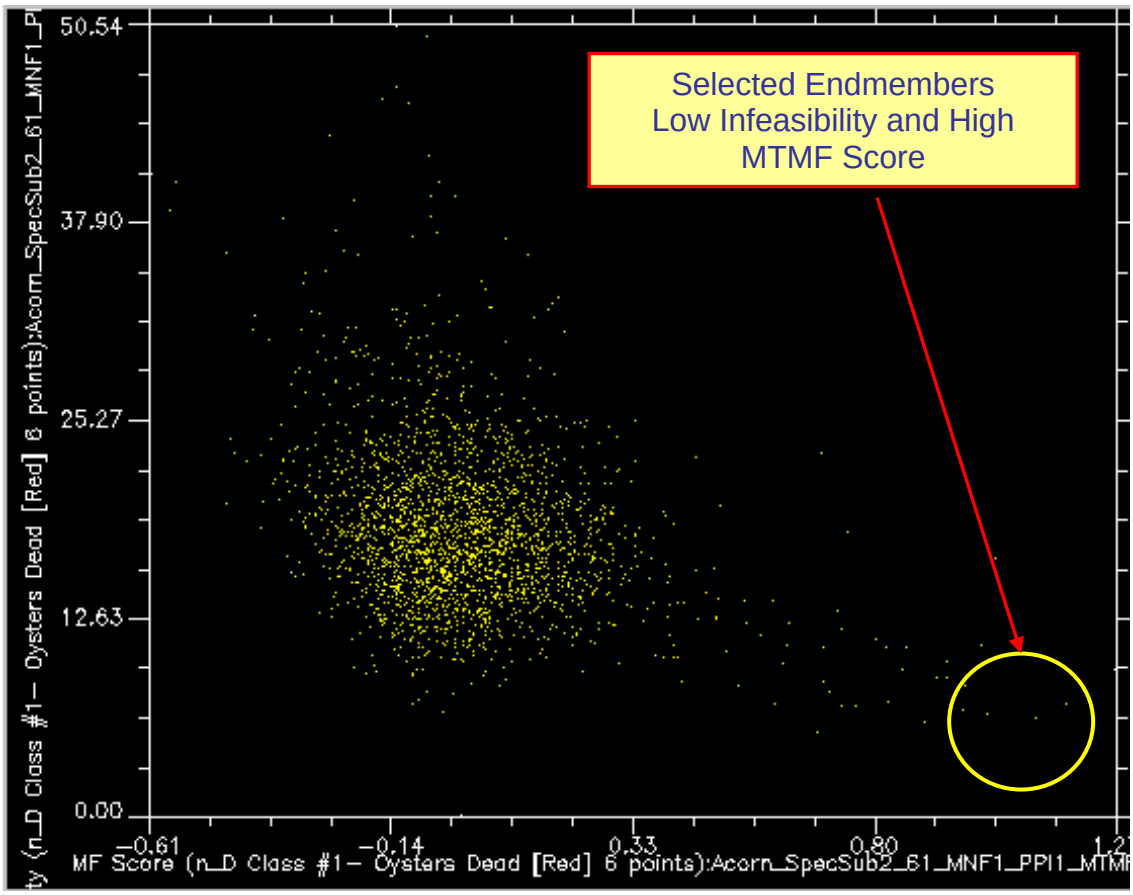

Figure 4.21 – Scatter-Plot of MTMF Scores vs. Infeasibility

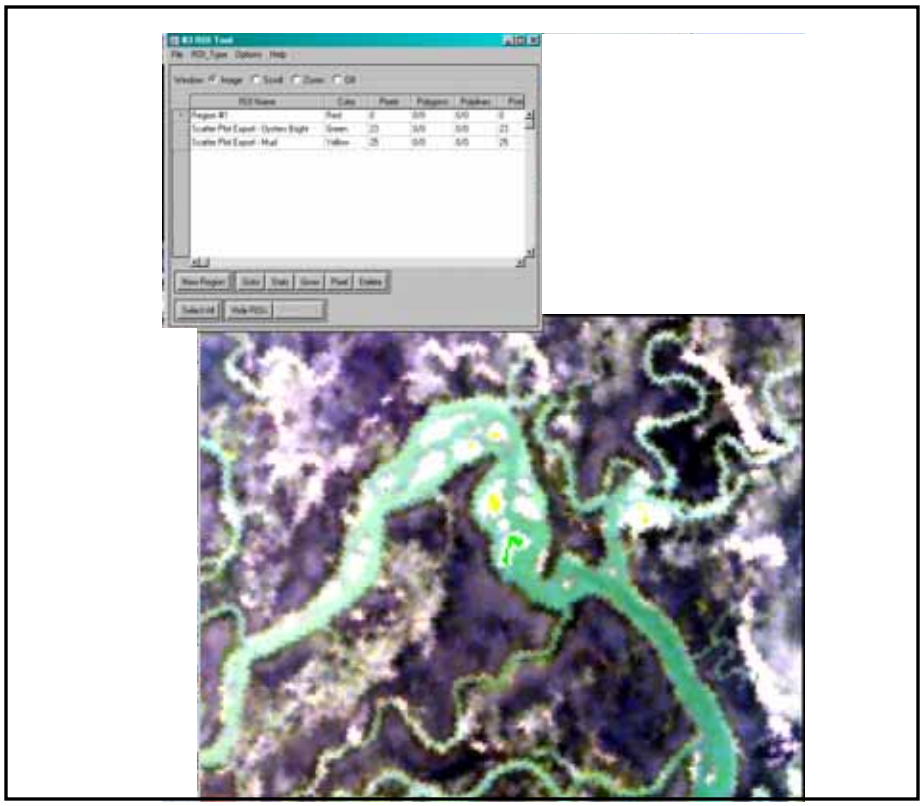

Figure 4.22 – Location of Library Spectra of Shellfish and Mud from Bands 2-61

Collection of these endmembers was accomplished by exporting the endmembers then saving as library spectra. After they have been exported they are viewable within the HyMAP image (figure 4.22) showing mud (yellow) and shellfish (green) endmember library spectra. These endmembers were used for input for the next round of MTMF mapping. From the first round of mapping the endmember values of the mapped shellfish pixels ranged from -0.55697 to 1.2690.

4.6.2.1 HyMAP Second Round MTMF

An item worth noting in figure 4.23 showing locations of pixels classified as shellfish, the area where the library spectra were located also have the most pixels classed as shellfish with fewer pixels classified as shellfish further away from the library spectra. Second round mapping for shellfish and mud (figures 4.24.and 4.25) produced results that showed an increase in the range of pixel probability values.

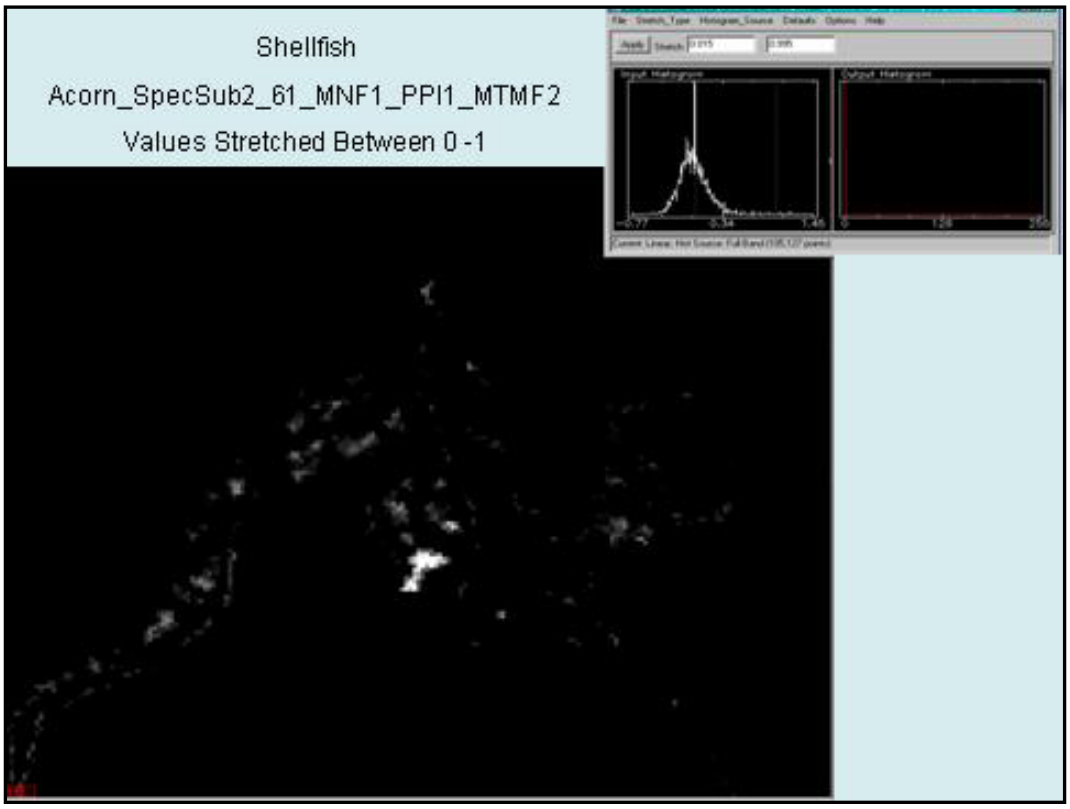

Figure 4.23 – MTMF Second Round Mapping of Shellfish

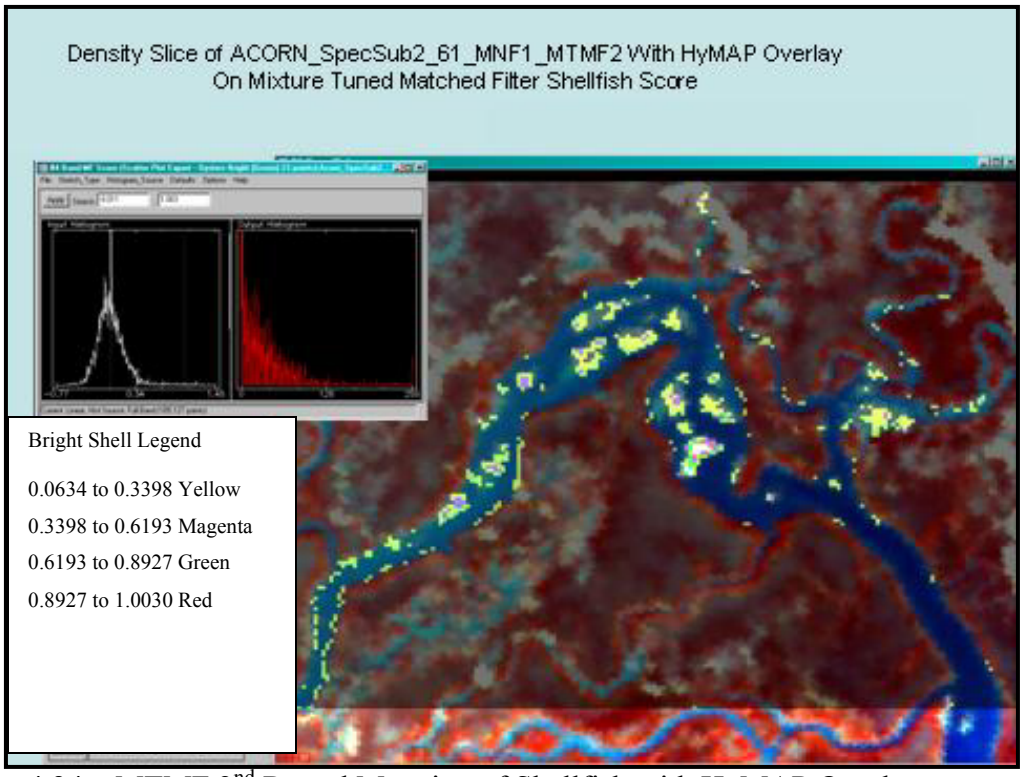

Figure 4.24 – MTMF 2nd Round Mapping of Shellfish with HyMAP Overlay

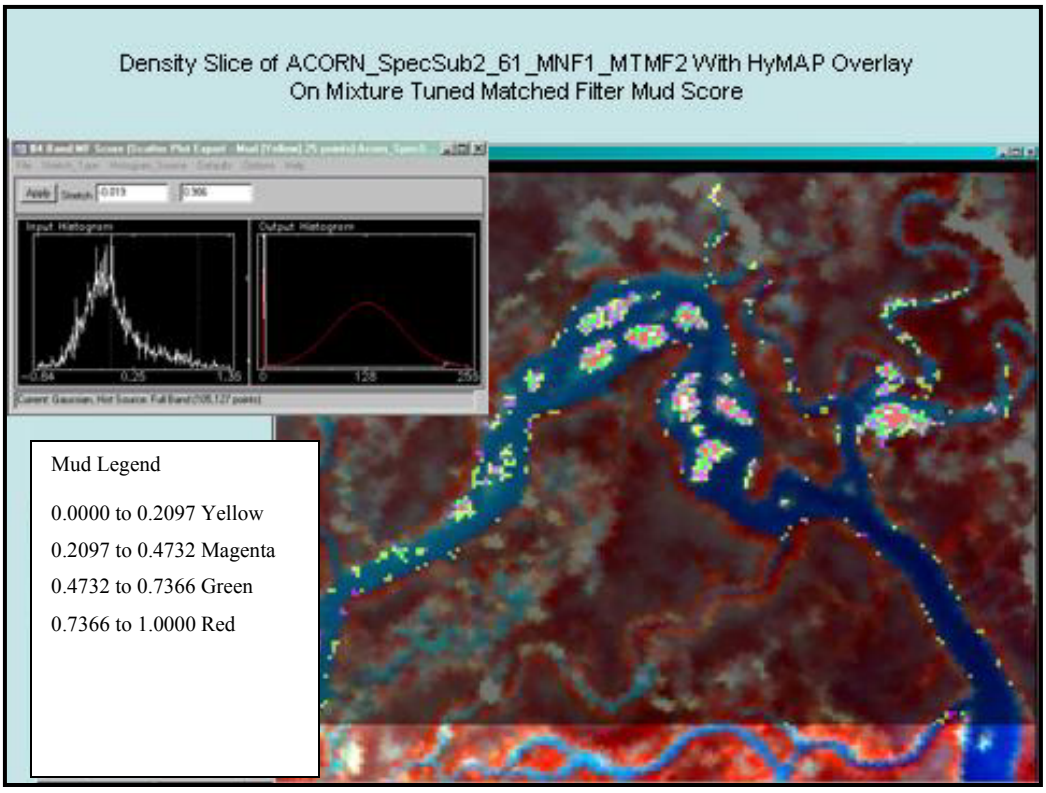

Figure 4.25 – MTMF Second Round Mapping of Mud

4.6.2.2 HyMAP Bands 2-44 Mixture Tuned Matched Filtering

Two bundles of endmembers representing shellfish and mud were derived from the HyMAP imagery bands 2-61 spectral subset and the same set of endmembers were utilized for the initial round of mapping using the MNF images derived from the bands 2-44 HyMAP spectral subset. These same endmembers were used to measure the change in results from using the same set of endmembers for both spectral subsets. Initial endmember selection was with the use of ENVI's N-Dimensional Visualizer utilizing a refining process using the 2-dimensional plot to select endmembers with the lowest infeasibility and highest score. Two sets of endmembers were the result after two iterations of refinement and are referred to as Bright Shell and Mixed Shell endmembers with each having 5 and 6 endmember bundles respectively. The endmember bundles are so named because the five Bright Shell endmembers are aggregated closely together on top of the BOB 4 study sight in an area that has oysters with a higher reflectance due to washed shells. The Mixed Shellfish are distributed throughout the study within locations that show areas of higher density live oysters.

The first endmember bundle, Bright Shell had the best accuracy within the general location of the endmembers, the top of BOB 4 patch reef. Figure 4.26 shows the results from the MTMF mapping using the Bright Shell endmember bundle.

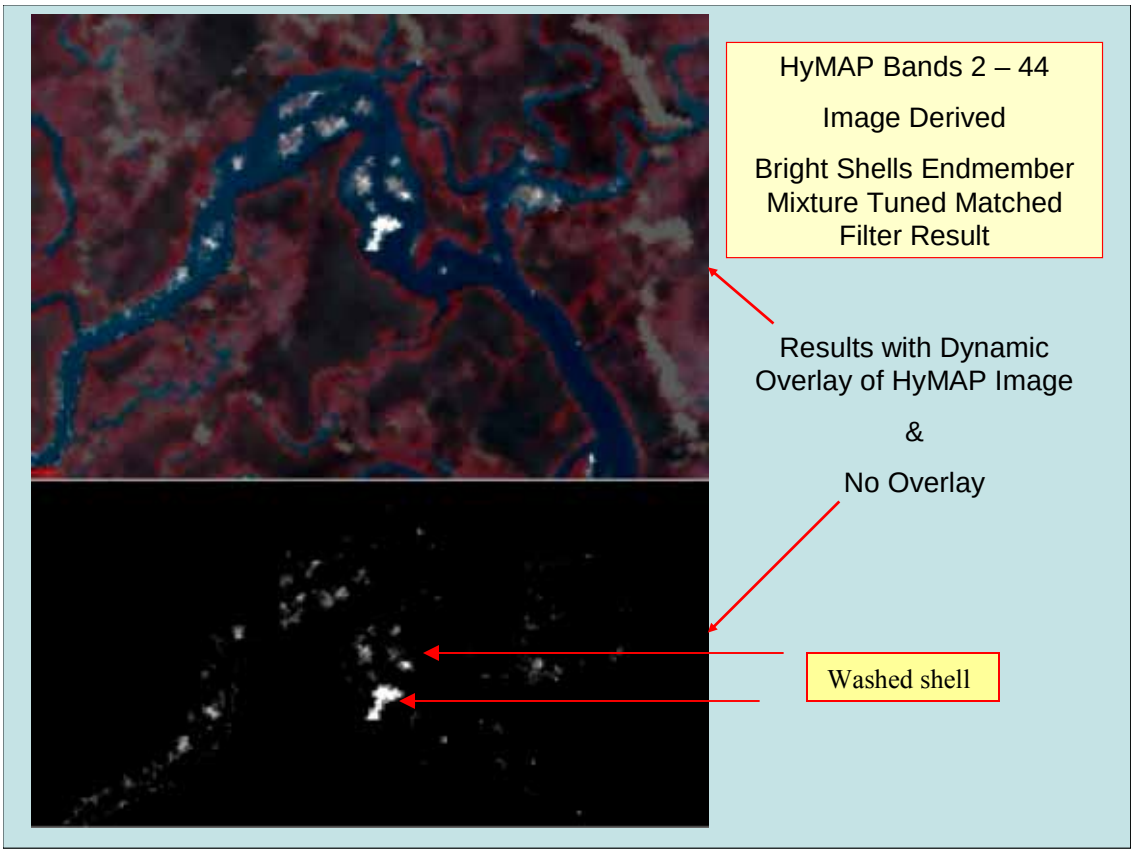

Figure 4.26 - MTMF Results for Bright Shell Bundle with HyMAP Bands 2-44

The image with the HyMAP over lay shows the best detail of BOB 4 study site and also the location of the best shellfish mapping accuracy. A smaller location just north of the BOB 4 study site also shows an area with washed shells. The results from the Mixed Shell endmember bundle is displayed in figure 4.27. The Mixed Shell endmember bundle indicates results with a distributed shellfish classification. A visual inspection shows the shellfish to be patchy and fragmented.

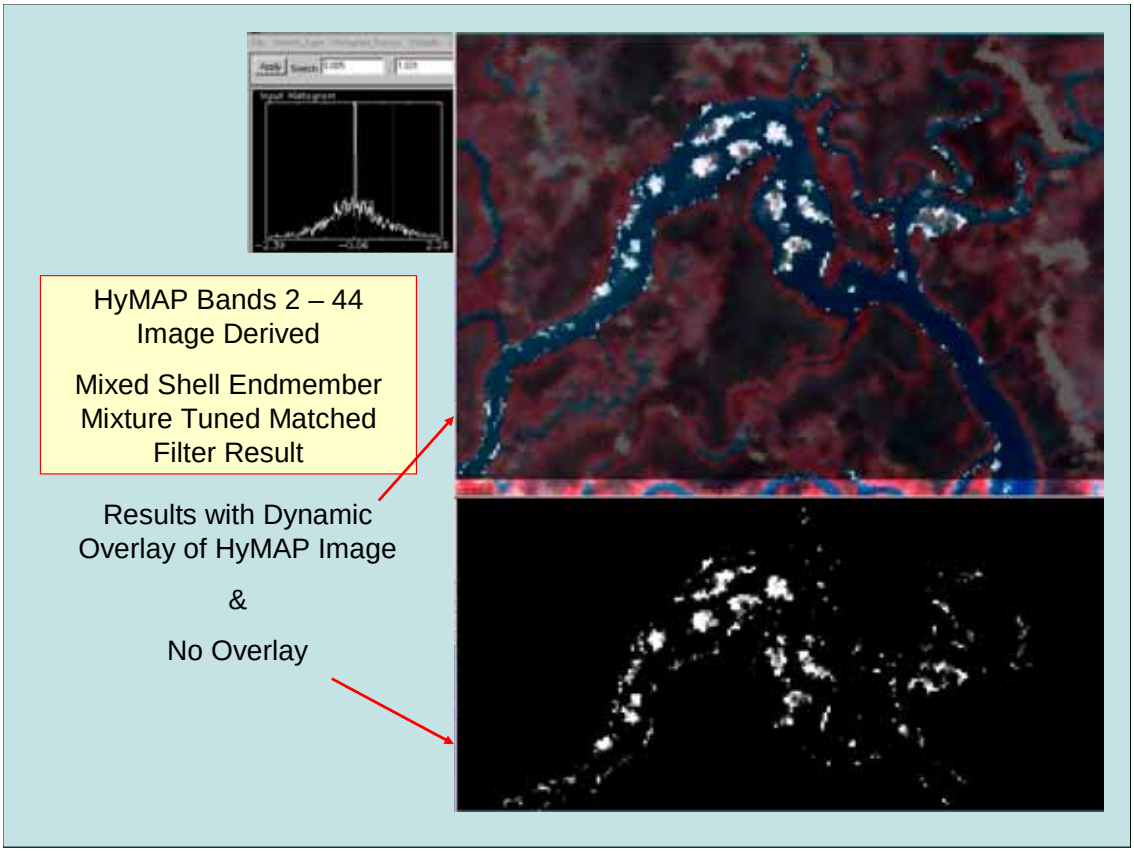

Figure 4.27 - MTMF Results for Mixed Shell Bundle with HyMAP Bands 2-44

4.7 MTMF from *In situ* Derived Endmembers

4.7.1 Mapping *In situ* Endmembers Using AISA Imagery

The mapping of the AISA remotely sensed imagery, as described in the Methodology section, started with masking then executing an MNFT to reduce the dimensionality of the data and eliminate any band-to-band correlations. This aspect of the methodology was the same for all datasets analyzed. Before the MTMF is executed, the user must decide on which endmember to use as inputs. If the user chooses to utilize *in situ* endmembers then the implementation of the Pixel Purity Index is skipped and the *in situ* endmembers are convolved to match the specific bandwidths of the imagery. A MNF transformation is then implemented on the *in situ* endmembers prior to inclusion into the MTMF algorithm.

4.7.1.1 MNF Rotation of *In situ* Endmembers

In order for *in situ* derived spectral endmembers to be utilized for spectral analysis, they must first be convolved to match the specific bandwidths of the imagery that was to be mapped. Because the remotely sensed images were transformed using the MNF rotation algorithm, the spectral signatures were also transformed. A graph of the spectral signatures from the image-derived endmembers taken from the BOB4 sample site alongside the aggregated in situ spectral signatures collected from the same sample site that have not been convolved to match the AISA band-width (figure 4.28). Visual inspection of this figure shows for the most part, the endmembers and *in situ* curves line up spectrally with little deviation except in magnitude of reflectance. The red/infrared shift for both the shorter AISA derived endmembers and the *in situ* spectral signatures all coincide. The AISA derived endmembers do not match the spectral range of the *in situ* endmembers due to the *in situ* spectral endmembers not having been convolved to match the AISA spectral range and bandwidth. Figure 4.29 shows after the *in situ* spectral endmembers have been convolved to match the AISA spectral bandwidth and range. The spectral signatures in red are *in situ* endmembers that have been aggregated and convolved to match the AISA imagery bandwidth and spectral range. The black spectral signatures are the AISA spectral endmembers that were derived from imagery at the BOB 4 sample site.

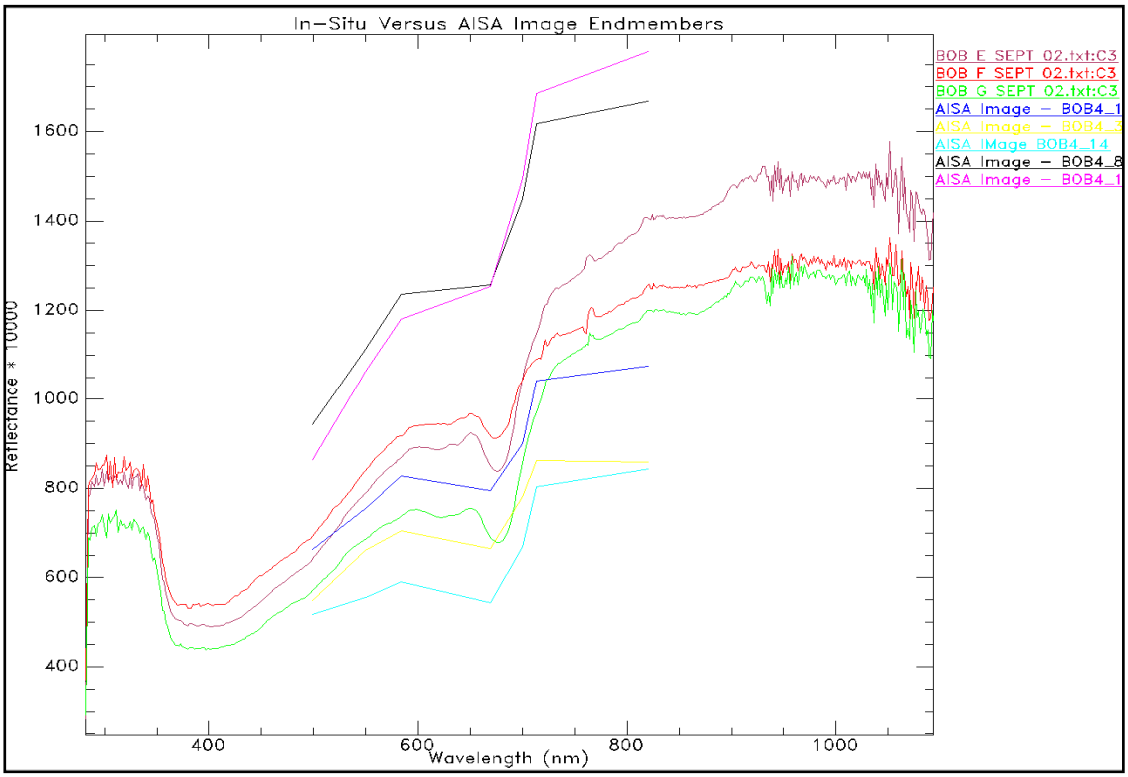

Figure 4.28 - Spectral Curves of *In Situ* and AISA Imagery Shellfish

The *in situ* endmembers align very closely with the image endmembers, the exception being that it appears the image-derived endmembers (black) have a lower reflectance than the *in situ* endmembers. This may be the result of image and *in situ* endmembers acquired on different dates or differences in radiometric corrections. This underscores a concern that is expressed in the literature on the accuracy of using *in situ* derived versus image-derived endmembers for mapping. The literature supports this contention that better results are obtained using imaged derived endmembers for the reasons stated above (Elmore, et al. 2000).

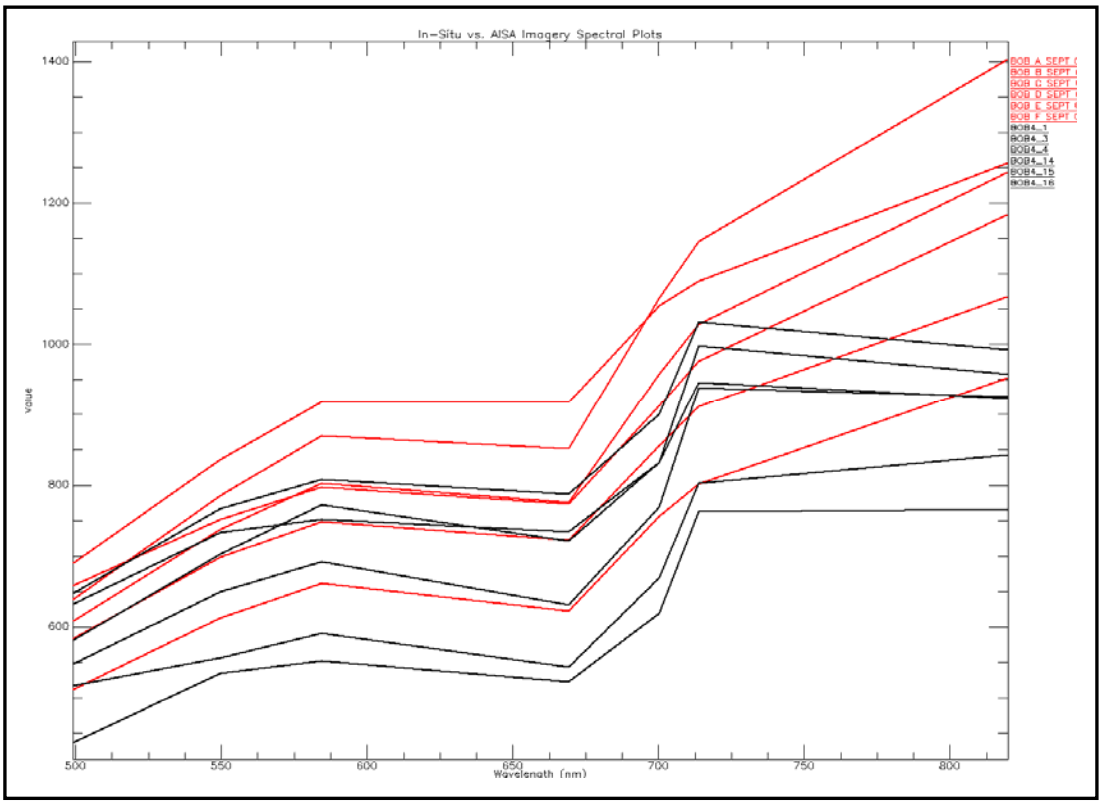

Figure 4.29 – Convolved *In Situ* Endmembers & AISA Image Endmembers

4.7.1.2 AISA Mixture Tuned Matched Filtering

Using the convolved *in situ* endmembers and the AISA image, the endmembers were mapped in two parts. The first part used the *in situ* endmembers aggregated from BOB 1 through 3, (aggregated clusters BOB A through C). The second part utilized *in situ* endmembers from BOB 4, (aggregated clusters D through G). The rationale for mapping the *in situ* endmembers in two parts is due to the *n-1* constraint. Additionally, the first set of endmembers were not native to the study area of interest but the sample sites BOB 1-3 are the closest to BOB 4 than any other sample site. Endmembers needed to be tested to see if those that were derived from the study site had the same level of mapping accuracy as endmembers derived from the area of interest. Figures 4.30 - 4.32 shows the last two revisions of mapping using BOB A through C *in situ* endmembers.

Figure 4.30 - BOB A *In Situ* MTMF Mapping Result

BOB B MTMF Score

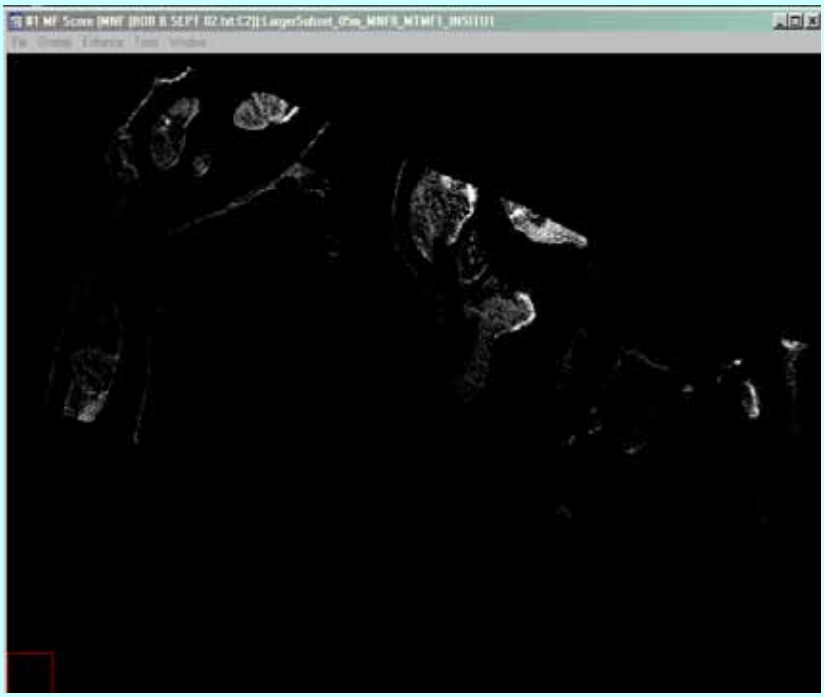

Infeasibility (y) vs. MTMF Score (x)

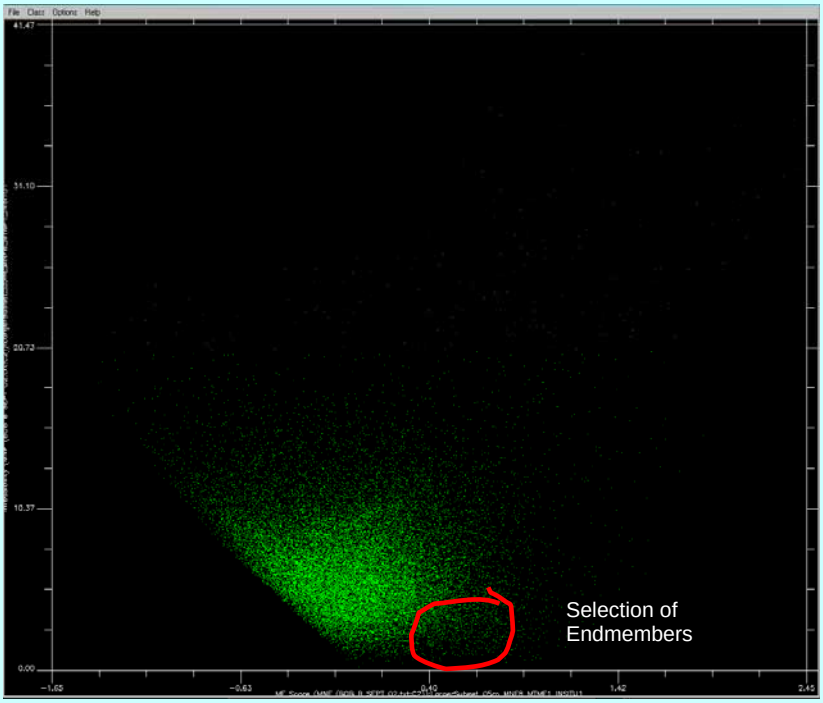

Figure 4.31 - BOB B *In Situ* MTMF Mapping Results & Scatter-Plot

BOB C MTMF Score

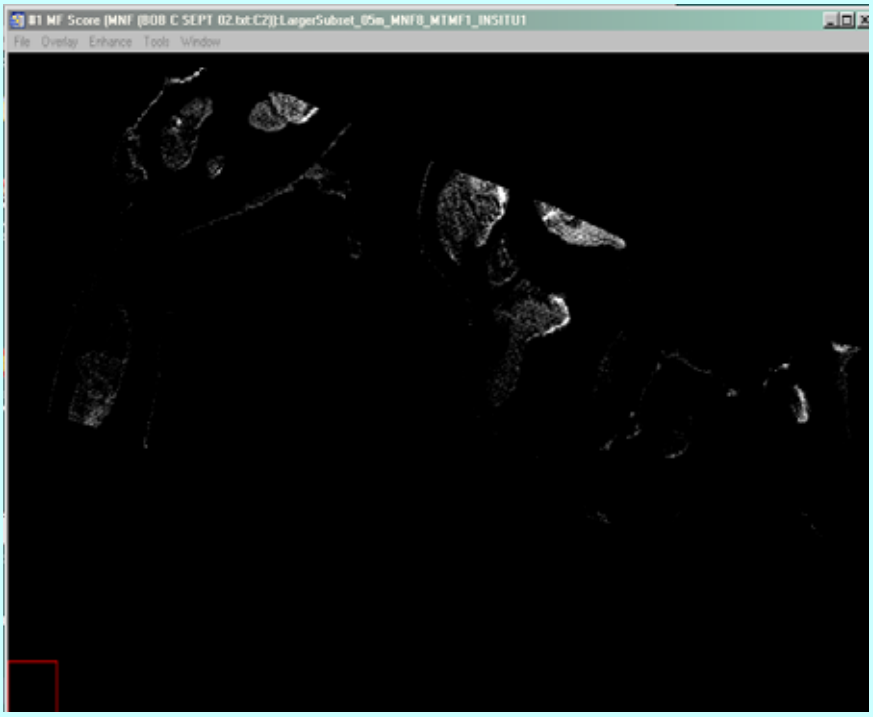

Infeasibility (y) vs. MTMF Score (x)

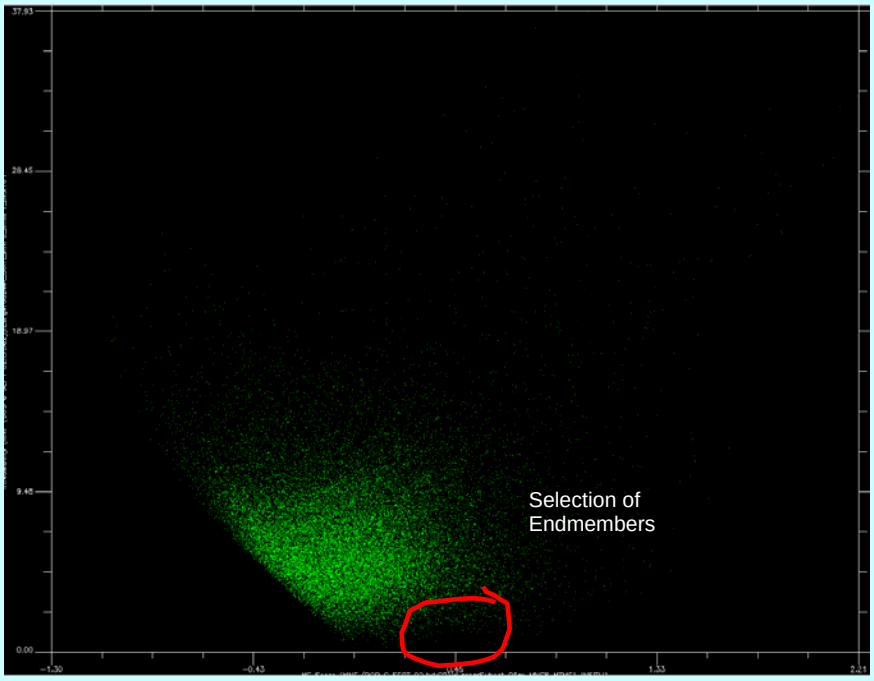

Figure 4.32 - BOB C *In Situ* MTMF Mapping Results & Scatter-Plot

The MTMF results were very similar between BOB A, BOB B, and BOB C *in situ* endmembers. Endmembers that were collected using the scatter-plots were unique as measured by the Jeffries-Matusita Transformed Divergence test (scores greater than 1.8). When *in situ* endmembers BOB D through F were utilized for mapping the AISA imagery and the subsequent endmember revisions were made using the 2-dimensional scatter-plots, the revised endmembers were not unique and were combined into a single endmember bundle. Figure 4.33 shows the result from mapping these single class endmembers.

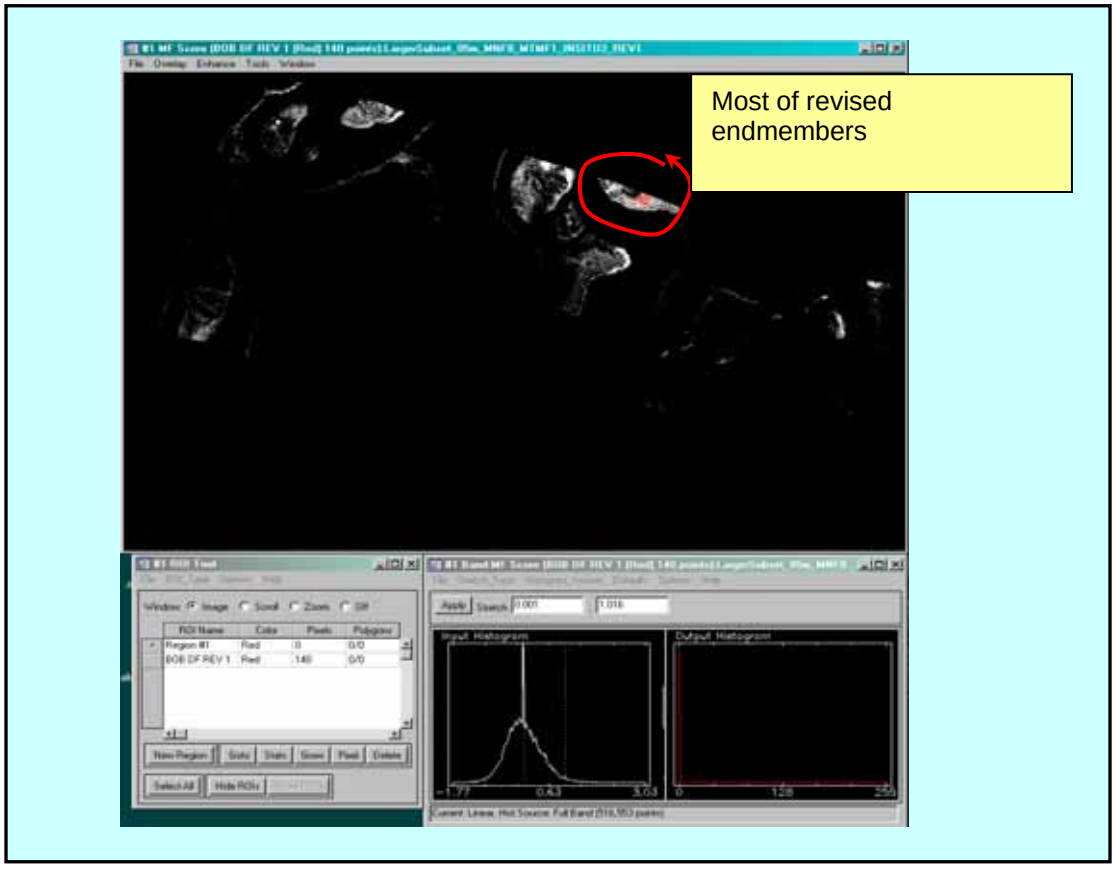

Figure 4.33 - BOB D Through F (combined) Revision 1 - Endmembers with AISA

Of interest to note that when the revised endmembers are shown on the MTMF score, their location is geographically different than where they were sampled in the field, but they are located in an area that contains dead brightly reflective shells, few live

shellfish and a similar type of strata as found on top of BOB4 (BOB D through G was sampled *in situ* from BOB 4).

4.7.1.3 *In situ* Spectral Mapping Using HyMAP Imagery

Mapping the 4.0 x 4.0 meter HyMAP imagery with *in situ* endmembers follows the same analysis flow schema as described in Figure 3.8 in the Methodology section. The spectral image analysis was performed using a subset of HyMAP bands 2 - 44. A limitation of the *in situ* spectral data is the GER 1500 spectroradiometer calibration is from 350 to 1050 nm, in contrast the HyMAP imagery spectral range is 439 nm to 2482 nm. To utilize the *in situ* endmembers, the HyMAP imagery had to be subset to the same relative spectral range of the *in situ* data. Consequently, the HyMAP subset that was utilized for the purpose of mapping the *in situ* endmembers were bands 2 through 44 (452.9 – 1078.8 nm). The *in situ* endmember sets were derived from BOB A through Bob G sample sites (see Appendix 7.3 – Shellfish Secondary Aggregation for specific sample points used) which were convolved to match the HyMAP band widths and spectral range. Figure 4.34 graph shows the convolved *in situ* endmembers with HyMAP endmembers of shellfish from the BOB 4 sample site.

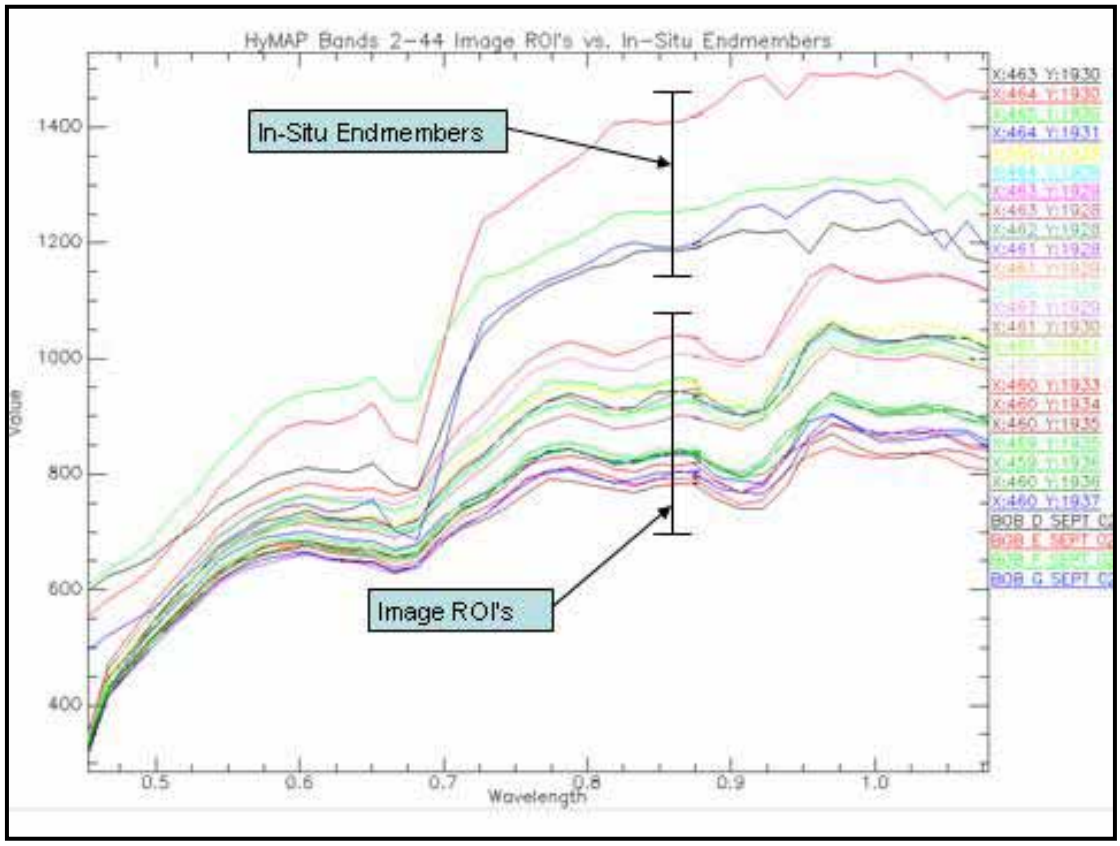

Figure 4.34 - Comparison Between HyMAP and *In Situ* Endmembers

The overall alignment between the HyMAP and *in situ* endmembers is very good but it is also interesting to see there is a greater slope increase in the red to infrared between the *in situ* and image endmembers. At approximately 700 nm, the *in situ* endmembers exhibit a greater overall reflectance than the *in situ* endmembers.

4.7.1.4 HyMAP *In Situ* Mixture Tuned Matched Filter (MTMF)

The initial runs used the convolved *in situ* spectral endmembers from BOB A through G and the endmembers from a shellfish patch reef located within the subset image. The success of using *in situ* endmembers for identifying patch reef was marginal. This set contained seven shellfish endmembers from the aggregated *in situ* endmembers with all but one resulting in the data range being extremely narrow (the data being centered on zero, representing the suppressed background data). The result of mapping BOB E *in situ* endmembers is shown in figure 4.35, which is an aggregate of mostly deceased shellfish that have higher over-all brightness.

Subsequent mapping efforts and refinement of the BOB G endmembers was accomplished using the 2-dimensional scatter-plot. After three successive rounds of mapping and refining endmembers, figure 4.36 shows the result displayed with density slice over-lay to identify pixels that are highest scoring for shellfish.

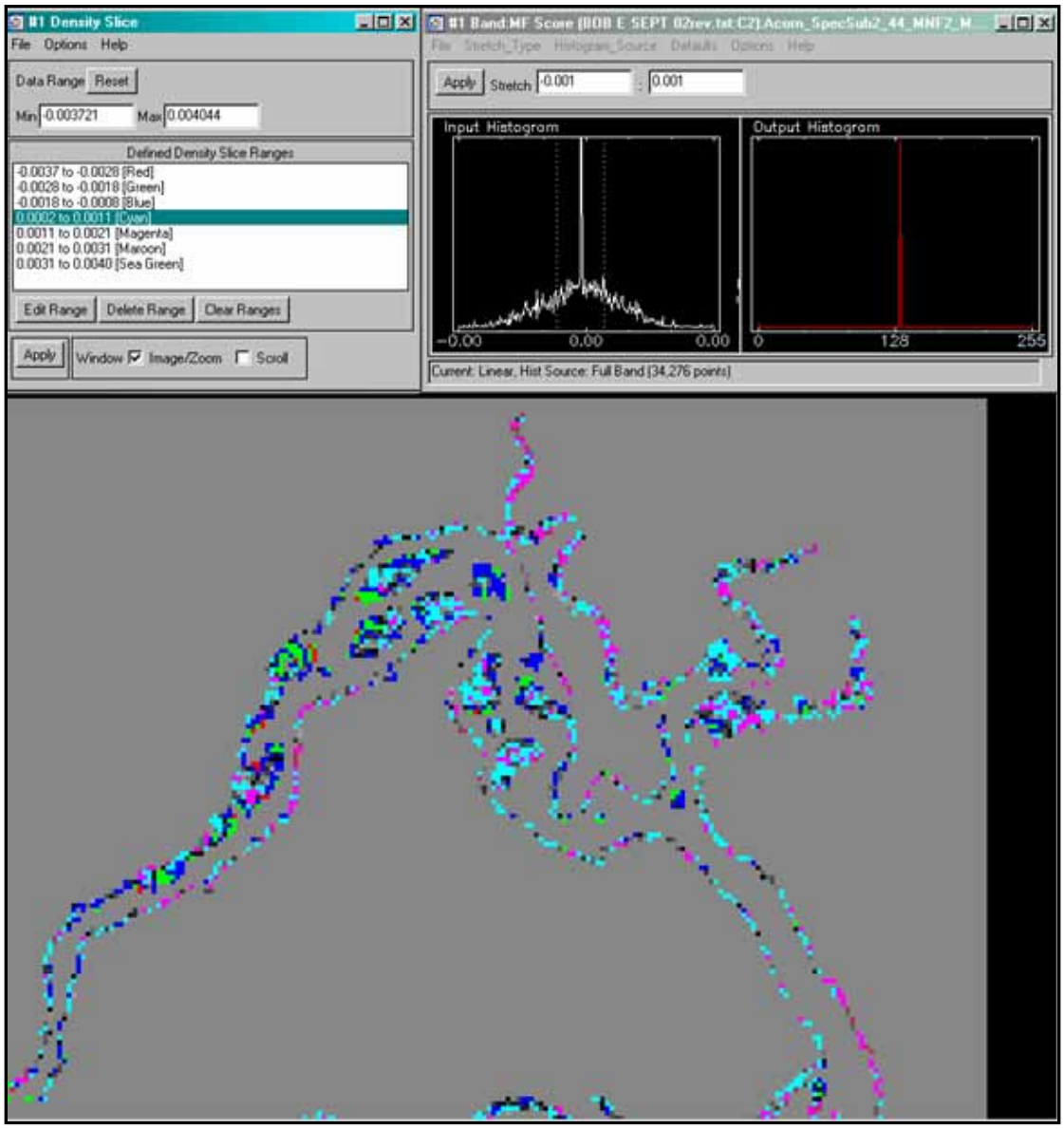

Figure 4.35 - MTMF Result for BOB E *In situ* Endmembers

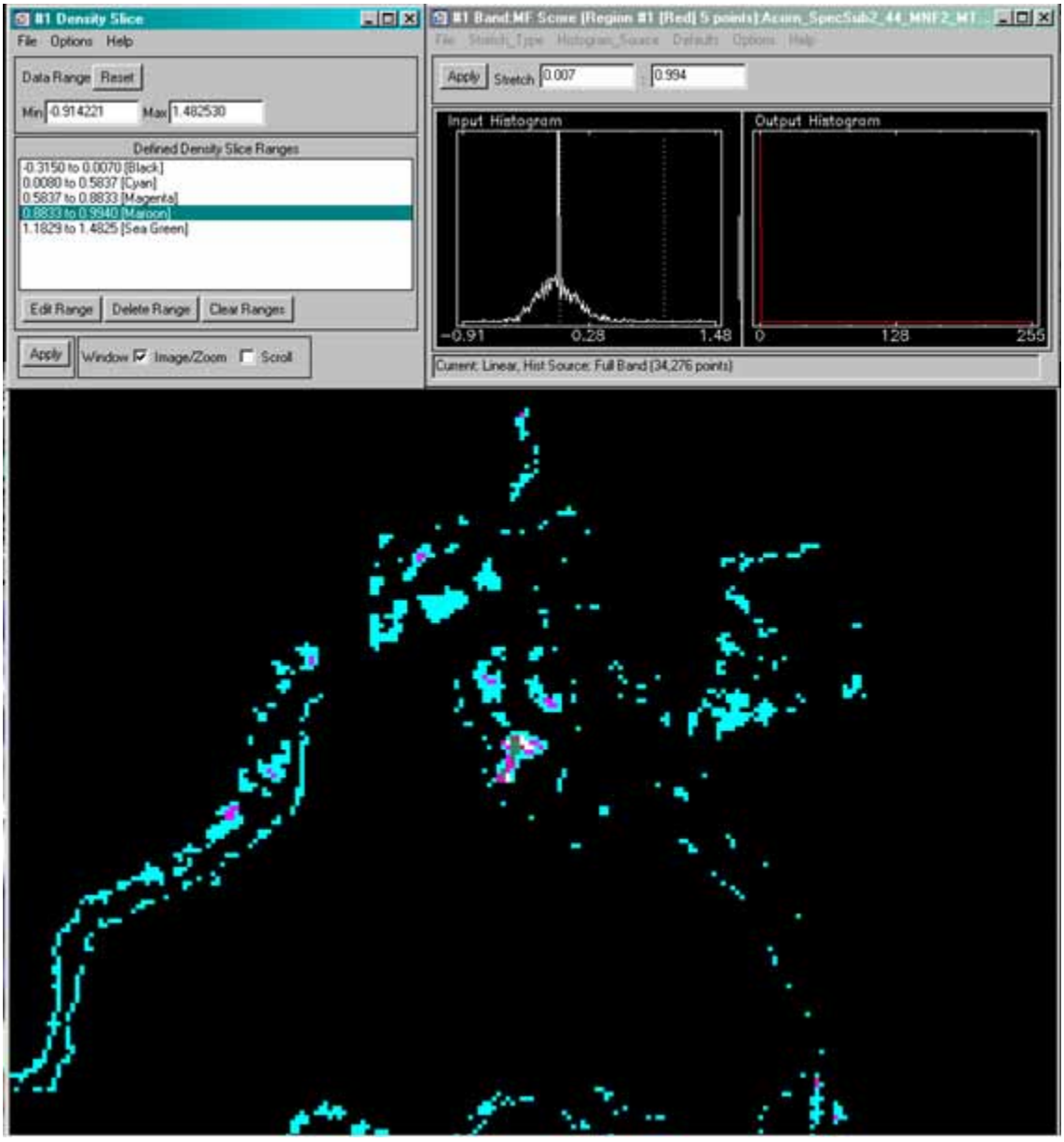

Figure 4.36 - MTMF 5 BOB "G" In Situ Endmembers

These runs were more promising, resulting in wide data range with values from -1.22 to 1.98. The image in Figure 4.36 was stretched between 0.013 and 0.995 to show pixels that have the highest probability of being shellfish. Of interest is BOB G which is primarily composed of shellfish from BOB 4. This sample site contains live vertical clustered shellfish with not as many dead washed shells that exhibit higher spectral reflectance. Since the *in situ* endmembers originated from BOB 4 (larger patch reef), it

was expected these features would map with a higher probability. This assumption proved correct. In addition, there were additional pixels mapped that showed higher probabilities of being correctly mapped as shellfish on the left side of the image and to the north. Pixels colored cyan indicate a lower probability of being correctly mapped than the sea green and magenta pixels.

4.8 Accuracy Assessment

The following show graphically with comment the creation of the "apparent truth" GeoVantage oyster map that was created to assess the "found" mapped AISA and HyMAP oyster maps. Only the resulting images of "found" oysters, correctly mapped, incorrectly mapped, omitted oysters, and a composite image showing correct, incorrect, and omitted are shown from each assessment.

The first treatment is the creation of an "apparent truth" oyster map that shows the locations of identified polygons of shellfish clusters that were found within the study area. The length of an individual shellfish ranges in size from 3 inches to 8 inches, but the smallest individual grouping of shellfish is determined by the spatial extent of the GeoVantage imagery used for the reference image. The spatial extent of the GeoVantage imagery and thus the minimum mapping unit (MMU) is 0.25 x 0.25 meter. The acquisition date and time of day of the imagery is unknown but was collected in 2005 (pers. comm. Coen, 2005). The imagery was collected as part of a statewide coastal survey in conjunction with the National Oceanic and Atmospheric Administration (NOAA) and the South Carolina Department of Natural Resources. The term "apparent truth" is used to denote that although every effort was used to accurately verify the degree of truthfulness of the "apparent truth" map through the use of field notes and pictures, but there is no guarantee to the degree of absolute truth of the "apparent truth" map. Additionally, there are some discrepancies between study area sizes between the HyMAP, AISA, and GeoVantage imagery. The GeoVantage 0.25 X 0.25 meter spatial resolution imagery retained an extent of the study site that was as big as or bigger than either of the other sets of data. Hence, only shellfish found within the AISA or HyMAP

data sets that were found contained within or partially contained within the GeoVantage "apparent truth" image were included in the accuracy assessment.

4.8.1 Creation of the GeoVantage "Apparent Truth" Map

The creation of the apparent truth oyster map was accomplished using a combination of several classification methods. The first treatment was to use Visual Learning System's Feature Analyst to classify the larger patch and fringing shellfish reefs. The results obtained were satisfactory with the exception that after considerable amounts of time and various shape representations within Feature Analyst, smaller clusters of shellfish isolated on larger patch reefs and fringing reefs were missed. With the aid of *a priori* field experience, field notes, and photographs, these areas were mapped by manual digitization techniques. The ability to visually identify small isolated clusters of shellfish was in part due to the 0.25 x 0.25 meter spatial resolution of the GeoVantage imagery. The use of visual classification and inspection was critical to the creation of the apparent truth oyster map. The following figure 4.37 exemplifies the high spatial resolution nature of the GeoVantage imagery and the ability to identify various classes of shellfish with an inset of the apparent truth oyster map.

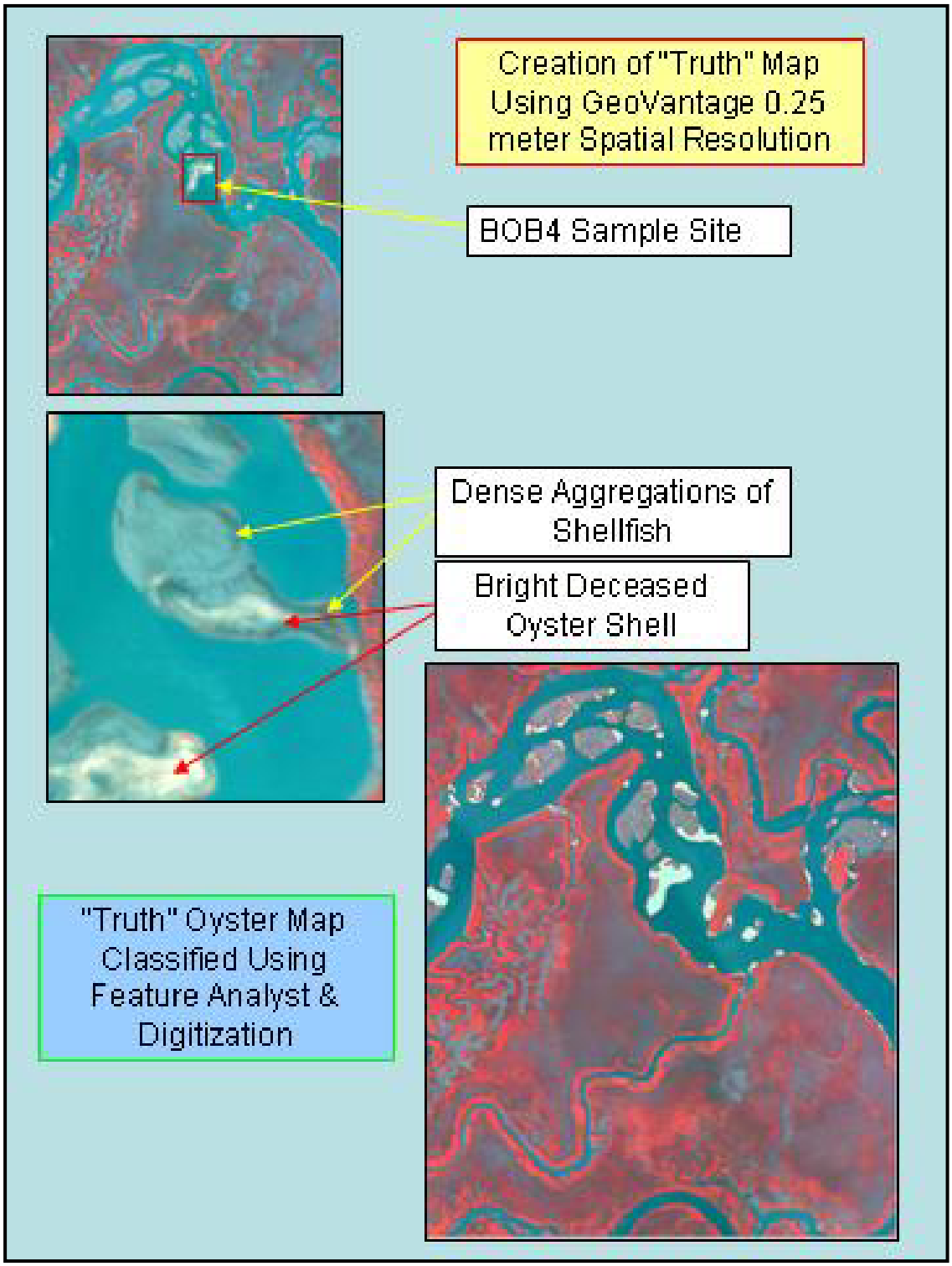

Figure 4.37 – Creation of GeoVantage "Apparent Truth" Map

4.8.2 HyMAP MTMF Assessment

4.8.2.1 HyMAP Spectral Subset Bands 2-61

The first results obtain with the HyMAP image was with the spectral subset of bands 2-61 (452.9 – 1324.7 nm). As previously stated, HyMAP was spectrally subset into two separate subsets so the image endmember analysis would approximate the spectral range that was used for the *in situ* derived spectral analysis. The inclusion of bands 45-61 constituted the inclusion through the short-wave infrared region of the electromagnetic spectrum. Earlier trials had indicated an increase in the detection of shellfish with the inclusion of the short-wave infrared bands. A spectral subset of the HyMAP bands 2-44 was necessary so as to compare with the field derived endmembers analysis. Figures 4.38a – 4.38c shows the results of the HyMAP bands 2-61 spectral subset accuracy assessment. The "oysters mapped" inset image shows the extent of the oysters mapped using the MTMF method. The correctly mapped oysters show those oysters from the oysters' mapped images that are correctly mapped. The remaining three inset images show oysters that were mapped but were incorrect, oysters that were not mapped but should have been mapped as oysters, and an image showing correctly mapped oysters, incorrectly mapped oysters, and omitted oysters are shown together in a single image.

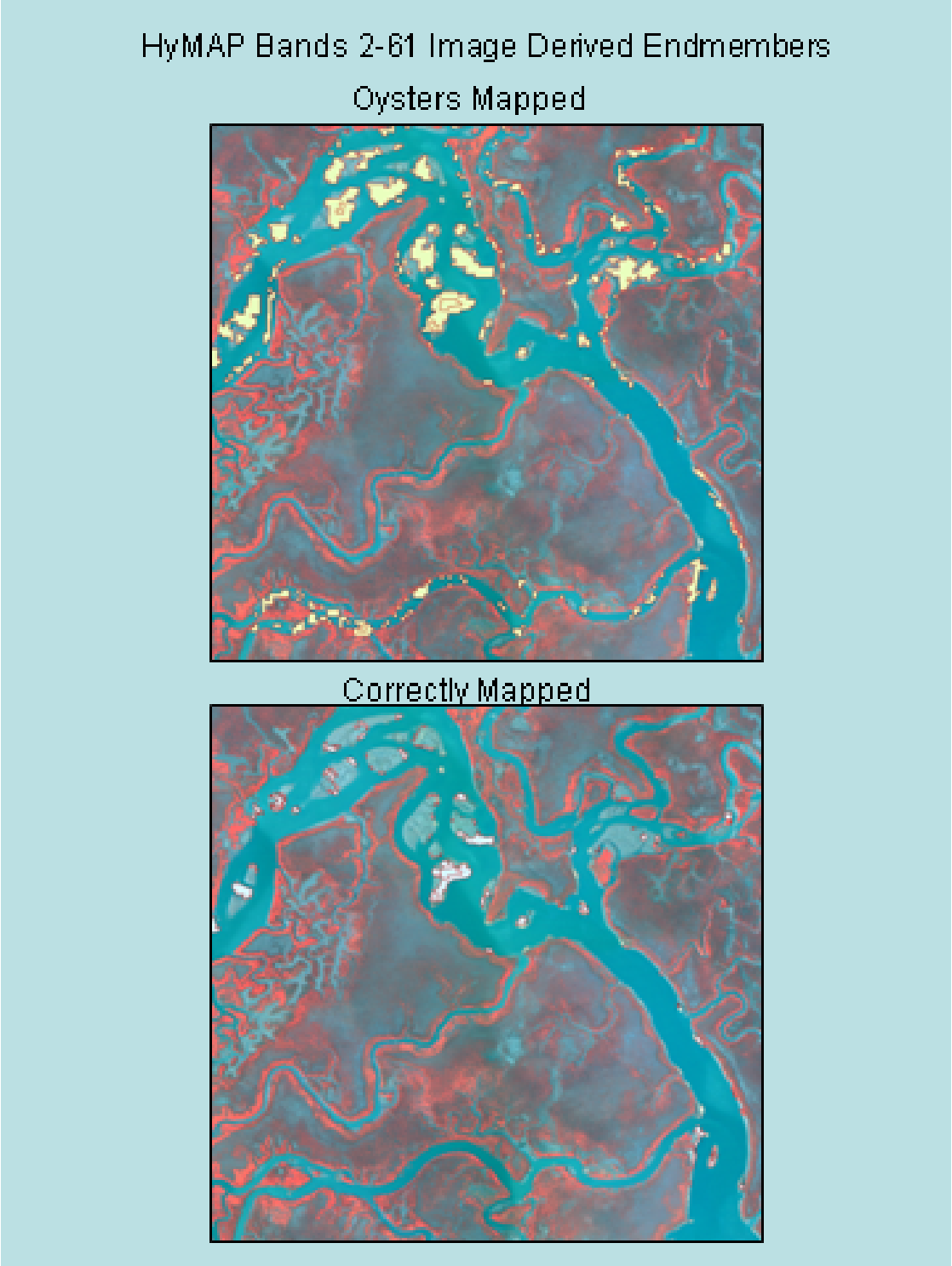

Figure 4.38a – HyMAP Bands 2-61 Oyster Mapping Accuracy Assessment Results

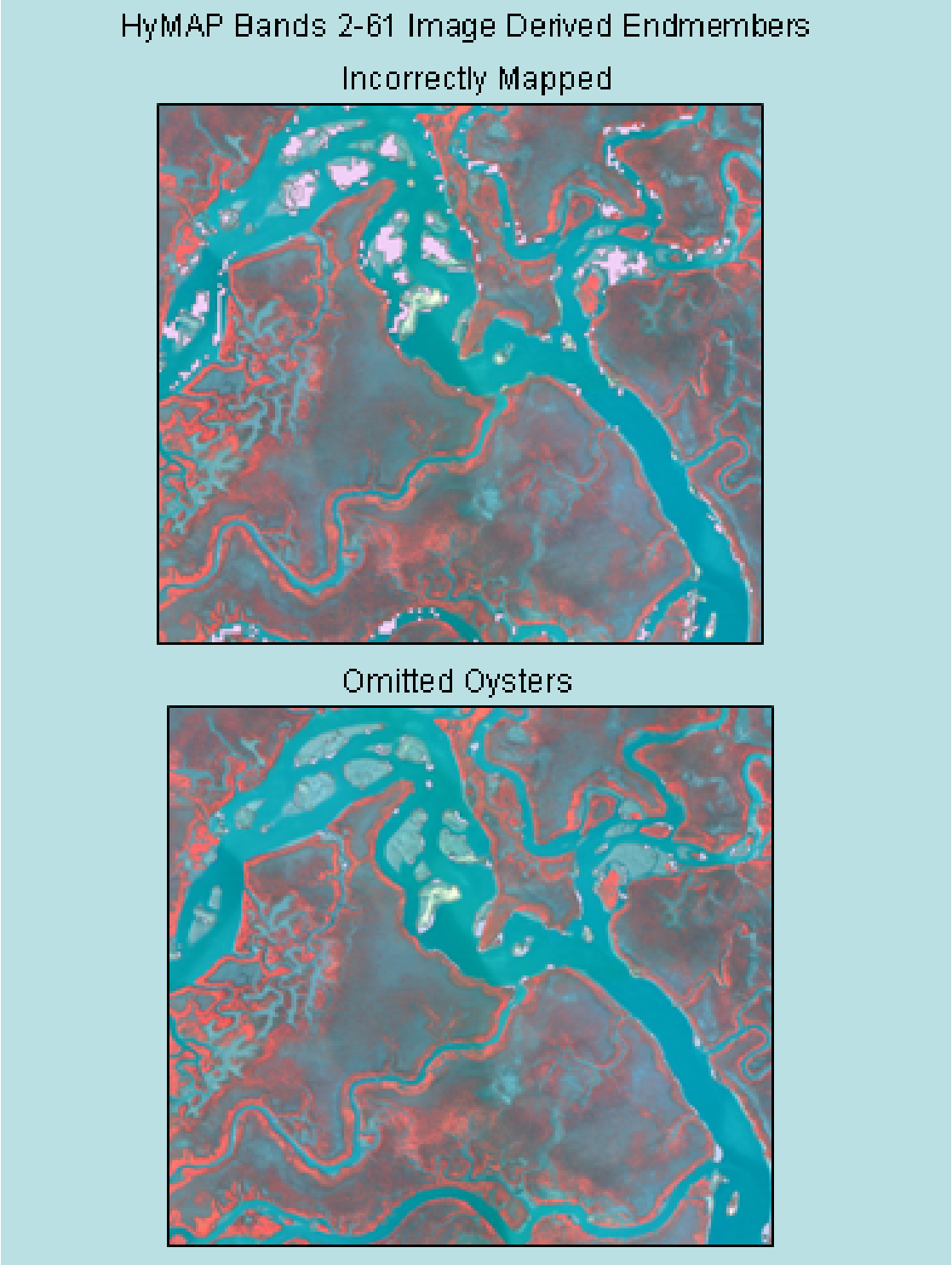

Figure 4.38b – HyMAP Bands 2-61 Oyster Mapping Accuracy Assessment

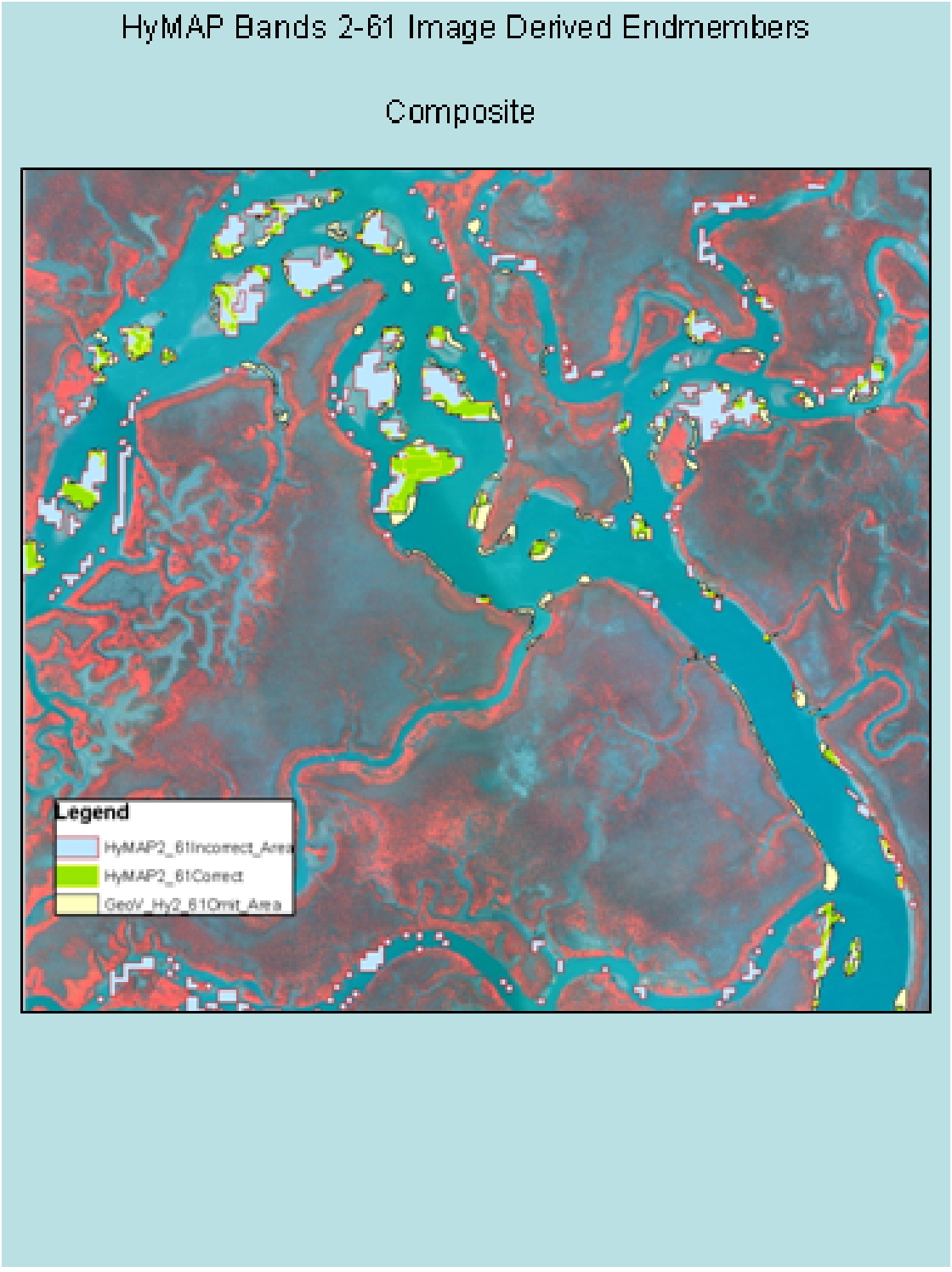

Figure 4.38c – HyMAP Bands 2-61 Oyster Mapping Accuracy Composite

Most notable for the HyMAP oyster maps is the larger extent of the raster converted polygons. As noted above the 4 x 4 meter spatial extent of the HyMAP imagery has inflated the total area of the area that is considered to have shellfish. The approach behind the analysis of using the 2-61 and 2-44 bands subset is to test if higher yields result from the addition of extra bands in the short-wave infrared region. Although it may have yield a higher probability of oysters contained within a cell, these result may not be apparent due to the inflated areal extent from the HyMAP. Put another way, the MTMF result tells only the probability of a cell having oysters but not the abundance or location of oysters within the polygon.

4.8.2.2 HyMAP Spectral Subset Bands 2-44

The HyMAP bands 2-44 spectral subset used endmembers that were derived from the imagery but was also subset to the spectral range that was comparable to the field hand-held spectroradiometer. Two endmembers were found from the MTMF analysis: Bright Shell from the top of the study site BOB 4; Mixed Shell composed of either F or F1 strata that show live scattered clusters of oysters.

Figures 4.39a - 4.39c visually shows the accuracy results from the HyMAP bands 2-44 image derived endmembers subset. What is notable is the near complete classification of all patch reefs as oysters. Very few portions of the patch reefs are not considered oysters.

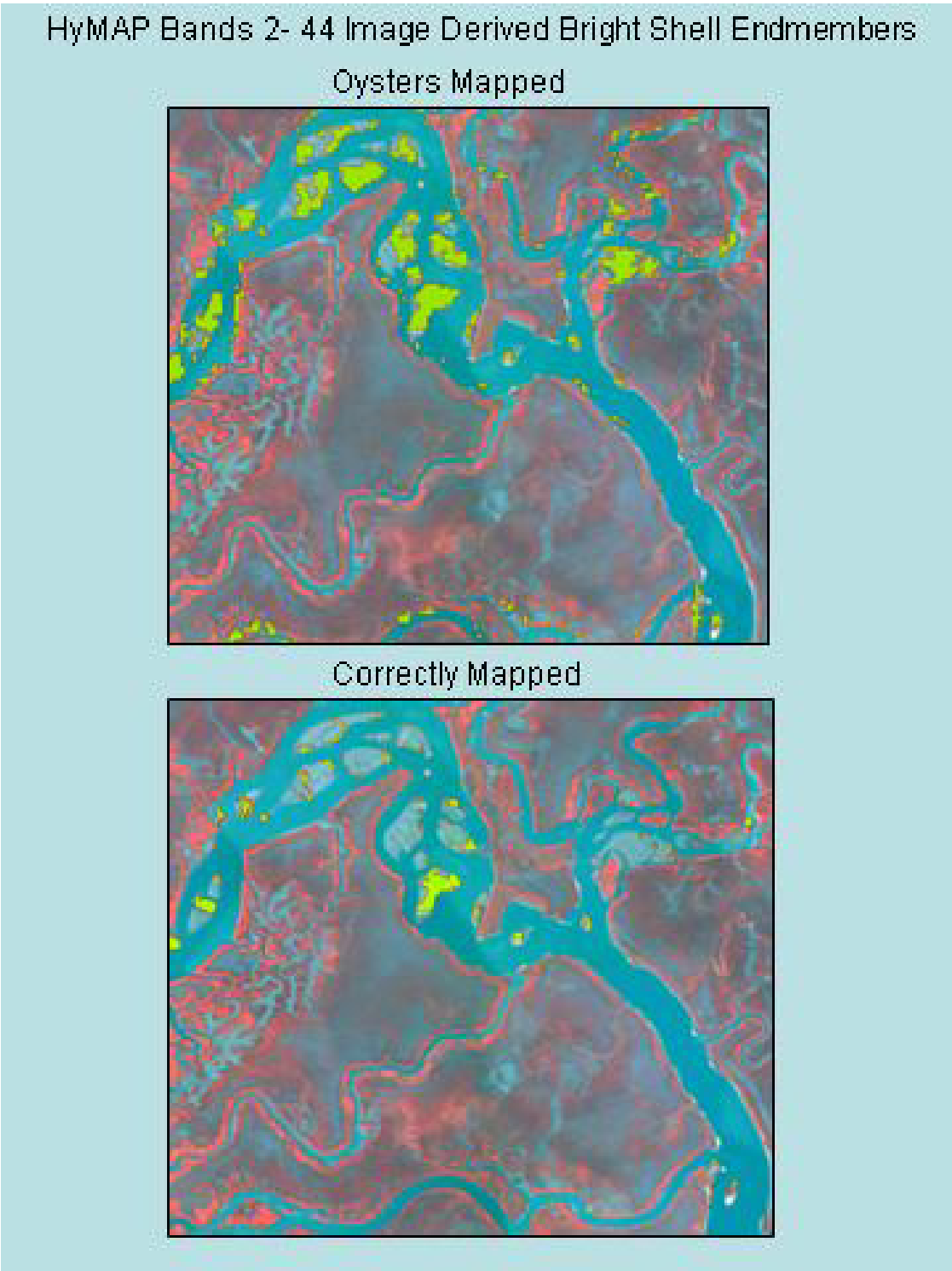

Figure 4.39a – HyMAP Bands 2-44 Bright Shell Accuracy Assessment Results

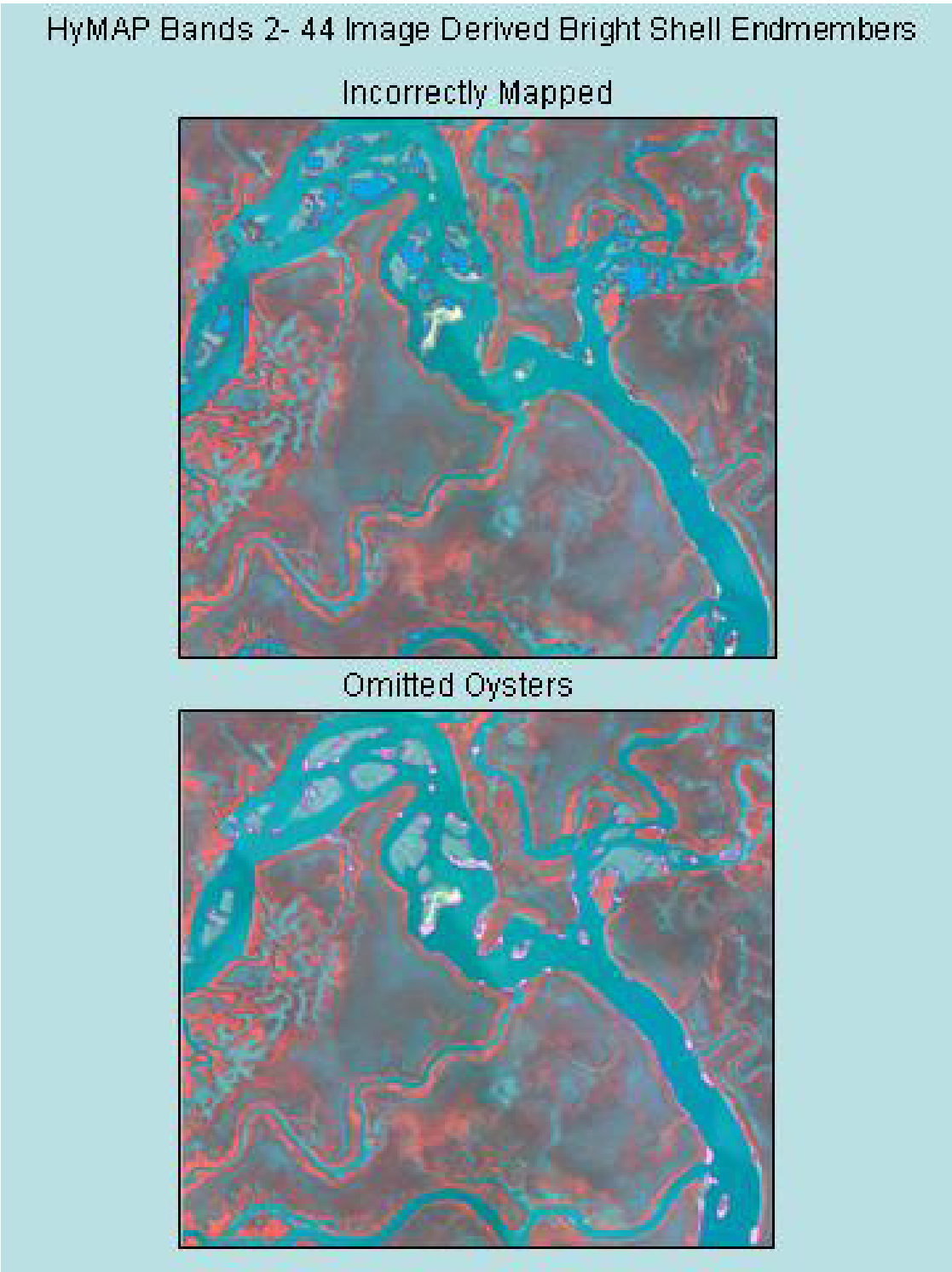

Figure 4.39b – HyMAP Bands 2-44 Bright Shell Accuracy Assessment Results

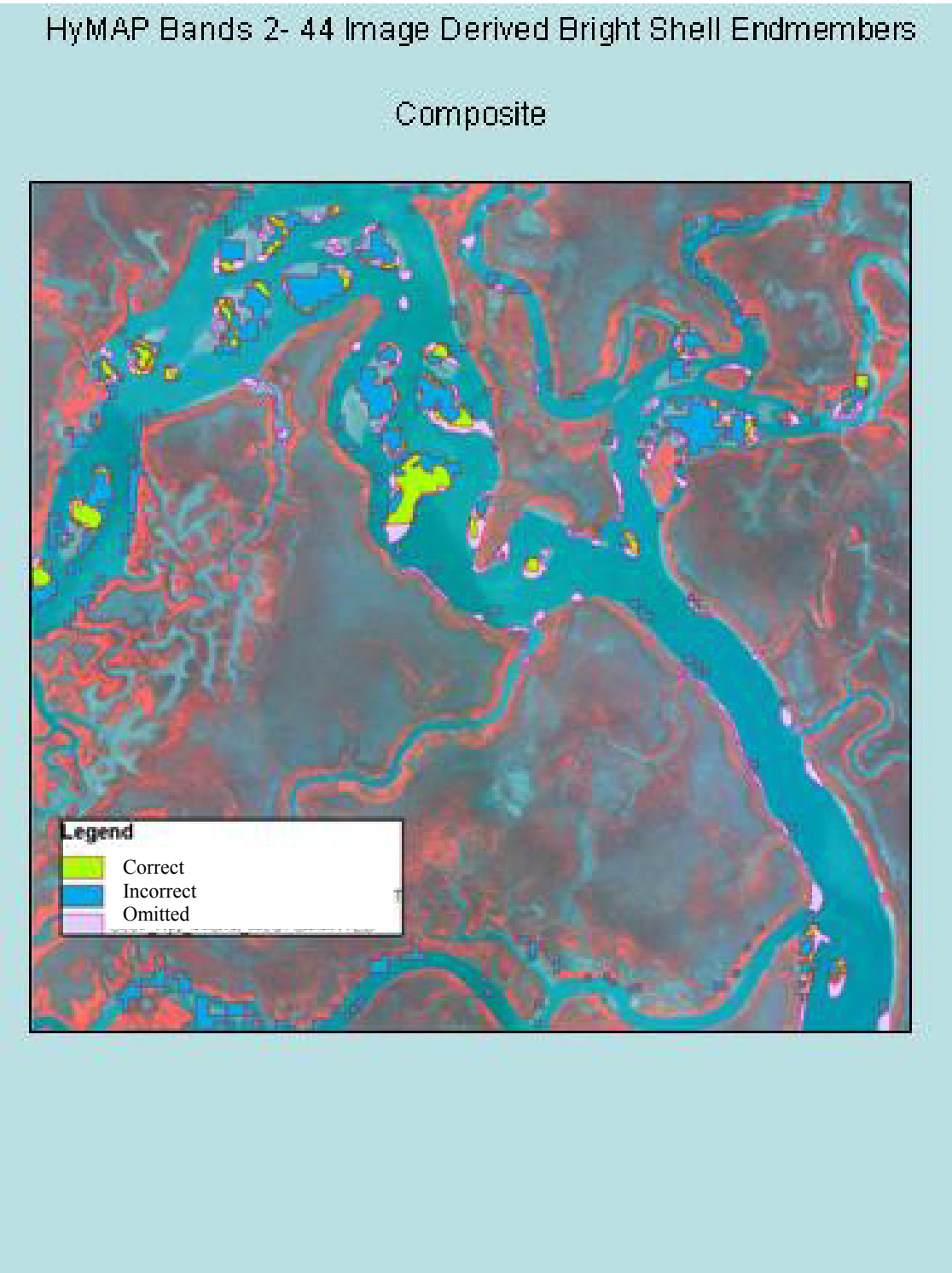

Figure 4.39c –HyMAP Bands 2-44 Bright Shell Accuracy Assessment Composite

The following figures 4.40a – 4.40c shows the accuracy assessment results from the mixed shell endmember analysis derived from the HyMAP image.

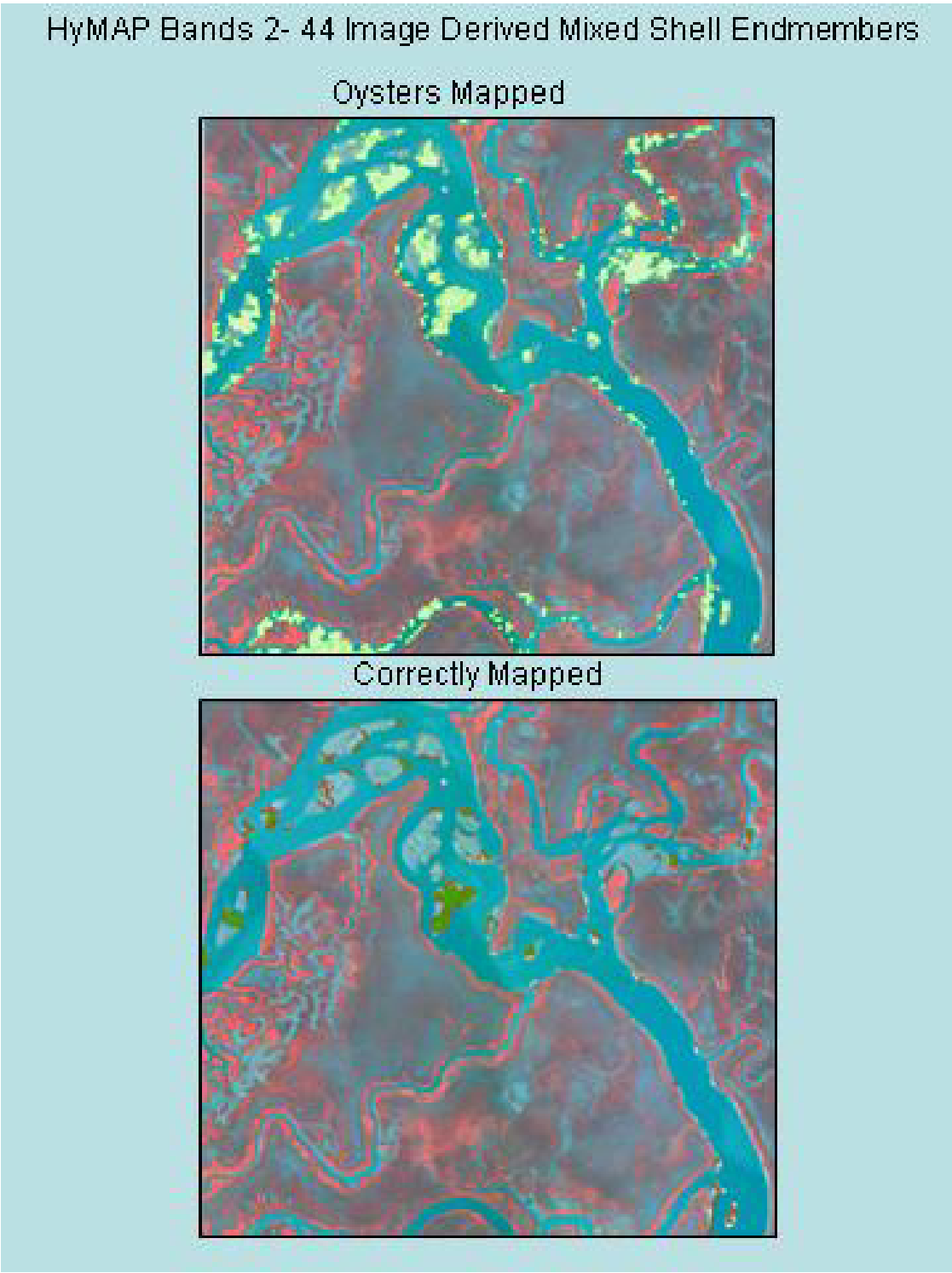

Figure 4.40a – HyMAP Bands 2-44 Mixed Shell Accuracy Assessment Results

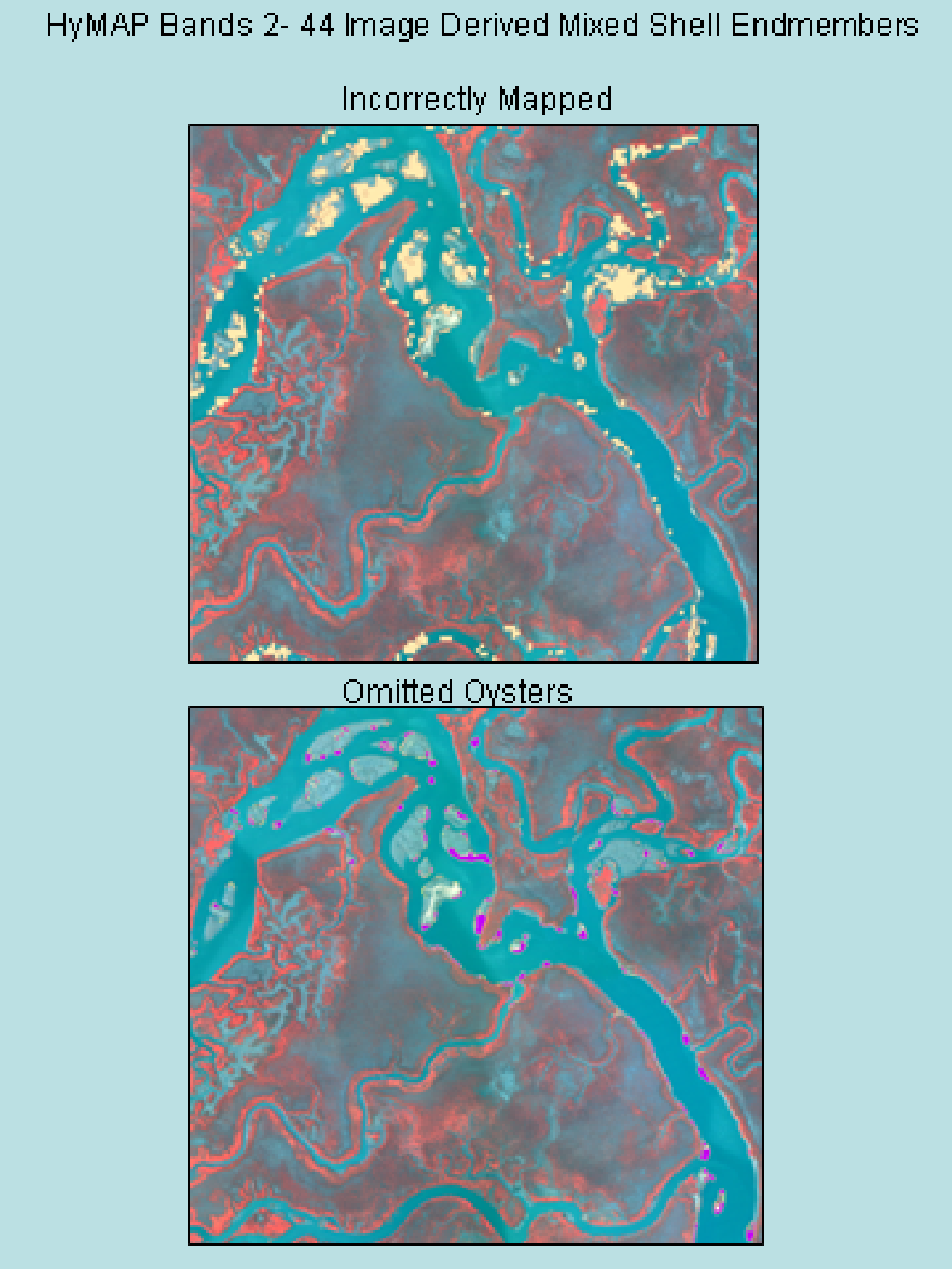

Figure 4.40b – HyMAP Bands 2-44 Mixed Shell Accuracy Assessment Results

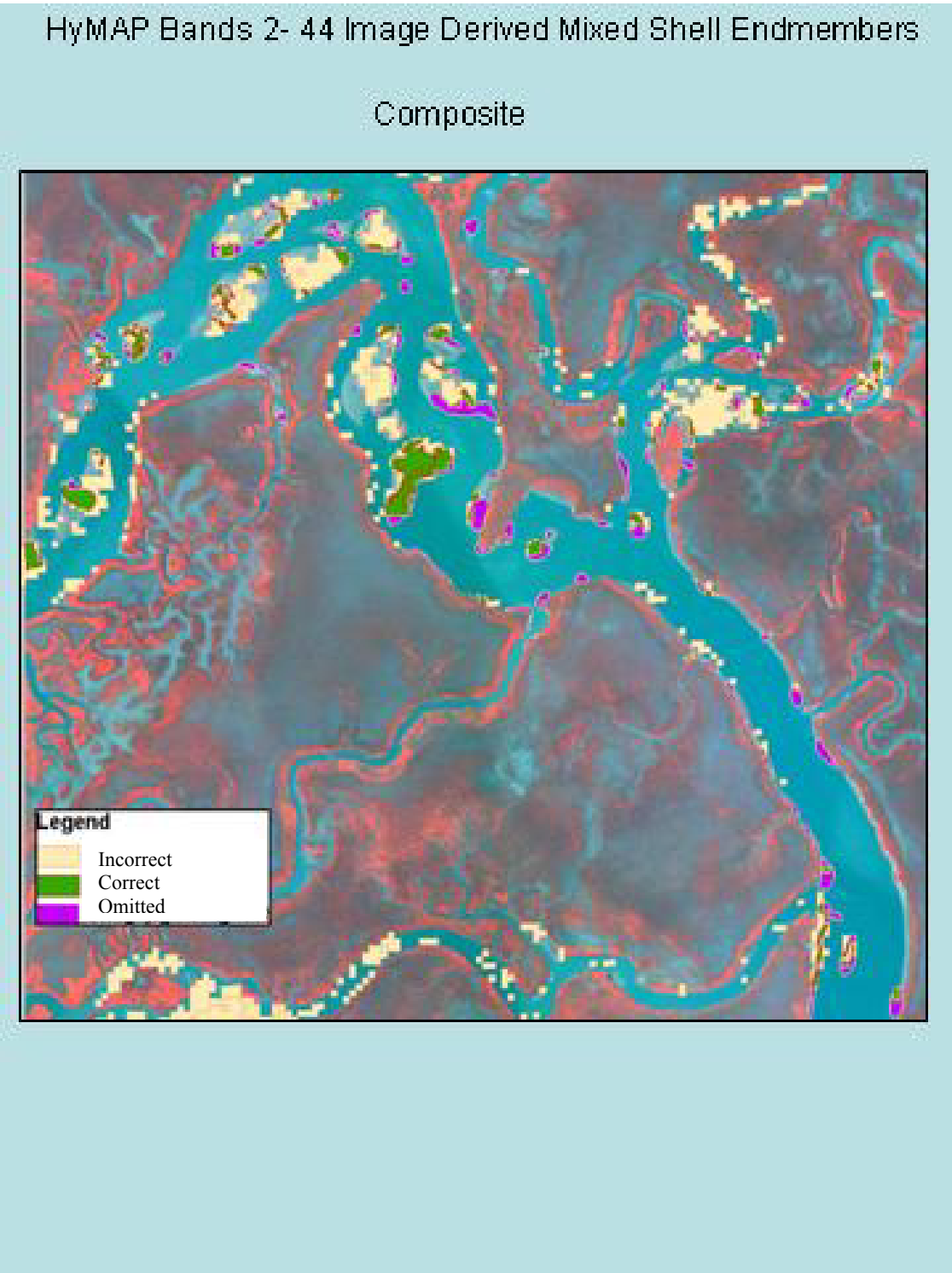

Figure 4.40c –HyMAP Bands 2-44 Mixed Shell Accuracy Assessment Composite

Visually comparing the two HyMAP accuracy assessments visually, one notes there is not a lot of difference between either the bright shell or mixed endmember bundles. The incorrectly mapped inset shows numerous small fragments of polygons that were incorrectly mapped while omitted polygons tend to be located near the edge of the patch reefs but are not as numerous as the incorrectly mapped oysters. It would appear that the HyMAP image over-estimated the number of pixels that contained oysters or because the "apparent truth map" was derived from a smaller spatial resolution image the areal extent of oysters is less than the areal extent of the HyMAP polygon oyster map and hence the mapped oystyers. The following figures 4.41 shows graphically the over-estimation encountered with using the HyMAP imagery.

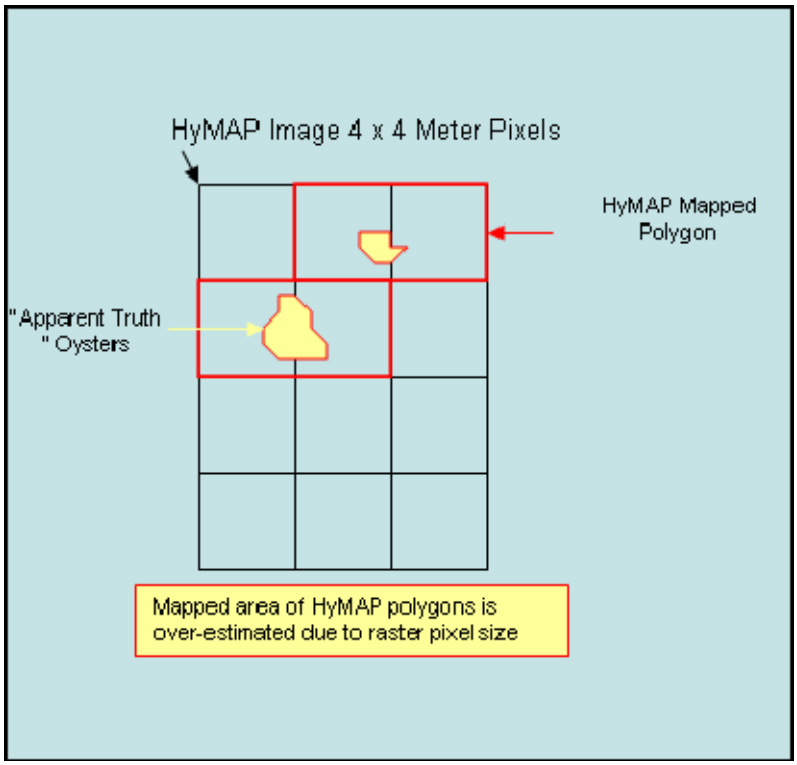

Figure 4.41 – Graphic Representation of HyMAP Over-Estimation

4.8.3 AISA MTMF Assessment

The AISA imagery accuracy assessment was accomplished on the endmember set that was derived from the AISA imagery and with mapping that used the in situ endmembers that were convolved from 512 bands of the hand-held spectroradiometer to match the 7 bands of the AISA image. One confounding issue with the use of the AISA imagery stems from the fact that the AISA image spatial extents are not the same as the HyMAP nor the GeoVantage imagery. The AISA image study area is a single flight line that is approximately 170 meters wide and 410 meters long. Viewing the following images it is apparent that the AISA image misses a portion of mapable oysters directly north of the BOB 4 study site. The problem of over-estimation that was described using the HyMAP imagery does not present itself with using the AISA imagery since due to the fact that the two sets of imagery utilized are closer in spatial resolutions, (GeoVantage is 0.25 meter and AISA is 0.50 meter spatial resolutions). The following figures 4.42a – 4.42c and 4.43a – 4.43c shows the accuracy assessment of the AISA imagery utilizing both image derived endmembers and *in situ* derived endmembers.

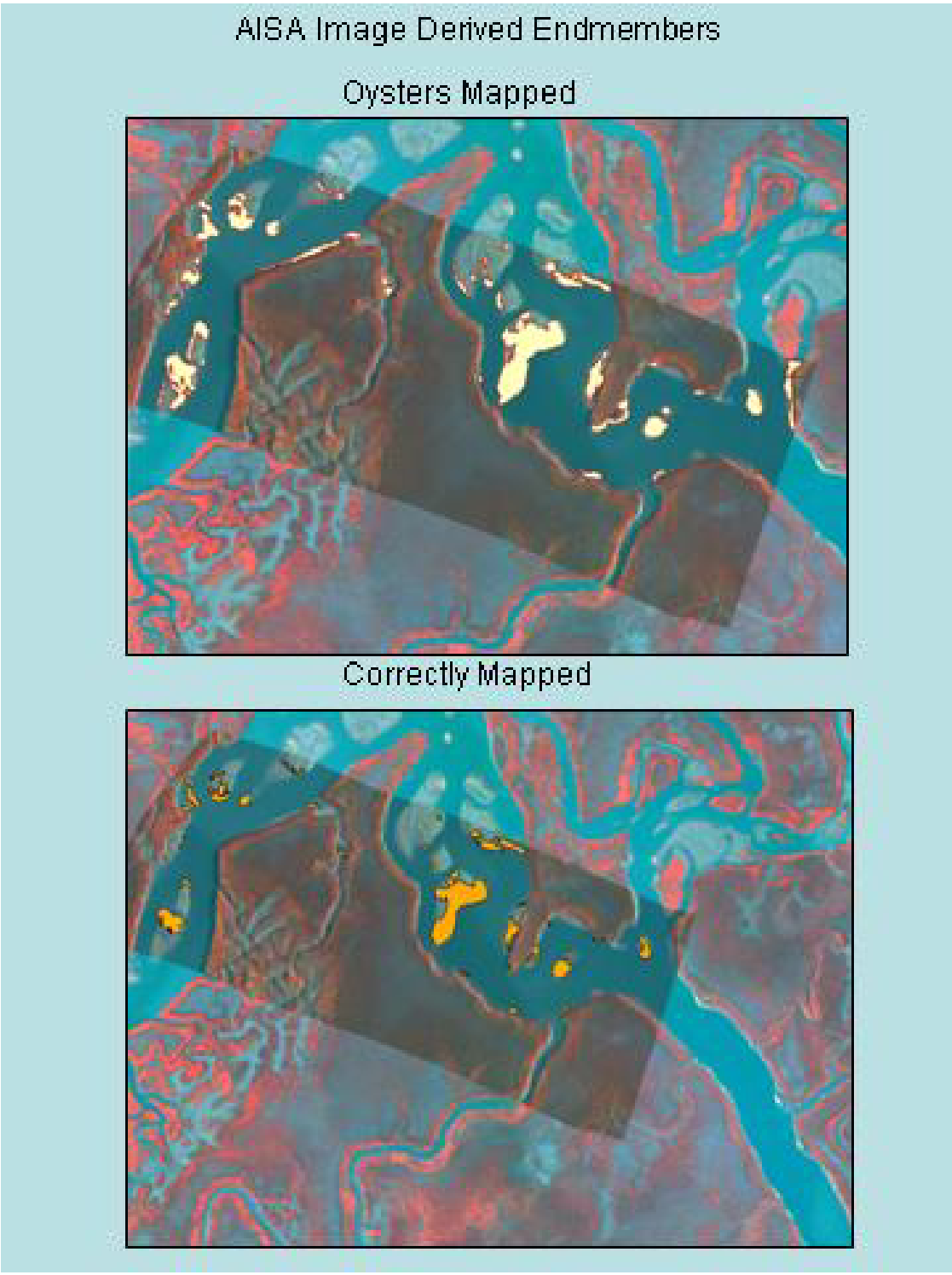

Figure 4.42a – AISA Image Derived Endmembers Accuracy Assessment

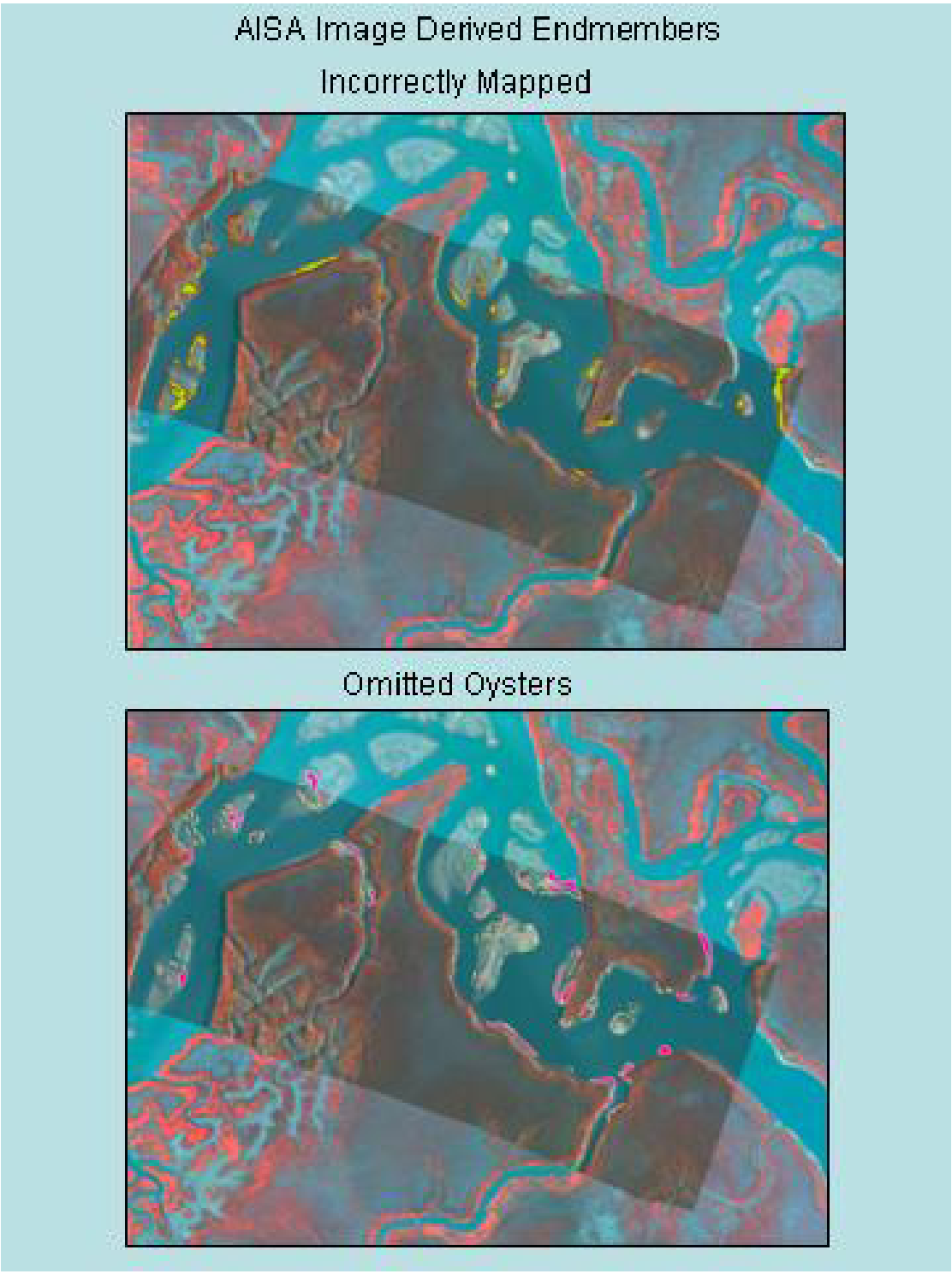

Figure 4.42b – AISA Image Derived Endmembers Accuracy Assessment

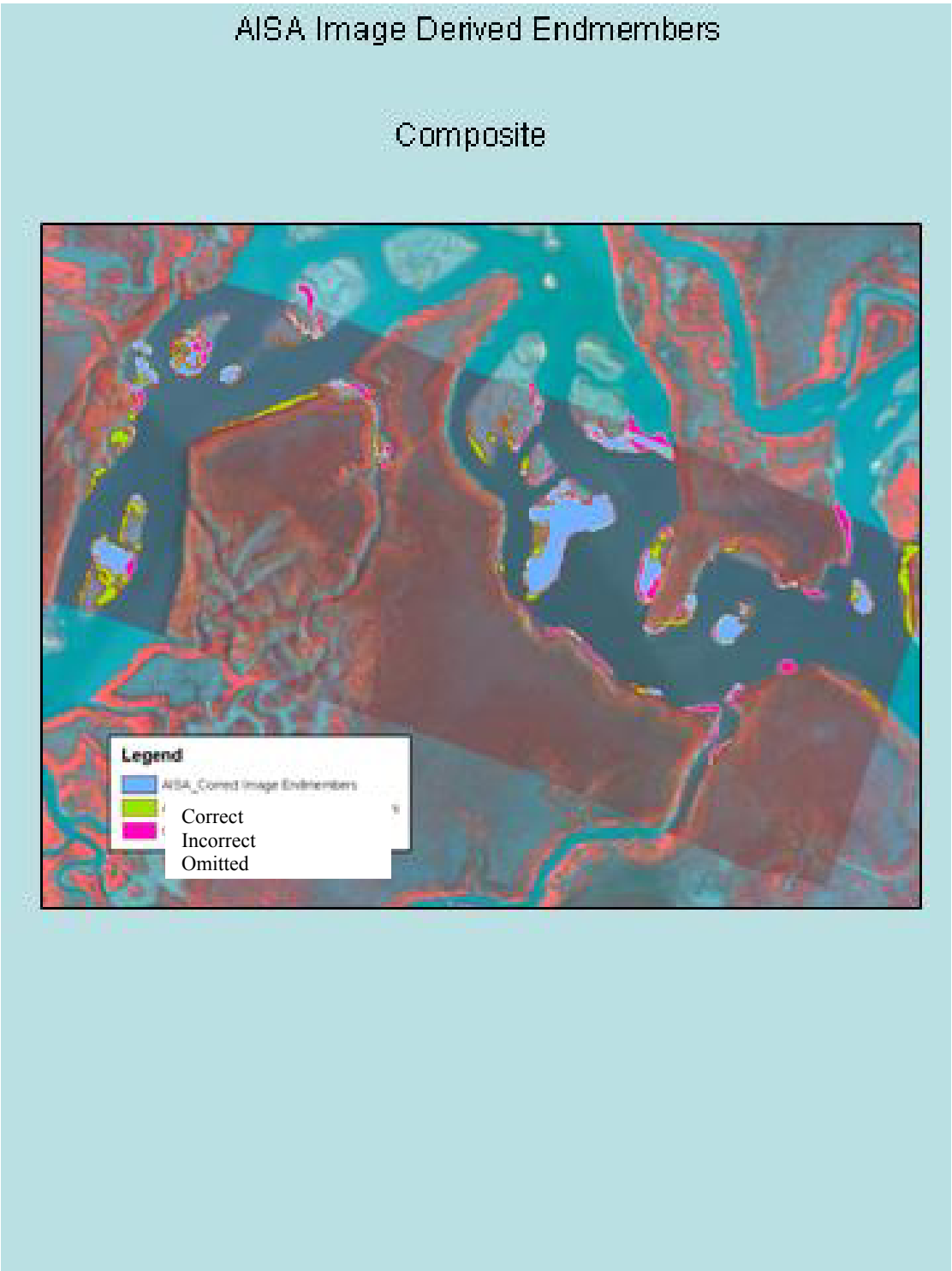

Figure 4.42c – Continued AISA Image Derived Endmembers Accuracy Assessment

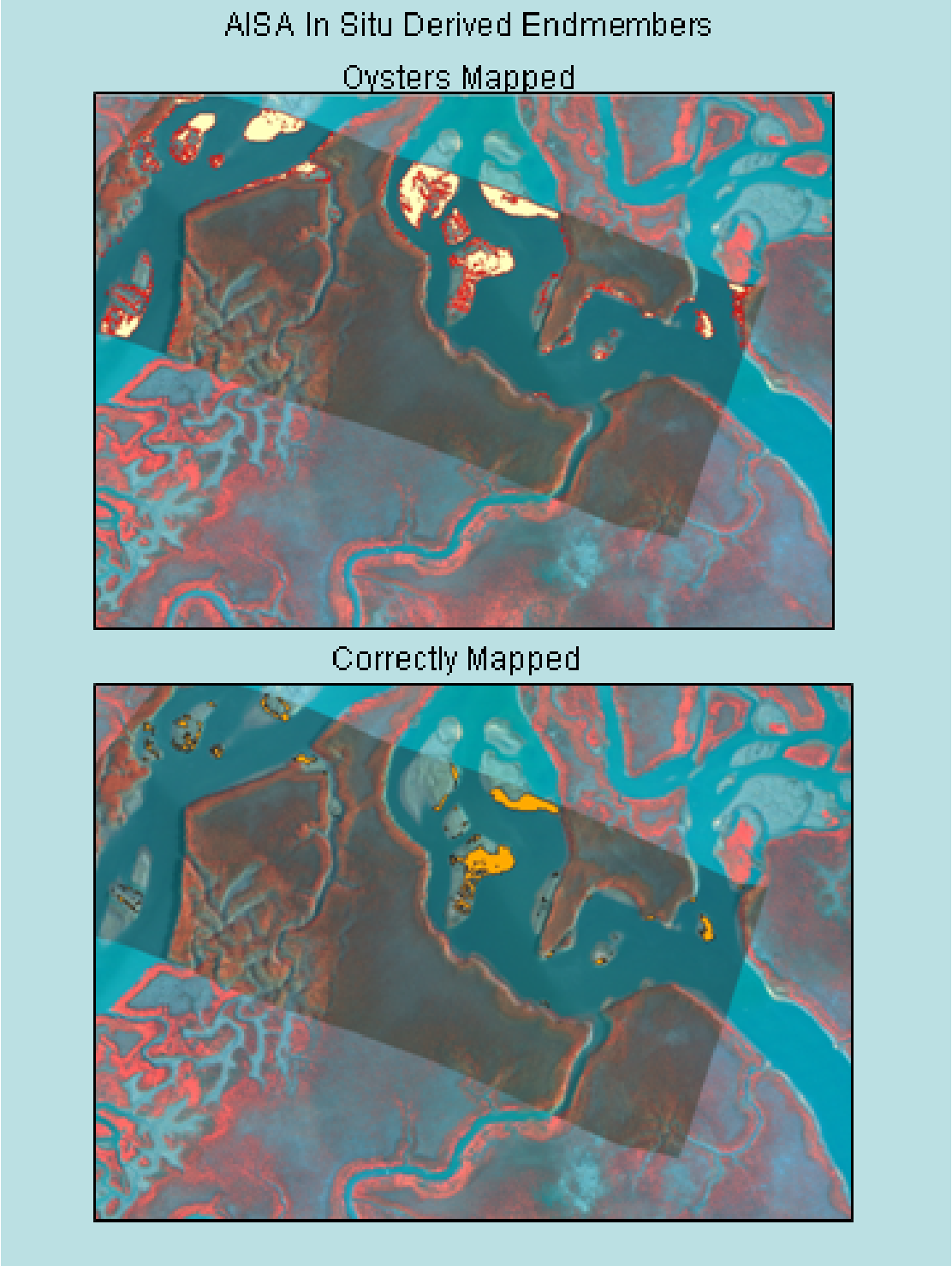

Figure 4.43a – AISA In Situ Derived Endmembers Accuracy Assessment

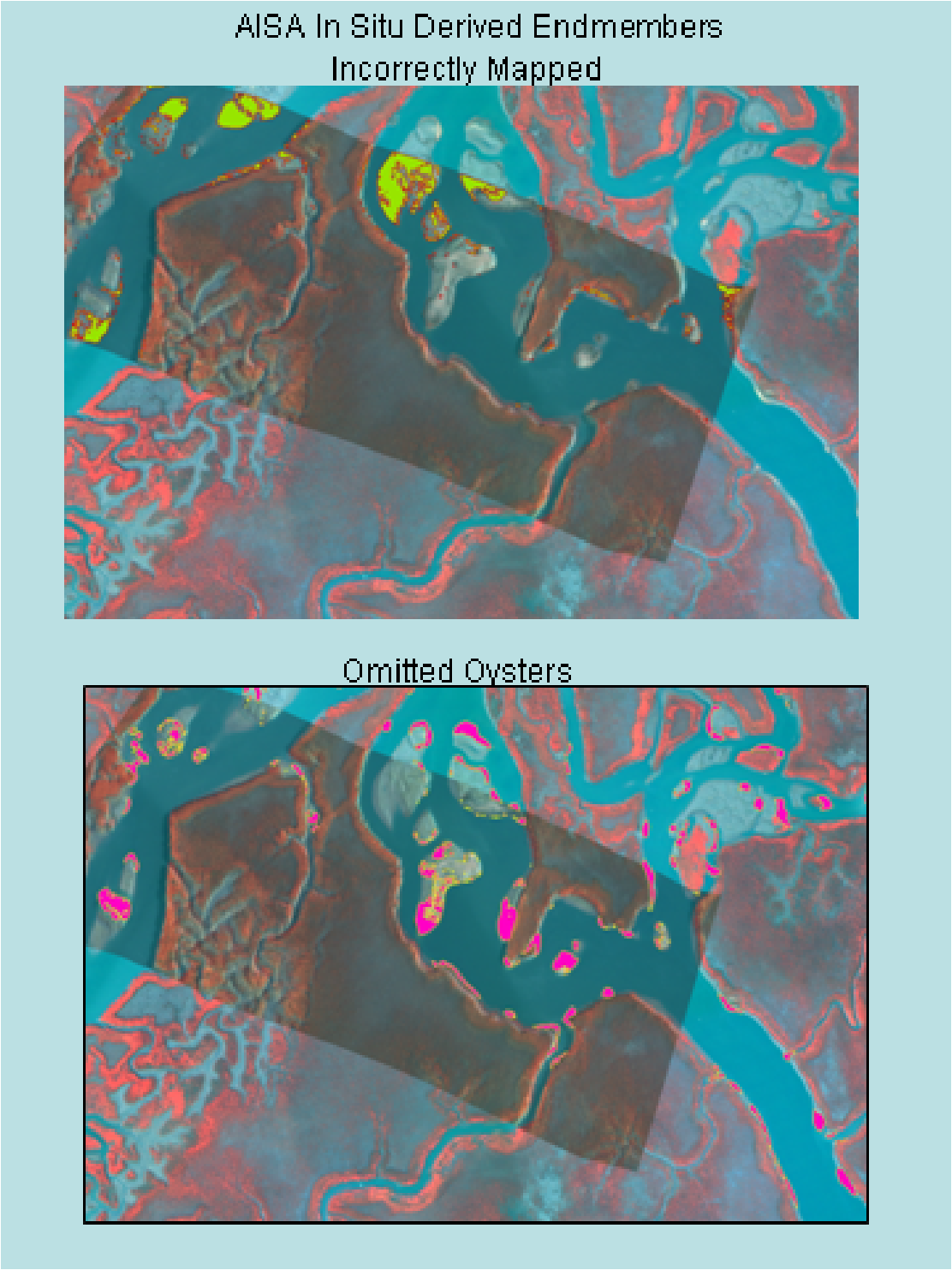

Figure 4.43b – Continued AISA In Situ Derived Endmembers Accuracy Assessment

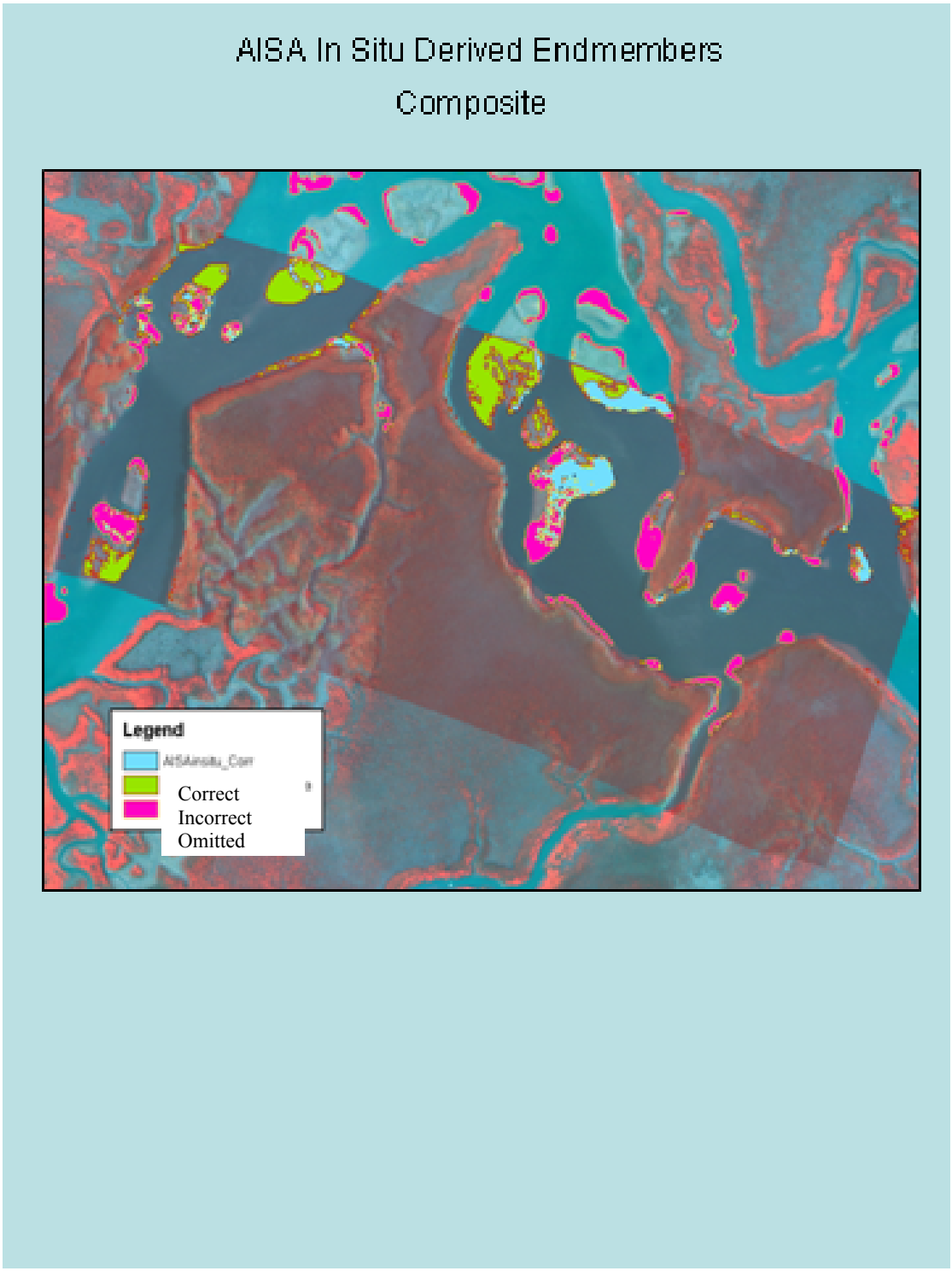

Figure 4.43c – AISA In Situ Derived Endmembers Accuracy Assessment

Some comments about the two assessments show that the *in situ* endmembers did a better job of mapping oysters correctly than the HyMAP imagery but not a well as the image derived endmembers from the AISA imagery. A rather large are of mud that is northwest of the BOB 4 study site was mistaken as oysters in the *in situ* derived analysis. Additionally, the southern portion of the BOB 4 sample site was omitted. This is interesting to note because the aggregated *in situ* spectral endmembers used were composed partly from the southern portion of the study area (BOB4_14, 15, & 16) but were not included in the mapped shellfish. The image derived oyster endmembers had far fewer incorrectly mapped and omitted oysters than any of the data sets analyzed. Table 4.8 shows the quantitative assessment of the accuracy assessment and shows the percent Producer's Accuracy, User's Accuracy, and Omission Error

Table 4.8 Accuracy Assessment Results

	Producer's Accuracy*	User's Accuracy**	Omission Error
HyMAP Spectral Subset Bands 2-61	44.25	22.89	55.41
HyMAP Spectral Subset Bands 2-44 Bright Shell	37.28	20.7	62.43
HyMAP Spectral Subset Bands 2-44 Mixed Shell	40.62	21.58	58.98
Insitu Spectral Endmembers HyMAP Bands 2-44	43.2	22.56	56.44
AISA Image Derived Endmembers	67.7	63.44	32.45
AISA In situ Derived Endmembers	39.03	35.48	59.92
* Total square meters correctly mapped / Total number of Square meters of apparent actual Oysters (truth)	** Total square meters correctly mapped / Total number of Square meters of MTMF mapped oysters		

The producers accuracy which is a measure of the percent area of correctly mapped oysters divided by the area of the total "apparent truth" from the GeoVantage imagery is as good a measure of overall accuracy varied from 37% to 67 % with the best accuracy found with the image derived endmembers from the AISA imagery. This is

repeated also with the User's Accuracy, which is a measure of classification accuracy, is repeated with the AISA image derived endmembers having 63% accuracy. The Omission Error was lowest with the AISA image derived endmembers (32%). It is not known if these accuracies are reasonable since there hasn't been any accuracy results published in the literature with which to compare. The HyMAP accuracy results showed considerable similarities with a small exception with the spectral subset of bands 2-61 having a slightly better accuracy and lower omission error than either of the 2-44 bands spectral subsets. Although between the two endmembers analyzed from the image derived bright shell and mixed shell from the 2-44 band subset, the Mixed Shellfish endmember displays a slightly better producer and user's accuracy and lower omission error than the bright shell. Overall, the AISA image derived endmember displayed the best accuracies and lowest omission error of all the endmembers tested. Also, the image derived endmembers had better accuracies and lower omission errors than the *in situ* derived endmembers.

Chapter 5. Conclusions and Future Research

As in any research, conclusions always divulge more than just an answer to the stated hypothesis' and objectives but invariably generate ancillary answers and many more questions that were unknown beforehand. This research project was no exception but before these aspects of the research is explored the answers to the initial stated hypothesis' are as follows:

Null Hypothesis one H_o1: There is no difference between maps produced by either reference library spectra and derived endmembers through MTMF analysis.

Rejected – Table 4.7 shows the results of the accuracy assessment and shows there is a difference between MTMF mapping using *in situ* generated endmembers than endmembers derived directly from the imagery. Both the Producer's Accuracy and User's Accuracy showed the best results were obtained using image derived endmembers. This was evident also between the two different remotely sensed data set utilized in the research. The AISA 0.5 x 0.5 meter with 7 bands had better mapping accuracy than utilizing HyMAP 4 x 4 meter with either of the two spectral subsets (subset 1: Bands 2-61 and subset 2: bands 2-44). The spatial resolution has been identified as a possible source of the lower mapping accuracy. As stated above the raster pixels that are 4 x 4 meter only identifies pixels that have a higher probability of shellfish occurring within the pixels and leaves out the amount or locations of shellfish within the pixel.

Null hypothesis two H_o2: There is no spectral difference between live oysters and mud.

Rejected – There is a significant spectral difference between live oysters and mud. A visual examination of figure 3.11 shows a graph of monthly averaged spectral signatures mud and shellfish. The shellfish utilized in this example was not exhaustive but is an example of bright shell, (BOB4_2), live healthy shellfish (BOB4_15 and NMF1_11). The mud spectral curve was compiled from BOB4_13 and NMF2 which has incorporated wet / dry and rough / smooth shellfish examples. One striking example is that while the mud and shellfish have relatively low reflectance values the range of reflectance values are very narrow. The slope of the curve from the visible spectrum to the short-wave infrared region is similar for both regions and is relatively flat. This is in contrast to the shellfish producing the infrared shift with the presence of photosynthesis producing organisms present (diatoms) but conspicuously absent in the mud spectral profile.

More importantly, in the MTMF mapping process in both AISA and HyMAP imagery data sets, the ability to map mud and shellfish was demonstrated. In each of the examples in the results section, the maps produced showed remarkable differences between mud as opposed to the shellfish map. Figures 4.21 and 4.22 on pages 104-106 show the mapping results for the AISA data set and figures 4.22 and 4.23, on pages 107-108 show the ability to map mud and shellfish endmembers.

This research spent more than a year measuring spectral responses of multiple sample sites and sample points for the creation of an *in situ* spectral library. A major contribution of this sample period is establishment of the shellfish phenology and ascertaining of optimal sampling times throughout the year to gain to optimal shellfish

spectra. It was found that during the winter months and early spring, macro-algae grew over the sites obfuscating the shellfish and thus the spectral response of the shellfish. This analysis utilized spectral library endmembers that were acquired in October to coincide with the same month of acquisition (different years) of the remotely sensed imagery. Additionally, future research should examine the effect of the changing environment with in the estuary over time leading to mapping discrepancies in the remotely sensed imagery and *in situ* data. This aspect is thought to partially explain the low accuracy results using the spectral library as noted by Elmore et al. 2000.

Overall, the ability to map shellfish and mud for both AISA and HyMAP imagery has been demonstrated within this report. Differences exist in the relative accuracy of each of the remotely sensed imagery data sets with the AISA imagery having a higher accuracy than the HyMAP imagery. Differences also exist in the use of *in situ* derived spectral endmembers and image derived spectral endmembers with the image derived spectral endmembers having a higher accuracy than *in situ* derived endmembers.

A future research question would be to examine some of the reasons for why the *in situ* spectral endmembers did not perform as well as the image derived spectral endmembers. A future study would examine the field acquisition of *in situ* endmembers to experiment with the number of sample points, in addition aggregating techniques of the sample points that demonstrate the optimal areal reflected signature and compared with "pure" laboratory spectra.

This research was able to only distinguish between two classes of shellfish, live shellfish that were relatively densely clustered and vertical, and dead horizontal shells that show the brightly reflective inside of the shell that has been sun bleached. Future research

should focus on the ability to differentiate more subtle differences and classes of shellfish. All of this research focused mainly on the larger patch reefs and to lesser extent fringing reefs along the shore. Future research should utilize imagery and classification techniques that emphasize not only on the smaller patch reefs but fringing reefs as well.

Chapter 6. References Cited

Accioly, L., Huete, A. R., and Batchily, K. 1998. Using mixture analysis for soil information extraction from an AVRIS scene at the Walnut Gulch Experimental Watershed – Arizona. *In* Green, R.O., ed., 7th *JPL Airborne Earth Sciences Workshop AVRIS*, Vol. 1. Jet Propulsion Laboratory, Pasadena, CA.

Adams, J. B., Smith, M. O., and Gillespie, A. R. 1992. Imaging spectroscopy: data analysis and interpretation based on spectral mixing analysis. *In* Remote Geochemical Analysis: Elemental and Mineralogical Composition. Eds. C. M. Pieters and P. Englert. LPI and Cambridge University Press. New York, NY.

Adams, J. B., Sabol, D. E., Kapos, V., Filho, R. A., Roberts, D. A., Smith, M.O., and Gillespie, A. R. 1995. Classification of multispectral images based on fractions of endmembers: application to land-cover change in the Brazillian Amazon. *Remote Sensing of Environment* 52:137-154.

Bateson, A., and Curtiss, B. 1996. A method for manual endmember selection and spectral unmixing. *Remote Sensing of Environment*. 55:229-243.

Bateson, A. Asner, G. P., and Wessman, C. A. 1998. Incorporating endmember variability into spectral mixture analysis through endmember bundles. *In* Green, R.O., ed., *7th JPL Airborne Earth Sciences Workshop AVRIS*, Vol. 1. Jet Propulsion Laboratory, Pasadena, CA.

Bertnes, M. D. 1999. *The ecology of Atlantic shorelines*. Sinauer Associates, Inc. Publishers. Sunderland, MA.

Bierwirth, P. N. 1990. Mineral mapping and vegetation removal via data-calibrated pixel unmixing, using multispectral images. *International Journal of Remote Sensing* 11(11):1999-2017.

Boardman, J. W., and Kruse, F. A. 1994. Automated spectral analysis: A geological example using AVRIS data, North Grapevine Mountains, Nevada. *Proceedings of the Tenth Thematic Conference on Geologic Remote Sensing: Exploration, Environment, and Engineering*: 9-12 May 1994. San Antonio, TX.

Boardman, J. W., and Kruse, F. A., and Green, R.O. 1995. Mapping target signatures via partial unmixing of AVIRIS data. *Summaries of the Fifth JPL Airborne Geosciences Workshop*, JPL Publications 95-1 pp. 230-26 Pasadena, CA: NASA Jet Propulsion Laboratory.

Breitburg, D. L. 1999. Are three-dimensional structure and healthy oyster populations the keys to an ecologically interesting and important fish community? *In: Oyster Reef Habitat Restoration: A Synopsis and Synthesis of Approaches*. Proceedings from the Oyster Reef Habitat Restoration Symposium. Eds. Luckenbach, M. W., Mann, R., and Wesson, J. A. Williamsburg, Virginia. Published by: Virginia Institute of Marine Science, School of Marine Science, College of William and Mary. VIMS Press.

Coen L. D., Knott, D. M., Wenner, E.L., Hadley, N. H., Ringwood, A. H., and Bobo, M. Y. 1999a. Intertidal oyster reef studies in South Carolina: design, sampling and experimental focus for evaluating habitat value and function. *In: Oyster Reef Habitat Restoration: A Synopsis and Synthesis of Approaches*. Proceedings from the Oyster Reef Habitat Restoration Symposium. Eds. Luckenbach, M. W., Mann, R., and Wesson, J. A. Williamsburg, Virginia. Published by : Virginia Institute of Marine Science, School of Marine Science, College of William and Mary. VIMS Press.

Coen, L.D, Luckenbach, M. W., and Breitburg, D. L. 1999b. The role of oyster reefs as essential fish habitat: a review of current knowledge and some new perspectives. *In: Fish Habitat: Essential Fish Habitat and Rehabilitation.* Ed. Benaka, L.R. American Fisheries Symposium 22. Hartford, CT. 26-27 August, 1998. American Fisheries Society. Bethesda MD.

Coen, L.D. and Luckenbach, M.W. 2000. Developing success criteria and goals for evaluating oyster reef restoration: ecological function or resource exploitation? *Ecological Engineering*. Vol.15: 323-343.

Cracknell, A. P. 1999. Remote sensing techniques in estuaries and coastal zones – an update. *International Journal of Remote Sensing* 19(3):485-496.

Curran, P. J. 1994. Imaging spectrometry. *Progress in Physical Geography*. 18(2):247-266.

Elmore, A. J., Mustard, J. F., Manning, S. J., and Lobell, D. B. 2000. Quantifying vegetation change in semiarid environments: precision and accuracy of spectral mixture analysis and the normalized difference vegetation index. *Remote Sensing of Environment* 73: 87-102.

Garcia-Haro, F. J., Gilabert, M. A., and Melia, J. 1996. Linear spectral mixture modeling to estimate vegetation amount from optical spectral data. *International Journal of Remote Sensing* 17(17):3373-3400.

Garcia-Haro, F. J., Gilabert, M. A., and Melia, J. 1999b. Extraction of endmembers from spectral mixtures. *Remote Sensing of Environment* 68:237-253.

Grizzle, R.E. 1990. Distribution and abundance of Crassotrea virginica (Gmelin, 1791) (Eastern Oyster) and Mercenaria SPP. (Quahogs) in a coastal lagoon. *Journal of Shellfish Research.* Vol. 9, no. 2: 347-358.

Gross, H. N. and Schott, J. R. 1996. Application of spatial resolution enhancement and spectral mixture analysis to hyperspectral images. *Proceedings of SPIE: Hyperspectral Remote Sensing & Applications*. Denver CPO. 4-9 August 1996, SPIE Vol. 2821.

Gross, H. N. and Schott, J. R. 1998. Application of spectral mixture analysis and image fusion techniques for image sharpening. *Remote Sensing of Environment* 63: 85-94.

Hackney, C.T. 2000. Restoration of coastal habitats: expectation and reality. *Ecological Engineering*. 15: 165-170.

Hall, F.G., Shimabukuro, Y.E., and Huemmich, K.F. 1995. Remote sensing of forest biophysical structure in boreal stands of picea mariana using mixture decomposition and geometric reflectance models. *Ecol. Appl*.5:993-1013.

Henderson, F. M., Hart, T. F., Heaton, B. P., and Portolese, J. E. 1999. Mapping coastal ecosystems over a steep development gradient using C-CAP protocols. *International Journal of Remote Sensing* 20(4):727-744.

Holden, H. M. 2001. Subpixel linear mixing within a coral reef environment based on in situ hyperspectral measurements. Presented at the *22nd Asian Conference on Remote Sensing*, November 5-9 Singapore, Malaysia.

Kracker, L. 1999. The geography of fish: the use of remote sensing and spatial analysis tools in fisheries research. *Professional Geographer* 51(3):440-450.

Ladner, S.D. and Arnone, R. A. 1998. Monitoring coastal environment using satellite time series. *Journal of Shellfish research*, 17(5):1445-1450.

Lyon, J. G. 2001. *Wetland landscape characterization: GIS, remote sensing, and image analysis*. Ann Arbor Press, Chelsea MI. U.S.A.

Maas, S. J. 1998. Method for estimating cotton canopy ground cover from remotely sensed scene reflectance. *Agronomy J*. 90(3):384-388.

Maas, S. J. 2000. Linear mixture modeling approach for estimating cotton canopy round cover using satellite multispectral imagery. *Remote sensing of Environment*. 72:304-308.

Mallin, M. A., Burkholder, J. M, and Cahoon, L. B. 2000. North and South Carolina coasts. *Marine Pollution Bulletin* 41(1-6):56-75.

McGwire, K., Minor, T., and Fenstermaker, L. 2000. Hyperspectral mixture modeling for quantifying sparse vegetation cover in arid environments. *Remote Sensing of Environment* 72:360-374.

Michener, W.K., Jefferson, W.H., and Karinshak, D.A. 1992. An integrated geographic information system, global positioning system, and spatio-statistical approach for analyzing ecological patterns at landscape scales. GIS/LIS Proceedings. Pgs. 546-576: vol. 2. American Society for Photogrammetry and Remote Sensing. Bethesda, MD.

Okin, W.J., Okin, G.S., Roberts, D.A., and Murray, B. 1999. Multiple endmember spectral mixture analysis: endmember choice in an arid shrubland. *In* Green, R.O., ed., 8^{th} *JPL Airborne Earth Sciences Workshop AVRIS*, Vol. 1. Jet Propulsion Laboratory, Pasadena, CA.

Okin, G.S. and Roberts, D.A. 2000. Linear unmixing of simulated, noisy spectra: Vegetation detection limits in areas of low cover. *In* Green, R.O., ed., 9^{th} *JPL Airborne Earth Sciences Workshop AVRIS*, Vol. 1. Jet Propulsion Laboratory, Pasadena, CA.

Okin, G. S., Roberts, D. A., Murray, B., and Okin, W. 2001. Practical limits on hyperspectral vegetation discrimination in arid and semiarid environments. *Remote Sensing of Environment* 77: 212-225.

Parker, M. R., Beal, B. F., Congleton, W. R., Pearce, B. R., and Morin, L. 1998. Utilization of GIS and GPS for shellfish growout site selection. *Journal of Shellfish research,* 17(5):1491-1495.

Pasqualini, V., Pergent-Martini, C., Fernandez, C., and Pergent, G. 1997. The use of airborne remote sensing for benthic cartography: advantages and reliability. *International Journal of Remote Sensing* 18(5):1167-1177.

Peddle, D. R., Hall, F.G., LeDrew, E.F. 1999. Spectral mixture analysis and geometric-optical reflectance modeling of boreal forest biophysical structure. *Remote Sensing of Environment* 67: 288-297.

Peddle, D. R., LeDrew, E. F., and Holden, H. M, 1995. Spectral mixture analysis of coral reef abundance from satellite imagery and in situ ocean spectra, Savusavu Bay, Fiji. Presented at the *Third Conference on Remote Sensing for Marine and Coastal Environments*, Seattle, WA. 18-20 September.

Ray, T. W. and Murray, B. C. 1996. Nonlinear spectral mixing in desert vegetation. *Remote Sensing of Environment* 55: 59-64.

Research Systems Incorporated. 2001. ENVI user's guide. Boulder Colorado.

Robinson, G.D., Gross, H. N., and Schott, J. R. 2000. Evaluation of two applications of spectral mixing models to image fusion. *Remote Sensing of Environment* 71: 272-281.

Sabol, D. A., Gillespie, A. R., Adams, J. B., Smith, M.O., Tucker, C.J. 2002. Structural stage in Pacific Northwest forests estimated using simple mixing models of multispectral images. *Remote Sensing of Environment* 80:1-16.

Smith G.F. and Greenhawk, K.N. 1998. Shellfish benthic habitat assessment in the Chesapeake Bay: progress toward integrated technologies for mapping and analysis. *Journal of Shellfish Research*. Vol. 17, No. 5: 1433-1437.

Smith G.F., Bruce, D.G., and Roach, E.B. 2001. Remote acoustic habitat assessment techniques used to characterize the quality and extent of oyster bottom in the Chesapeake Bay. *Marine Geodesy*. Vol. 24: 171-189.

Smith, M. O., Ustin, S.L., Adams, J.B., and Gillespie, A.R. 1990. Vegetation in deserts I: A regional measure of abundance from multispectral images, *Remote Sensing of Environment*, 31:1-26.

Smith, M. O., Ustin, S.L., Adams, J.B., and Gillespie, A.R. 1990. Vegetation in deserts II: A regional measure of abundance from multispectral images, *Remote Sensing of Environment*, 31:27-52.

Smith, M. O., Adams, J. B., Ustin, S. L., and Roberts, D. A. 1992. Using endmembers in AVRIS images to estimate changes in vegetative biomass. *In* Green, R.O., ed., *JPL Airborne Earth Sciences Workshop AVRIS*, Vol. 1. Jet Propulsion Laboratory, Pasadena, CA.

Smith, G.F. and Greenhawk, K.N. 1998. Shellfish benthic habitat assessment in the Chesapeake Bay: progress toward integrated technologies for mapping and analysis. *Journal of Shellfish research*, 17(5):1433-1437.

Tompkins, S., Mustard, J. F., Pieters, C. M., and Forsyth, D. W. 1997. Optimization of endmembers for spectral mixture analysis. *Remote Sensing of Environment* 59:472-489.

Yuhas, R.H, Boardman, J. W., and Goetz, A. F. H. 1993. Determination of semi-arid landscape endmembers and seasonal trends using convex geometry spectral unmixing techniques. *In* Green, R.O., ed., 4th *JPL Airborne Earth Sciences Workshop AVRIS*, Vol. 1. Jet Propulsion Laboratory, Pasadena, CA.

Chapter 7. Appendix

7.1 Intertidal Oyster Strata Description

Strata "A"	Approximately 11,974 bushels of live oysters per acre. Most productive oyster strata in the intertidal zone and having the greatest yield per acre of densely clustered live oysters. Exhibits little exposed dead shell or mud and the shell matrix is not visible.
Strata "B"	Approximately 2,905 bushels of live oysters per acre. Characterized by having little vertical or clustered crop. Found in the lower intertidal zone and are frequently single. Located on heavily shelled grounds with thin shell matrices.
Strata "C"	Approximately 2,164 bushels of live oysters per acre. Characterized by vertical clusters with spatial separation. Substrate is usually mud with little or no surrounding shell. Spatial separation between clusters ranges from a distance equal to the height of an individual cluster to approximately one meter.
Strata "D"	Approximately 225 bushels of live oysters per acre. Characterized by scattered live oysters usually integrated with large quantities of washed or dead shell. Found in the lower tidal zone on hard substrate. Hard clams live sympatrically in this area.
Strata "E"	Approximately 7,638 bushels of live oysters per acre. Characterized by heavily overgrown and difficult to harvest. Oysters are tightly clustered and completely cover the substrate. Occasional mud and sand infiltration within interstitial spaces and Spartina alterniflora growing within in-filled areas. Found at the highest oyster growing elevation and is further characterized by oysters with thin, sharp shells.
Strata "F"	Approximately 4,597 bushels of live oysters per acre. Characterized by mostly vertical clusters. Very similar to "C" strata except substrate is composed mostly of shells and very little amounts of mud with few horizontal oysters.
Strata "F1"	Approximately 2,598 bushels of live oysters per acre. Characterized by small vertical clusters evenly dispersed within a substrate of small horizontally oriented oysters. Very little exposed mud.
Strata "G"	Approximately 5,385 bushels of live oysters per acre. Characterized by vertical, clustered oysters that predominate. Spatial separation between clusters is equal to or less than height of the standing crop.
Strata "M"	Less than 20 bushels of oysters per acre. Characterized by scattered live oysters, which are small and show negligible aggregation. Surrounded by highly permeable mud substrate.
Strata "P"	Near minimum density of oysters in intertidal zone. Characterized by recently harvested zone with very few marketable oysters remaining. Considered to be productive since recent condition is due to harvesting and they will propagate to the next higher category by natural or artificial recovery.

Source: South Carolina Department of Natural Resources, Intertidal Oyster Survey.

7.2 Field Sample Locations

Sample Site	Sample Point	Easting	Northing
Jones Creek	JONES CREEK 3 REF	669276.7672	3685877.6819
Jones Creek	JC1_1	670043.7899	3687198.1627
Jones Creek	JC1_2	670043.7543	3687201.5818
Jones Creek	JC1_3	670043.7543	3687202.6503
Jones Creek	JC1_4	670043.7543	3687203.5763
Jones Creek	JC2_1	670051.7678	3687199.1956
Jones Creek	JC2_2	670051.5898	3687201.7599
Jones Creek	JC2_3	670051.5185	3687202.6503
Jones Creek	JC2_4	670051.4829	3687203.7188
Jones Creek	JC3_1	669279.5539	3685875.8580
Jones Creek	JC3_2	669279.4311	3685877.6998
Jones Creek	JC3_3	669279.0014	3685879.5416
Jones Creek	JC3_4	669278.2033	3685881.6289
Bob's Garden	BOB1_REF	669236.9192	3687467.5518
Bob's Garden	BOB1_1	669238.1615	3687467.3164
Bob's Garden	BOB1_2	669240.0173	3687464.8586
Bob's Garden	BOB1_3	669236.3635	3687468.1815
Bob's Garden	BOB1_4	669237.7885	3687465.5452
Bob's Garden	BOB1_5	669235.6967	3687465.6597
Bob's Garden	BOB1_6	669238.4052	3687463.4205
Bob's Garden	BOB2_REF	669232.9159	3687471.5942
Bob's Garden	BOB2_1	669234.1219	3687472.9988
Bob's Garden	BOB2_2	669233.4280	3687472.3156
Bob's Garden	BOB2_3	669232.1599	3687471.0794
Bob's Garden	BOB2_4	669231.0509	3687469.9704
Bob's Garden	BOB3_1	669231.4774	3687476.3257
Bob's Garden	BOB3_2_REF	669230.6826	3687475.4348
Bob's Garden	BOB3_3	669229.8993	3687474.8328
Bob's Garden	BOB3_4	669228.7523	3687473.5778
Bob's Garden	BOB4_REF	668981.9413	3687654.1416
Bob's Garden	BOB4_1	668982.2619	3687652.2184
Bob's Garden	BOB4_2	668982.4182	3687651.0349
Bob's Garden	BOB4_3	668982.6143	3687649.8305
Bob's Garden	BOB4_4	668982.7448	3687648.6244
Bob's Garden	BOB4_5	668983.0077	3687646.7638
Bob's Garden	BOB4_6	668983.3747	3687644.2947
Bob's Garden	BOB4_7	668989.9653	3687647.9513
Bob's Garden	BOB4_8	668990.8673	3687646.1135
Bob's Garden	BOB4_9	668998.3891	3687652.9457
Bob's Garden	BOB4_10	668999.6562	3687652.9892

Bob's Garden	BOB4_11	668994.5842	3687661.2875
Bob's Garden	BOB4_12	668995.8713	3687662.3824
Bob's Garden	BOB4_13	668983.8106	3687662.1515
Bob's Garden	BOB4_14	668963.0273	3687621.7905
Bob's Garden	BOB4_15	668962.4440	3687620.0907
Bob's Garden	BOB4_16	668962.0215	3687618.6197
Bob's Garden	BOB4_17	668960.8549	3687615.0498
Bob's Garden	BOB4_18	668961.9255	3687613.4081
Bob's Garden	BOB4_19	668971.5387	3687627.3714
Bob's Garden	BOB4_20	668973.2441	3687627.0020
Bob's Garden	BOB4_21	668973.0278	3687637.3203
Bob's Garden	BOB4_22	668974.9505	3687637.3442
No Man's Friend	NMF1_Reference Post	667329.5542	3687470.2526
No Man's Friend	NMF1_1	667336.1839	3687466.8292
No Man's Friend	NMF1_2	667336.9749	3687466.8774
No Man's Friend	NMF1_3	667337.5231	3687466.1555
No Man's Friend	NMF1_4	667336.4530	3687466.1892
No Man's Friend	NMF1_5	667331.8690	3687463.2383
No Man's Friend	NMF1_6	667332.2426	3687462.5891
No Man's Friend	NMF1_7	667332.4999	3687461.6144
No Man's Friend	NMF1_8	667326.0631	3687463.4448
No Man's Friend	NMF1_9	667325.6330	3687462.7938
No Man's Friend	NMF1_10	667327.7505	3687469.4961
No Man's Friend	NMF1_11	667325.1321	3687471.5327
No Man's Friend	NMF1_12	667320.1863	3687484.4499
No Man's Friend	NMF1_13	667315.5896	3687484.9736
No Man's Friend	NMF1_14	667330.8343	3687469.3216
No Man's Friend	NMF1_15	667332.9290	3687468.0415
No Man's Friend	NMF1_16	667334.6164	3687467.1105
No Man's Friend	NMF1_17	667326.4704	3687463.9685
No Man's Friend	NMF 2 MUD	3688194.1614	667325.1321

All Eastings and Northings derived from UTM, Zone 17N, NAD83

7.3 Table of Spectral Aggregation

IN-SITU SPECTRORADIOMETIC DATA 2ND LEVEL AGGREGATION		
CLUSTER	**DESCRIPTION**	**SAMPLE POINTS**
	(BOB A-C are aggregated from BOB 1-3 sample sites)	
BOB A		BOB1_1 BOB1_2 BOB2_1 BOB3_1
BOB B		BOB1_3 BOB1_4 BOB2_2 BOB3_2
BOB C		BOB1_5 BOB1_6 BOB2_3 BOB2_4 BOB3_3 BOB3_4
	(BOB D- G are aggregated from BOB4 sample site)	
BOB D		BOB4_1 BOB4_2 BOB4_3 BOB4_4
BOB E		BOB4_7 BOB4_8 BOB4_11 BOB4_12 BOB4_17 BOB4_18 BOB4_20 BOB4_22
BOB F		BOB4_9 BOB4_10
BOB G		BOB4_5 BOB4_14 BOB4_15 BOB4_16 BOB4_19 BOB4_21

	(NMF A – C are aggregated from NMF 1 sample site)
NMF A	NMF1_1 NMF1_2 NMF1_3 NMF1_4 NMF1_5 NMF1_6 NMF1_7 NMF1_8 NMF1_9
NMF B	NMF1_10 NMF1_11
NMF C	NMF1_12 NMF1_14 NMF1_15 NMF1_16
NMF D	NMF2 ALL SAMPLE POINTS
	(JC A & B are aggregated from JONES CREEK sample sites 1 & 2)
JC A	JC1_1 JC2_1
JC B	JC1_2 JC1_3 JC1_4 JC2_2 JC2_3 JC2_4
	(JC C & D are aggregated from JONES CREEK sample site 3 WASHED SHELL are separated into WET and DRY)
JC C DRY	JC3_1 JC3_2 JC3_3 JC3_4
JC D WET	JC3_1 JC3_2 JC3_3 JC3_4

MISCELLANEOUS CLASSES	
WET U	Sample points that are submerged or partially submerged. Classed as either NMF (No Man's Friend) or BOB (includes BOB sample sites 1-4).
MUD	BOB4_13 mud sample point.
CONCRETE PAD	Concrete pad at clambank used as reference and control.
WATER	Spectroradiometer samples of deep water at sample sites.
SPARTINA	Jones Creek sample sites 1 and 2 & No Man's Friend 1_13.

7.4 Table of Sampling Dates and Tide Levels

Sampling Schedule for 2002-2003			
Month	**Date**	**Time**	**Height**
July, 2002	9th & 10th	1:34 PM / 2:21 PM	-.01 / -0.03
August, 2002	20th & 21st	12:29 PM	0.3
September	19th & 20th	12:10 PM / 12:55 PM	0.6 / 0.5
October	2nd & 3rd	10:35 AM/11:36 AM	0.6 / 0.4
November	14th & 15th	09:21 AM /10:13 AM	1.1 / 1
December	30th & 31st	10:39 AM/11:36 AM	0 / -0.2
January, 2003	29th & February 1st	11:54 AM / 2:17 PM	-0.6 / -.04
February	March 3rd & 4th	2:29 PM / 3:05 PM	-0.2 /-0.2
March	31st & April 1st	1:19 PM / 1:55 PM	0.0 / -.01
April	14th & 15th	12:58 PM / 1:47 PM	-0.3 / -0.7
May	Monday, 12th	12:36 PM	0.2
June	24th & 25th	10:55 AM / 11:40 AM	0.3/ 0.3
July	9th & 27th	10:34 AM / 1:20 PM	-.03 / 0.2